STRESS RELAXATION TESTING

Alfred Fox, *editor*

ASTM STP 676

AMERICAN SOCIETY FOR TESTING AND MATERIALS

STRESS RELAXATION TESTING

A symposium
sponsored by ASTM
Committee E-28 on
Mechanical Testing
AMERICAN SOCIETY FOR
TESTING AND MATERIALS
Kansas City, Mo., 24, 25 May 1978

ASTM SPECIAL TECHNICAL PUBLICATION 676
Alfred Fox, Bell Telephone
Laboratories, editor

List price $23.75
04-676000-23

AMERICAN SOCIETY FOR TESTING AND MATERIALS
1916 Race Street, Philadelphia, Pa. 19103

Library of Congress Catalog Card Number: 78-74563

NOTE

The Society is not responsible, as a body,
for the statements and opinions
advanced in this publication.

Printed in Baltimore, Md.
June 1979

Foreword

The symposium on Stress Relaxation Testing for Improved Material and Product Reliability was presented at Kansas City, Mo., 24, 25 May 1978. The symposium was sponsored by the American Society for Testing and Materials through its Committee E-28 on Mechanical Testing. Alfred Fox, Bell Telephone Laboratories, presided as symposium chairman and editor of this publication.

Related ASTM Publications

Reproducibility and Accuracy of Mechanical Tests, STP 626 (1977), $15.00, 04-626000-23

Recent Developments in Mechanical Testing, STP 608 (1976), $14.50, 04-608000-23

Cyclic Stress-Strain and Plastic Deformation Aspects of Fatigue Crack Growth, STP 637 (1977) $25.00, 04-637000-30

The Influence of State of Stress on Low-Cycle Fatigue of Structural Materials: A Literature Survey and Interpretive Report, STP 549 (1974), $5.25, 04-549000-30

Cyclic Stress-Strain Behavior—Analysis, Experimentation, and Failure Prediction, STP 519 (1973), $28.00, 04-519000-30

A Note of Appreciation to Reviewers

This publication is made possible by the authors and, also, the unheralded efforts of the reviewers. This body of technical experts whose dedication, sacrifice of time and effort, and collective wisdom in reviewing the papers must be acknowledged. The quality level of ASTM publications is a direct function of their respected opinions. On behalf of ASTM we acknowledge with appreciation their contribution.

ASTM Committee on Publications

Editorial Staff

Contents

Hold-Times Cyclic Effects and Residual Stress

Summary

Introduction

Stress relaxation[1] is the time and temperature dependent decrease of stress in a solid due to the conversion of elastic into inelastic strain. Stress relaxation data can be used to develop stress-relief heat treatments for reducing residual stresses and for the design of such mechanical elements as joints, gaskets, and springs. Stress relaxation data are also an important tool for evaluating the constitutive relations governing a material's inelastic behavior.

Until approximately 1960, stress relaxation was primarily of interest only to those concerned with the design and manufacture of steam and power generating equipment and, to a lesser extent those concerned with the design of gaskets, reinforced concrete, and electric motors. Thus we find that a considerable amount of the early work in this field has been done by the ASTM-ASME Joint Committee on the Effect of Temperature on the Properties of Metals and by individuals associated with this committee.

Microminiaturization in the computer and electronics industries coupled with the high reliability of the missile and nuclear reactor industries created a need for standard testing techniques for measuring this mechanical property. This led to the creation of ASTM Subcommittee E28.11 on Stress Relaxation of ASTM Committee E-28 on Mechanical Testing and to the development of an ASTM Standard Recommended Practice (E 328).

The present symposium was organized, and this Standard Technical Publication was prepared primarily to permit those studying the phenomenon to share technical skills, procedures, and analytical tools. We also hoped to direct the attention of those teaching materials engineering and machine design to the importance of this property in evaluating the time and temperature dependence of stresses and strains in components intended for long term operation.

In selecting subdivisions for this publication we arbitrarily followed the arrangement of the three symposium sessions, and the papers were arranged into three groups involving (1) constitutive relations and modeling,

[1]These terms are more precisely defined in ASTM Standard Definitions of Terms Relating to Methods of Mechanical Testing (E 6) and ASTM Standard Recommended Practices for Stress Relaxation Tests for Materials and Structures (E 328), *ASTM Annual Book of Standards*, Part 10.

(2) test methods as applied to materials and products, and (3) effects of hold times, residual stress, and cycling.

This publication is a contribution of Subcommittee E28.11 on Stress Relaxation of ASTM Committee E-28 on Mechanical Testing. As chairman of the Subcommittee I should like to acknowledge the contribution made by the authors, reviewers, the session chairmen Karl Schmieder and Prakash Parikh, both of whom also helped in organizing the symposium, Anton Sinisgalli who represented the ASTM Publications Committee, and Miss Jane Wheeler and her ASTM editorial staff.

It is hoped that this volume will help design engineers by providing sorely lacking data on stress relaxation of engineering materials as well as provide an incentive to develop more data by highlighting some of the techniques by means of which this may be accomplished.

Alfred Fox

Bell Laboratories, Murray Hill, N.J. 07974;
symposium chairman and editor.

Constitutive Relations

E. W. Hart[1]

Load Relaxation Testing and Material Constitutive Relations

REFERENCE: Hart, E. W., "**Load Relaxation Testing and Material Constitutive Relations**," *Stress Relaxation Testing, ASTM STP 676,* Alfred Fox, Ed., American Society for Testing and Materials, 1979, pp. 5-20.

ABSTRACT: The phenomenon of load relaxation for a specimen in a tension test configuration is not in itself a material property. The resultant record of load P as a function of elapsed time t is dependent on the conditions of loading in the test as well as on the material elastic and inelastic properties. For this reason, the term "load" relaxation seems preferable to "stress" relaxation as a nomenclature for the test, and we shall employ this term in the paper.

In order to deduce the intrinsic material flow properties from the testing results it is desirable to convert the load-time record $P(t)$ to a specimen record of stress versus strain rate $\sigma(\dot{\epsilon})$. In some cases the explicit time dependence is significant, and so each stress-strain rate point can also be associated with the current time t if desired. This data conversion can be always accomplished.

In the following we shall describe the method of data analysis that is desirable for determining the inelastic constitutive relations of a material. We shall discuss some refinements of the experimental technique that have proven very important in such analysis. We shall then illustrate the expected results for several types of ideal material behavior and finally show the type of results and conclusions for some real materials and test conditions.

KEY WORDS: load relaxation, stress relaxation, constitutive relations, inelastic deformation

Load Relaxation Test

Conditions of the Test

In a load relaxation test, as generally performed on a screw-driven tensile machine, the specimen is pulled at a predetermined extension rate (cross-head speed) to some desired extension or load level, at which point the machine cross-head motion is stopped. The specimen continues to strain inelastically under the action of the load exerted by the load train. As the

[1]Professor of Mechanics and Materials Science, Cornell University, Ithaca, N. Y. 14853, and General Electric Co., Schenectady, N. Y. 12345.

specimen extends inelastically, the applied load relaxes according to the elastic compliance of the specimen and load train. The time rate of change of the applied load $\dot{P}$ is a direct measure of the specimen nonelastic extension rate $\dot{L}$, and, of course, P at each instant determines the operative applied stress σ. Therefore, if, during such a test, P is measured as a function of time t with sufficient precision that P can be differentiated with respect to t, the relaxation history of specimen strain rate $\dot{\epsilon}$ as a function of σ and t can be generated. For metals, the dependence on t is significant only for anelastic transients, and most of the cases of interest concern the nontransient dependence of $\dot{\epsilon}$ solely on σ and the accumulated strain hardening. We shall discuss this aspect in detail next.

Deduction of $\sigma(\dot{\epsilon})$

The analytical relationships in the load relaxation test have been discussed by many authors, among which the more recent are listed in the references [*1-4*].[2] We shall follow here the treatment of Lee and Hart [*4*].

For a specimen mounted in a tension testing machine, let L be the current "relaxed length" of the specimen, that is, the length of the real gage section less its elastic extension. Let L_1 be the distance of the movable crosshead from a fixed fiducial point chosen in such a way that $L_1 = L$ when the load $P = 0$. Then at any instant

$$CP = L_1 - L \tag{1}$$

where C is the elastic compliance of the entire load train including load cell and specimen.

Now, differentiating with respect to time, we obtain an expression for the nonelastic extension rate of the specimen as

$$\dot{L} = \dot{L}_1 - C\dot{P} \tag{2}$$

If A_0 and A are, respectively, the initial and current specimen relaxed cross sections, and L_0 is the initial value of L, we have the general relations

$$LA = L_0A_0 \tag{3}$$
$$\sigma = P/A$$
$$= PL/A_0L_0 \tag{4}$$
$$\dot{\epsilon} = \dot{L}/L \tag{5}$$

[2]The italic numbers in brackets refer to the list of references appended to this paper.

We obtain the current value of L from Eq 1 and $\dot{L}$ from Eq 2. During the load relaxation stage of a test, $\dot{L}_1 = 0$, and then

$$\dot{L} = -C\dot{P} \tag{6}$$

Some Experimental Aspects

Since for most testing configurations the value of C is about five to ten times what the compliance would be if all elements of the load train except the specimen were perfectly rigid, the total nonelastic strain of the specimen during the relaxation history is equal to not more than ten times the change of elastic strain during the same history. This corresponds to an inelastic strain increment typically of about 10^{-4} and seldom more than 10^{-3}. The specimen therefore undergoes negligible strain hardening during the relaxation straining, and so all the points σ versus $\dot{\epsilon}$ from a single relaxation run correspond to a single state of hardness.

This aspect of the test was exploited by Hart and Solomon [5] in their study of high-purity aluminum at 25°C. In that same study, some experimental refinements were introduced that made it possible to measure the stress–strain rate characteristics of that material over a large range of hardness levels and over as much as six decades of strain rate in each run. Those techniques are described in detail in Lee and Hart [4] and Hart and Solomon [5]. We shall describe them only briefly here. The most important modifications of the technique are as follows:

1. The use of high precision digital instrumentation to measure and record the load cell readings $P(t)$. This provides good time resolution of the load readings in the early stages of the relaxation and permits strain rate determinations up to a factor of 10^2 higher than is possible with the usual chart recorders. The digital data also facilitates numerical analysis.
2. Careful temperature stabilization of the entire load train. This step minimizes the signal fluctuations normally caused by thermal expansion and contraction of elements of the load train. It is especially important at the very low-strain-rate end of the run. With this precaution the rate measurements can be extended to rates as much as 10^3 slower than is otherwise possible.
3. The replacement of direct numerical differentiation in the data analysis by a nonlinear optimization routine that discriminated strongly against "noise" in the $P(t)$ record. This technique is described in Appendix I of Hart and Solomon [5].

It should be noted that the time of measurement of a single relaxation run to accomplish this broad range of strain rate measurement is as long as 2 days. The usual statements in the literature that the specimen ceases to relax after an hour or so of observation are simply not correct. Such conclusions reflect only the high level of noise fluctuation in the data in the usual test.

There is a possible additional modification of the experimental configuration of the load relaxation test that can make a significant improvement in the test results. This consists in introducing direct measurement of the extension rate of the specimen by use of strain gages or extensometers. This technique seems to have been employed so far only by Woodford in tests on Cr-Mo-V steel [*6*].

Presentation of the Data

As we have discussed previously, the significant test result is the record of observed stress as a function of strain rate. Since most metal flow properties involve ratios of σ and of $\dot{\epsilon}$, it is best to plot the data as log σ versus log $\dot{\epsilon}$. Furthermore, since the observable strain rate range is the same for all tests, it is convenient to employ the log $\dot{\epsilon}$ variable for the abscissa of the plot. We shall follow this procedure in this paper.

Test Data and Material Properties

The formal model of the inelastic deformation properties of a material is now generally termed the material inelastic "constitutive relations" or "constitutive equations." A complete set of constitutive relations permits the prediction of the material response to any history of loading. A knowledge of such a set of equations is necessary to make proper mechanical design calculations of engineering structural elements. They also serve to characterize the material with respect to the problem of controlling the mechanical properties by material processing procedures.

The load relaxation test is a valuable test procedure for deducing some of the relations that are needed to develop and critically test constitutive equations. Some caution must be exercised, however, in such deductive procedures, since the constitutive relations are rarely simple. This point can be best illustrated by looking at the results that would be obtained for tests on materials that exhibit a variety of idealized constitutive relations. We shall examine, therefore, the resultant stress-strain rate curves that would be produced in load relaxation tests for (*a*) a simple viscous flow relation, (*b*) nonlinear viscosity plus an internal stress, and (*c*) a nonlinear anelastic element. Of these three examples, the first two lead to explicit σ-$\dot{\epsilon}$ relations that are dependent on the loading history only insofar as the parameters of the relations are assumed to evolve (as in strain hardening) with prior straining. The third case depends more immediately on the abruptness of initial loading and so represents to some extent an explicit time history in relaxation.

Viscous Flow Law

A "viscous relation," in modern usage, means a flow relation in which the strain rate is determined directly by the current value of the stress. Thus, it is represented by a functional relationship of the type

$$\dot{\epsilon} = \dot{\epsilon}(\sigma) \tag{7}$$

For application to metal flow, there is generally included a dependence on temperature T as well, and, if strain hardening is described through a state variable σ^*, that state variable appears in the functional relation also. Thus, in this general case

$$\dot{\epsilon} = \dot{\epsilon}(\sigma; \sigma^*, T) \tag{8}$$

In any case, so long as T is held constant and σ^* does not vary during the test, the load relaxation data will produce precisely the viscous relation itself. Clearly, the log σ-log $\dot{\epsilon}$ plot of the load relaxation data for a material can be directly analyzed for the form of such a relation if it is known that there are no transient phenomena generated at the initiation of the test.

Viscous Flow with an Internal Stress

It is sometimes assumed that a material satisfies a viscous flow relation that takes a simple functional form when the relation is stated in terms of an "effective stress" σ_f that is equal to the applied stress σ less an "internal stress" σ_a. Thus, for $\sigma \geq \sigma_a$

$$\sigma_f = \sigma - \sigma_a \tag{9}$$

and σ_a is assumed constant during the test. A simple power law viscous relation might be of the form

$$\begin{aligned} \dot{\epsilon} &= \dot{a}^*(\sigma_f/\mathfrak{M})^M \\ &= \dot{a}^*[(\sigma - \sigma_a)/\mathfrak{M}]^M \end{aligned} \tag{10}$$

where

$\mathfrak{M}$ is a reference modulus,
M is a constant, and
$\dot{a}^*$ is a rate factor that depends on T.

Now

$$\log \frac{\sigma - \sigma_a}{\mathfrak{M}} = \frac{1}{M} \log \frac{\dot{\epsilon}}{\dot{a}^*} \tag{11}$$

and the plot of log σ versus log $\dot{\epsilon}$ is a curve that is concave upward. Such a behavior is actually found for most metals at low homologous temperature. This is illustrated in the measurements of Gupta and Li [*7*] and Yamada and Li [*8*].

Anelastic (Viscoelastic) Element

We show in Fig. 1 a diagram representing the typical anelastic element. In this model the viscous element (represented by the dashpot) is not necessarily Newtonian. The strain storage element (represented by the spring) is considered here to be linear with a modulus $\mathfrak{M}$.

For this element, the strain rate at any stress level during relaxation depends on the current value of the stored strain a, and that depends on the prior loading history. Thus this case, unlike the prior two, is explicitly relaxation history dependent.

The response law of this element will be assumed to be that for which the dashpot represents a viscous flow with a power law like that in the immediately preceding model. Thus

$$\dot{\epsilon} = \dot{a}^*[(\sigma - \sigma_a)/\mathfrak{M}]^M \tag{12a}$$

$$\dot{\epsilon} = \dot{a} \tag{12b}$$

$$\sigma_a \equiv \mathfrak{M}a \tag{12c}$$

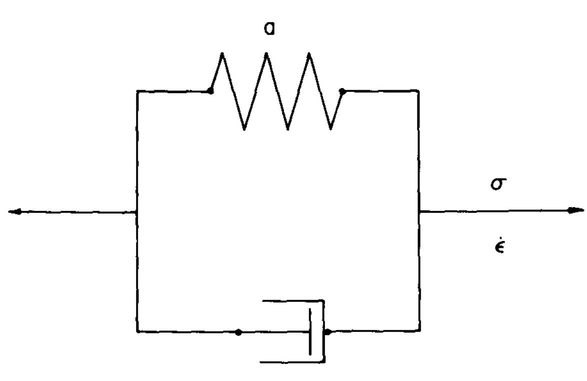

FIG. 1—*A schematic anelastic element. The spring is linear; the dashpot is not necessarily linear.*

We restrict our example to the case where $\sigma \geq \sigma_a$.

If at the start of the relaxation stage of the test $\sigma = \sigma_0$ and $a = a_0$, and, if

$$\kappa \equiv KL/A \tag{13}$$

where K is the machine-specimen elastic constant, equal to $1/C$, then at any time during the relaxation

$$\sigma = \sigma_0 - \kappa(a - a_0) \tag{14}$$

Then, during the run

$$\frac{\sigma - \mathfrak{M}a}{\mathfrak{M}} = \left(\frac{1}{\kappa} + \frac{1}{\mathfrak{M}}\right)\left[\sigma - \frac{\sigma_0 + \kappa a_0}{1 + (\kappa/\mathfrak{M})}\right] \tag{15}$$

If we write

$$\frac{1}{\mathfrak{M}'} \equiv \frac{1}{\kappa} + \frac{1}{\mathfrak{M}} \tag{16}$$

$$\frac{(\sigma_0 + \kappa a_0)}{1 + (\kappa/\mathfrak{M})} \equiv \sigma_a' \tag{17}$$

we can represent the resultant relaxation data in the form

$$\log[(\sigma - \sigma_a')/\mathfrak{M}'] = (1/M)\log(\dot{\epsilon}/\dot{a}^*) \tag{18}$$

This is remarkably like the result of the previous example given by Eq 11. Note well, then, that an experimental result that can be fitted by a formula like that of Eq 18 can in fact be due to either of two quite different models. These can be distinguished only by additional tests of other types.

Testing Results for Some Materials

Actual materials exhibit the simple constitutive properties described previously only for restricted testing conditions. The usual behavior is more complex. Typical forms of stress-strain rate relations from refined load relaxation testing are exhibited and discussed by Hart et al [9]. It is specially noted in that paper that there is a fundamental difference in the aspect of the σ-$\dot{\epsilon}$ relation measured in load relaxation between the results obtained at high and low homologous temperature. Specifically, the high-temperature curves are concave downward, while the low-temperature curves are concave upward. A complete model and set of constitutive equations was proposed then by Hart [10] that quantitatively accounted for both modes of behavior.

We can discuss this model and its application only very briefly in the present paper. The model is shown schematically in Fig. 2. There, an auxiliary strain rate component α is shown as well as a stored anelastic strain a. The total nonelastic strain rate $\dot{\epsilon}$ is given by

$$\dot{\epsilon} = \dot{\alpha} + \frac{d}{dt} a \tag{19}$$

The $\dot{\alpha}$ component is assumed to obey a viscous relation that depends on the stress component σ_a, the temperature T, and on a hardness-state variable σ^*. Thus

$$\dot{\alpha} = \dot{\alpha}(\sigma_a; \sigma^*, T) \tag{20}$$

as in the parametric viscous model we discussed previously. The rest of the diagram elements are like those in the anelastic model mentioned previously, and

$$\sigma = \sigma_a + \sigma_f \tag{21}$$

The hardness σ^* changes incrementally with increments of strain according to an experimentally determined relation

$$d \ln \sigma^*/dt = \Gamma(\sigma^*, \sigma_a)\dot{\alpha} - \mathcal{R}(\sigma^*, T) \tag{22}$$

The first term of the right-hand side represents strain hardening, and the

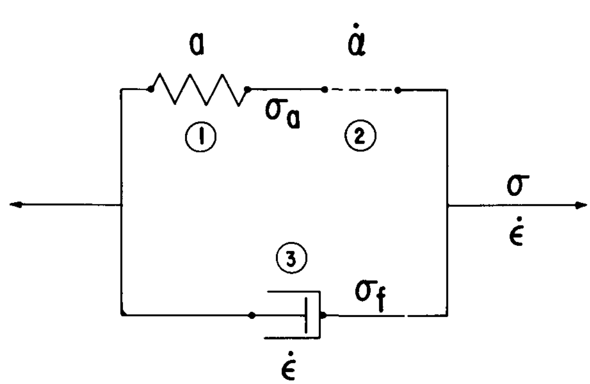

FIG. 2—*A diagram representing constitutive relations for metal grain matrix nonelastic flow. Element 1 is Hookeian; Element 2 is a viscous element with strain hardening as described in the text; Element 3 is a nonlinear viscous element.* (*From Hart* [10].)

second term represents static thermal recovery. The term $\mathcal{R}$ is relatively unimportant below about one half the melting temperature.

The application of the model to high- and low-temperature behavior is discussed in detail in Hart [10]. We note here only that at high temperature, for relatively pure metals, $\sigma_f \ll \sigma_a$ and so, substantially, $\sigma = \sigma_a$ and $\dot{\epsilon} = \dot{\alpha}$ after transient loading is completed. We illustrate this case next by the data for high-purity aluminum. At low temperature, the strain rate component $\dot{\alpha}$ behaves much like classical plasticity in which $\dot{\alpha} = 0$ if $\sigma_a < \sigma^*$, and $\dot{\alpha}$ is nonzero and arbitrary when $\sigma_a = \sigma^*$. Thus, in that case, $\sigma_a = \sigma^*$ when flow occurs, and then $\dot{\alpha} = \dot{\epsilon}$. We illustrate this case by data for niobium.

High-Temperature Case

Two curves from the measurements of Hart and Solomon [5] are shown in Fig. 3. Those authors noted that all of their curves satisfied a scaling relation, shown in Fig. 4, such that all measured curves could be derived from a single master curve by simple translation in the $\log \sigma - \log \dot{\epsilon}$ plane as shown in the figure. The master curve, so deduced, yielded the functional form of the $\dot{\alpha}(\sigma_a)$ relationship of Eq 21. A plot of the resultant function together with the experimental points is shown in Fig. 5. The deduction of the function is described in Hart et al [9]. A remarkable later development was Woodford's discovery [6] that the same function also fit the results for a low alloy steel at elevated temperature.

Low-Temperature Case

There is considerable data now available for the low homologous temperature behavior. A set of curves for niobium due to Yamada and Li [11] is shown in Fig. 6. These and other low-temperature curves exhibited a scaling also. This scaling is not related to that in the high-temperature case, but rather derives from the fact that equations of the sort described previously for viscous behavior with an internal stress in fact obey a scaling with respect to σ_a. This fact was shown by Hart [10] in analysis of the niobium data, and it was used effectively in a detailed analysis on 316 stainless steel by Nir et al [12].

An earlier analysis of low-temperature behavior in terms of an internal stress was carried out by Gupta and Li [7]. Their measurements covered only a narrow range of strain rate and did not find the scaling relationship, but the more recent work cited here confirms their methodology.

Complex Loading Histories

It is, of course, possible to carry out load relaxation subsequent to prior

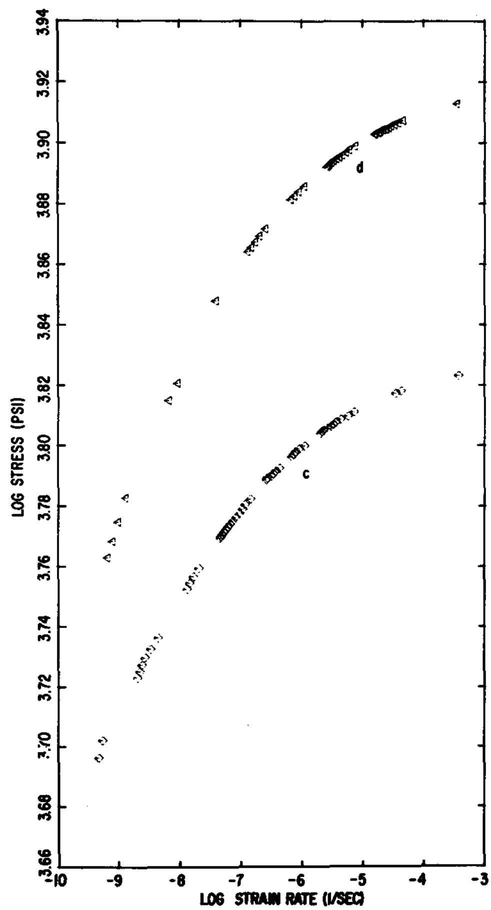

FIG. 3—*Two load relaxation curves for high-purity aluminum. (After Hart and Solomon* [5].) *The total accumulated strain at about* 10^{-3} s^{-1} *at the start of each run is 6 percent for the lower curve and 14 percent for the upper curve.*

loading histories that are more complex than the simple monotonic loading we have considered so far. The effect of the prior loading on the load relaxation result depends on the constitutive relations of the material being tested.

In the case of the viscous flow law given by Eq 8, the prior deformation determines the value of σ^* that will be effective during the test. The test then simply measures the normal viscous relation with that value of σ^*.

In the case of the anelastic element, as well as with the more complete Hart model, the prior history determines the value of a_0, the initial value of a at start of test, as well as σ^*, where it is applicable.

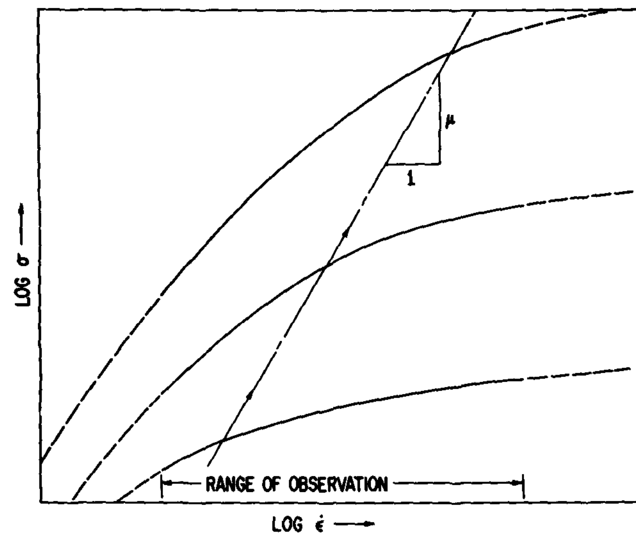

FIG. 4—*Schematic representation of log σ — log $\dot{\epsilon}$ scaling for curves of different hardness. (After Hart and Solomon* [5]). *Each curve shown is the same master curve translated along the oblique direction shown. The region of $\dot{\epsilon}$ designated range of observation defines the measured curves.*

Anelastic Element

In our previous discussion, we restricted our considerations to the case where $\sigma_0 \geq \mathfrak{M}a_0$, or more generally, for $\sigma \geq \sigma_a$. When this is not the case we note first that Eq 12*a* must be modified as follows

$$|\dot{\epsilon}| = \dot{a}^*[|\sigma - \sigma_a|/\mathfrak{M}]^M \tag{23}$$

and

$$\text{sgn}\,\dot{\epsilon} = \text{sgn}(\sigma - \sigma_a) \tag{24}$$

where sgn x means "the algebraic sign of x."

Now, if at start of the relaxation run $\sigma_0 < \mathfrak{M}a_0$, the resultant relaxation data will be given by

$$\log[\sigma_a' - \sigma)/\mathfrak{M}'] = (1/M)\log(-\dot{\epsilon}/\dot{a}^*) \tag{25}$$

where $\mathfrak{M}'$ and σ_a' are as defined in Eqs 16 and 17. The observed strain rate $\dot{\epsilon}$ will be negative during the run, and σ will rise from the value σ_0 to σ_a' as an upper bound.

The specimen, therefore, contracts during the relaxation as in the familiar

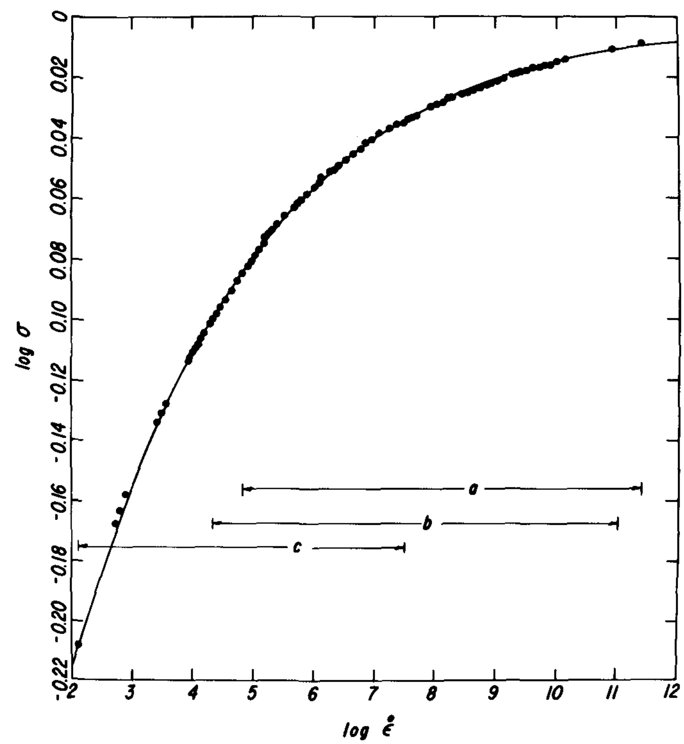

FIG. 5—*Master hardness curve for high-purity aluminum generated from three room temperature curves by scaling. (After Hart* [10].) *The drawn curve is a plot of the analytical function describing the* $\dot{\alpha}$ *element as described in Hart* [10].

case of the creep strain recovery attendent upon unloading a creep test specimen.

The Hart Model

In the case of the full inelastic constitutive equations given by Hart [*10*], the resultant behavior can be even more complex. The effects can range from the simple loading transients discussed by Hart and Solomon [*5*] and by Hart et al [*9*] to quite bizarre behavior when a_0 is large enough. In the latter case, it is possible to have relaxation histories during which $\dot{\epsilon}$ begins negative, increases continuously up to a maximum positive value, and then decreases continuously but remains positive. During that history, σ increases from σ_0 to a maximum value and then decreases monotonically.

It is clear, then, that considerable caution must be exercised in the interpretation of load relaxation tests that follow complex loading patterns. Such complex loading tests are of use as crucial tests for constitutive equations that have been fully stated for the material. The constitutive

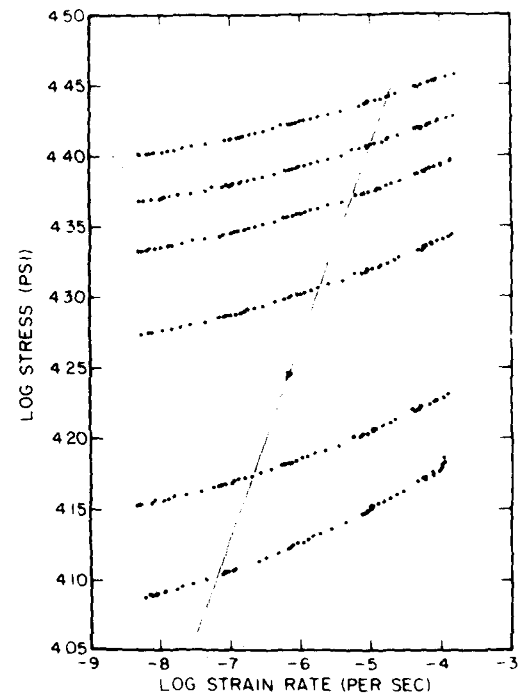

FIG. 6—*Stress-strain rate curves from load relaxation tests of high-purity niobium. (After Yamada and Li* [11].) *The diagonal line represents the scaling translation direction.*

equations should be able to predict the test results even for quite complex loading histories.

On the other hand, it is somewhat pointless to attempt to deduce the constitutive equations *ab initio* solely on the basis of complex tests.

Conclusions

Load relaxation testing is an indispensible tool for the development of inelastic constitutive relations. The test is fully effective only if refined experimental techniques are employed so that the tests explore a sufficiently large range of strain rate. The test data should generally be analyzed for the resultant stress-strain rate relationship. Considerable caution must be exercised in test interpretation when complex loading routines are employed.

Acknowledgments

The preparation of this paper was supported by the U.S. Department of Energy (formerly USERDA).

References

[1] Noble, F. W. and Hull, D., *Acta Metallurgica*, Vol. 12, 1964, pp. 1089-1092.
[2] Li, J. C. M., *Canadian Journal of Physics*, Vol. 45, 1967, pp. 493-509.
[3] Hart, E. W., *Acta Metallurgica*, Vol. 15, 1967, pp. 351-355.
[4] Lee, D. and Hart, E. W., *Metallurgical Transactions*, Vol. 2, 1971, pp. 1245-1248.
[5] Hart, E. W. and Solomon, H. D., *Acta Metallurgica*, Vol. 21, 1973, pp. 295-307.
[6] Woodford, D. A., *Metallurgical Transactions*, Vol. 6A, 1975, pp. 1693-1697.
[7] Gupta, I. and Li, J. C. M., *Metallurgical Transactions*, Vol. 1, 1970, pp. 2323-2330.
[8] Yamada, H. and Li, C-Y., *Metallurgical Transactions*, Vol. 4, 1973, pp. 2133-2136.
[9] Hart, E. W., Li, C-Y., Yamada, H., and Wire, G. L. in *Constitutive Equations in Plasticity*, A. S. Argon, Ed., Massachusetts Institute of Technology Press, Cambridge, Mass., 1975, pp. 149-197.
[10] Hart, E. W., *Transactions ASME Journal of Engineering Materials and Technology*, Vol. 98, Series H, 1976, pp. 193-202.
[11] Yamada, H. and Li, C-Y., *Acta Metallurgica*, Vol. 22, 1974, pp. 249-253.
[12] Nir, N., Huang, F. H., Hart, E. W., and Li, C-Y., *Metallurgical Transactions*, Vol. 8A, 1977, pp. 583-588.

DISCUSSION

A. K. Miller[1] *(written discussion)*—We have just conducted a series of experiments on high-purity aluminum (the same material which you utilized in developing your model). We were able to reach steady-state flow at very low temperatures and therefore at very high stresses by using torsion at constant strain rate as the testing mode. Our new data, when combined with the classic work of Servi and Grant, results in a set of data for temperature-compensated steady-state strain rate $(\dot{\epsilon}_{ss}/D_{EFF})$[2] versus modulus-compensated steady-state flow stress σ_{ss}/E which covers an extremely broad range in both variables; in particular, the $\dot{\epsilon}_{ss}/D_{EFF}$ values extend for 15 orders of magnitude above power-law breakdown. The combined data are fit very well by the hyperbolic sine relation first suggested by Garofalo et al. Is there a way in which your equations will predict this hyperbolic-sine type of behavior at steady-state?

E. W. Hart (author's closure)—I do not know how low your measurements were in temperature. I presume the testing was done with thin walled cylinders. If they were done with solid cylinders, the interpretation of the results depends on the assumed constitutive law. There is an effect that is quite important in torsion testing that is almost always ignored. This effect is the rotation of the material elements of the specimen that occur in torsional deformation. The influence of that on the results was reported

[1]Department of Materials Science and Engineering, Stanford University, Stanford, Calif. 94305.
[2]D_{EFF} is the effective diffusion coefficient incorporating lattice diffusion and dislocation pipe diffusion.

recently by VanArsdale, Hart, and Jenkins, at the Eighth U.S. Congress of Applied Mechanics, University of California-Los Angeles, Los Angeles, June 1978.

It would be necessary to know the type of specimen, torsion rate, and temperature to find what the predictions of the constitutive equations are in this case.

A. K. Miller (written discussion)—In order for a material to obey your constitutive equations, it must first be prestrained enough to build up σ_a to the appropriate (saturated) level. How large of a prestrain is required to reach this condition where the equations become applicable?

E. W. Hart (author's closure)—The constitutive equations, as described in Ref *10* of the paper and in the present paper, fully describe the loading phase as well as the nontransient régime.

K. Amin[3] *(written discussion)*—Does the author see any future feasibility of applying this approach and constitutive relations in general to unstable structures (mainly age-hardenable alloys)?

E. W. Hart (author's closure)—There is already formal provision for accounting for aging effects through the term $\mathcal{R}$ in Eq 23. That term, which is included principally to handle static thermal recovery, could clearly describe other aging phenomena as well. However, no systematic investigation has been done with this yet, and it is not clear whether or not, in the case of aging, there must also be some time dependence of other parameters such as $\dot{a}^*$.

Ray Stentz[4] *(written discussion)*—Since the compliance of the testing machine (in the author's technique) affects the time-load relaxation of the material, would it not be better to actually control the strain in the gage length of the specimen, rather than controlling the crosshead displacement of the machine?

E. W. Hart (author's closure)—No. The only effect of that is to reduce C to a value determined by the specimen elastic modulus. As noted in the paper this reduction would be by a factor of from 1/5 to 1/10. The practical result of this in testing would be that the relaxation process would speed up by a factor of about 10. Under those circumstances there is insufficient time for data collection in the early stages of the test, and about two decades of strain rate data is lost.

[3] Bendix Research Laboratories, Southfield, Mich. 48076.
[4] Mar-Test Inc., Cincinnati, Ohio 45215.

R. W. Swindeman[5] *(written discussion)*—Do your constitutive relations recognize the existence of diffusional creep mechanisms at low stresses?

E. W. Hart (author's closure)—I am not sure whether the question concerns diffusional creep of the Herring-Nabarro type of diffusional processes such as affect dislocation climb. The constitutive equations described by Hart do not include the Herring-Nabarro creep. On the other hand, the processes responsible for the $\dot{\alpha}$-component of flow (described in detail in Ref *10* and noted briefly here in Eq 21) certainly reflect diffusion mechanisms. In fact, the activation energy for $\dot{\alpha}$ is commonly the self-diffusion activation energy.

[5]Oak Ridge National Laboratory, Oak Ridge, Tenn.

R. W. Rohde[1] *and J. C. Swearengen*[2]

Metal Deformation Modeling—Stress Relaxation of Aluminum

REFERENCE: Rohde, R. W. and Swearengen, J. C., "**Metal Deformation Modeling—Stress Relaxation of Aluminum,**" *Stress Relaxation Testing, ASTM STP 676,* Alfred Fox, Ed., American Society for Testing and Materials, 1979, pp. 21-35.

ABSTRACT: Experiments designed to test the validity of a model for rate-dependent inelastic deformation in metals are presented and discussed. The stress dependence of the strain rate in 99.99 percent pure aluminum was determined at 308 K from stress relaxation and creep experiments, and at 373 K from stress relaxation experiments. Deformation history was examined by conducting experiments subsequent to either monotonic tensile or reversed strain cyclic loading. At both temperatures and for both deformation histories, evidence of microstructural recovery was identified during the course of a relaxation experiment. The exponent characterizing recovery was found to be 20 at 308 K for both stress relaxation and creep; indicating that plastic deformation during creep and relaxation may be governed by the same kinetic law. The model is also found to predict correctly transient behavior observed in some relaxation experiments. This model apparently provides a physical basis for predicting relaxation subsequent to a variety of deformation conditions, thereby functioning as an evolutionary material law.

KEY WORDS: plastic deformation, mechanical properties, stress relaxation, creep recovery, creep properties, polycrystals, dislocations, aluminum

Design of highly reliable structures and components often requires knowledge of material response to loads or strains after long service time. This response may manifest itself in terms of general yielding, creep, load relaxation, or fracture. External loads and temperatures may be steady or time varying, so that in principle a material may experience an infinite variety of thermomechanical histories prior to the time or event of interest. The wide diversity of service conditions and the need for material properties after long service times usually eliminate the possibility of obtaining design data under conditions that duplicate service lives. Therefore, designs for long times are usually based on predictions of mathematical models.

[1] Supervisor, Physical Metallurgy Division, Sandia Laboratories, Albuquerque, N. Mex. 87115.
[2] Supervisor, Materials Science Division, Sandia Laboratories, Livermore, Calif. 94550.

Models for describing material behavior have been usually empirical or phenomenological. While such models often permit reliable interpolation in the regions between existing experimental data, extrapolation to predict behavior beyond measured data must be considered hazardous. This prediction is especially important for the case of time-varying loads and temperatures. Extrapolation with confidence requires, at a minimum, the knowledge that the physical processes of deformation remain the same in the regions of measurement and extrapolation. Several investigators have recently attempted to write physically based descriptive equations for nonsteady loading conditions at temperatures sufficiently high so that thermal instability of the microstructure must be accounted for [*1-4*].[3] A number of excellent examples are also found in Argon [*5*]. Since it is obviously impossible to require detailed knowledge of the deformation history of a material in order to predict subsequent response, attempts are being made to develop models that predict material response with only the requirement that the current state of a material be known [*4,6,7*]. Often these relationships are called "mechanical equations of state," because they postulate a unique relationship between stress, strain, and their time derivatives, and temperature. More recently, however, it has been shown that, if material models are to be useful in describing deformation after some arbitrary thermal and mechanical history, they must contain at least one and perhaps several variables that are dependent upon the microstructure [*6,8,9*]. This microstructure related variable is often called an internal state variable. In principle, then, adequate specification of the internal state variable allows calculation of material response without explicit knowledge of history.

If a material deformation model considers microstructure, it may be written to describe deformation occurring concurrently with microstructural change, such as recovery. Since the state of a material is constantly changing in this case the description "mechanical equation of state" is misleading. Rather, we choose to call such relations "evolutionary material laws."

In this paper we consider the application of a model proposed by Kocks [*2,10*] to stress relaxation and creep behavior of aluminum. The model assumes inelastic deformation occurs by the thermally activated glide of dislocations in a microstructure, which itself changes as a result of the combined effects of work hardening and recovery. The kinetic relationship between inelastic strain rate and applied stress is taken (at fixed temperature) to be a power law

$$\dot{\epsilon}_p = \epsilon_0\left(\frac{\sigma}{\sigma_D}\right)^m \tag{1}$$

[3] The italic numbers in brackets refer to the list of references appended to this paper.

where

$\dot{\epsilon}_p$ = inelastic strain rate,
ϵ_0 = material constant,
σ = applied stress,
σ_D = drag stress, and
m = isostructural rate sensitivity exponent.

This power law is assumed to be an approximation to the usual Arrhenius equation for thermal activation; it is useful because it is analytically simple yet still provides an excellent description of the usual experimental data, which is taken over a limited range of strain rates.

In this equation, ϵ_0 and m are assumed to depend on temperature; ϵ_0 is expected to be rather insensitive, varying only as the shear modulus. The fact that ϵ_0 is constant with stress or strain implies the assumption that the density of the thermally activated mobile dislocations is constant. The drag stress is a microstructure-dependent internal state variable related to the mechanical strength of obstacles in the dislocation glide planes. In a study of the work-hardening behavior of high-purity aluminum and copper polycrystals, Kocks [10] concluded that the drag stress changed both through microstructural hardening and recovery. He proposed that σ_D evolves in the following manner

$$\frac{d\sigma_D}{d\epsilon_p} = \theta_0\left(1 - C\frac{\sigma_D}{\dot{\epsilon}_p{}^{1/n}}\right) \qquad (2)$$

where

θ_0 = work-hardening coefficient at 0 K,
C = material constant related to the kinetics of recovery, and
n = recovery rate exponent.

The material constant n is related to the steady state creep exponent n' by $1/n = 1/n' + 1/m$. Usually m is much greater than n' so $n \cong n'$.

Equations 1 and 2 represent an evolutionary material law. This law in the present form is difficult to test by simple experimental techniques. It may, however, be integrated in a closed form for the case of one-dimensional stress relaxation and for the case of $m \gg n$ to produce [2]

$$\frac{\dot{\epsilon}_p}{\dot{\epsilon}_i} = \left[(1 - A)\left(\frac{\sigma}{\sigma_i}\right)^{m/n} + A\left(\frac{\sigma}{\sigma_i}\right)\right]^n \qquad (3a)$$

with

$$A = \frac{S\theta_0 C}{(1 - n/m)(1 - S\theta_0)^2}\,\frac{\sigma_i}{\dot{\epsilon}_i{}^{(1/n+1/m)}} \qquad (3b)$$

where

$\dot{\epsilon}_i$ = strain rate at the beginning of relaxation,
σ_i = stress at the beginning of relaxation, and
S = combined compliances of the machine and specimen.

Equations 3*a* and 3*b* now represent the evolutionary material law for the special case of stress relaxation. As will be shown subsequently, all the constants in these equations are easily determined, so the proposed law may be experimentally verified. It will be shown that application of the model given in Eqs 1 and 2 and expressed in Eq 3 for stress relaxation provides insights about the mechanisms responsible for the plastic strain accumulated in a stress relaxation event and for the observed strain-rate sensitivity of the stress. At early times, where the plastic strain rate is nearly the initial strain rate, the kinetics of deformation are controlled by simple, thermally activated glide. Recovery is unimportant, and the constant m controls the stress dependence of the plastic strain rate. At long times, when the plastic strain rate is small, microstructural recovery becomes important and dominates the kinetics. For the case of $n \ll m$, the recovery (or creep) exponent controls the stress dependence of the plastic strain rate.

Kocks [2] showed his model to be reasonably successful in reproducing stress relaxation data obtained by Hart and Solomon [11]. More recently, we found that the model produced an excellent description of stress relaxation in a 50Sn-50In alloy [3] and of Type 304 stainless steel [12] at temperatures above about 30 percent of the absolute melting temperatures. However, it was found necessary to include a backstress term to allow modeling stress relaxation at lower temperatures [12].

While these past successes of the model for stress relaxation are encouraging, some additional critical tests must be passed before the model can be used for long-term prediction. In particular, the model has not yet been examined to determine if history can be accounted for solely through the microstructural variable A. It is also desirable to determine if the long-time relaxation behavior follows the steady-state creep kinetics (that is, $n = n'$) as was postulated. Thus, in this work, creep and stress relaxation experiments are conducted on high-purity aluminum subsequent to both monotonic tensile and reversed strain tensile-compressive cyclic deformation. Material properties are determined from the creep experiments and are used in predicting stress relaxation data. Calculations are then performed to determine if the model is capable of predicting the transient behavior observed by Hart and Solomon [11].

Experimental Procedure

All specimens were made from 99.99 percent pure aluminum obtained from Alcoa in the form of 16-mm-thick rolled plate. Chemical analysis of the material is given in Table 1. Specimens having a 25.4-mm gage length and 6.4-mm gage diameter were prepared with their axes parallel to the rolling direction. Button ends were utilized to facilitate reversed-strain cyclic deformation. The specimens were annealed 30 min at 573 K and furnace-cooled, producing an average grain diameter of 0.25 mm.

Creep-Stress Relaxation Tests

Creep and stress relaxation experiments were conducted subsequent to both monotonic and reversed strain cyclic loading on a servocontrolled electrohydraulic machine especially modified to enhance stability [*3*]. Several relaxation events were conducted on each specimen at progressively larger initial strains. For the cyclic histories, ten complete cycles of reversed strain were applied before each creep or relaxation experiment. After the experiment, another ten cycles of reversed strain, of increased amplitude, were imposed and another creep or relaxation test conducted. Strain was measured with a clip-on strain gage extensometer having a 12-mm gage length. The sensitivity was better than ± 10 μm/m. Load was measured with an accuracy of 0.3 percent and a precision of 0.2 N. Strain could be controlled to better than ± 50 μm/m; load was controlled to better than 1 N.

The temperature of the specimen was precisely maintained by controlling room temperature to ± 0.5 K and by immersing the specimen and grips in a 23-litre silicon oil bath. The bath temperature was maintained by using immersed resistance heating elements connected to a proportioning controller. Temperature stability was better than ± 0.05 K during a typical stress relaxation experiment and ± 0.2 K for an extended creep measurement. Initial strain rates were 10^{-4} s^{-1}, with triangular strain-time functions used for reversed cyclic strain control.

TABLE 1—*Emission spectrographic analysis of aluminum plate.*

Element Detected	Amount, ppm	Element Not Detected	Sensitivity Limit, ppm
Manganese	6	Zinc	20
Iron	10	Chromium	10
Magnesium	2	Lead	15
Silicon	20	Zirconium	20
Copper	4	Nickel	20
Gallium	20	Titanium	1
		Beryllium	5
		Vanadium	2
		Boron	6

Data Reduction

Strain–time and load–time data were digitized and stored on magnetic tape for subsequent analyses. At short times, when the load or strain values were changing rapidly, data were sampled and stored every 0.3 s. Time resolution was better than 0.01 s. At longer times, when changes were minimal, greater time intervals were used. Typically, one experiment was characterized by 3000 to 4000 data points over a period of 40 min. Strain rates were determined by differentiating curves that had been spline-fitted to the data.

Results and Discussion

Most of the stress relaxation and all of the creep experiments were conducted at 308 K. This temperature was chosen because Bradley et al [*13*] found the effect of cyclic deformation on subsequent creep response was maximized at 308 K. A few relaxation experiments were conducted at 373 K in order to determine the temperature sensitivity of the material constants m and n and the variable A.

Creep Behavior

Results of the creep experiments are shown in Fig. 1, where the logarithm of the steady-state creep-strain rate is plotted versus the log of applied stress. The creep rate exponent n' ($\dot{\epsilon}_p = \epsilon_0 \sigma^{n'}$) is simply the slope of a best-fit line through the data. A linear least-squares fit gave $n' = 19.5$. Kocks [*10*] obtained a value of 15 for the stress exponent from an analysis of "saturation stress" data during work-hardening of aluminum. The difference in values found for n' in Kocks work and the value of 19.5 determined in Fig. 1 is well within the combined errors of the independent measurements. The two open circles in Fig. 1 are steady-state creep data taken subsequent to ten cycles of reversed strain at amplitudes of 0.12 and 0.22 percent for the smaller load and 0.12, 0.22, and 0.32 percent at the larger load. There is no apparent dependence of the steady-state creep rate upon cyclic or monotonic history.

Load Relaxation at 308 K

Stress relaxation behavior was measured at 308 K in 24 experiments subsequent to monotonic loading and in 13 experiments subsequent to cyclic loading. These data were processed to determine the relationship between stress and strain rate and plotted as log stress versus log strain rate as shown in Fig. 2 for monotonic loading. The model for stress relaxation (Eq 3) was then examined for its ability to fit the data using constants

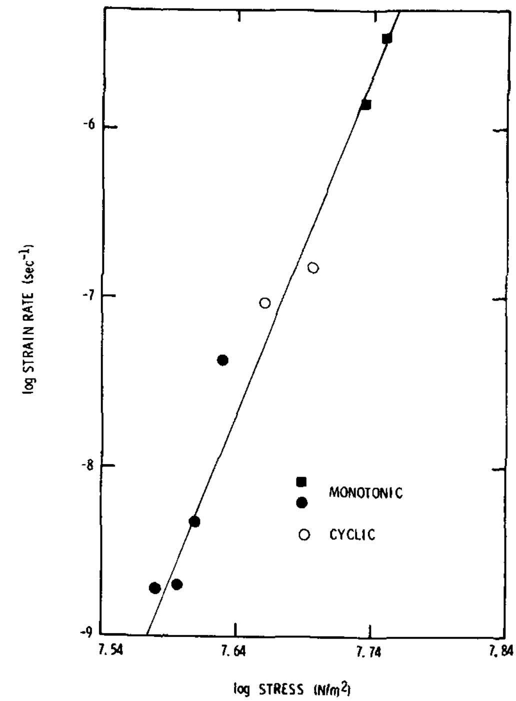

FIG. 1—*Log steady-state creep rate versus log applied stress. Line is a linear least squares fit.*

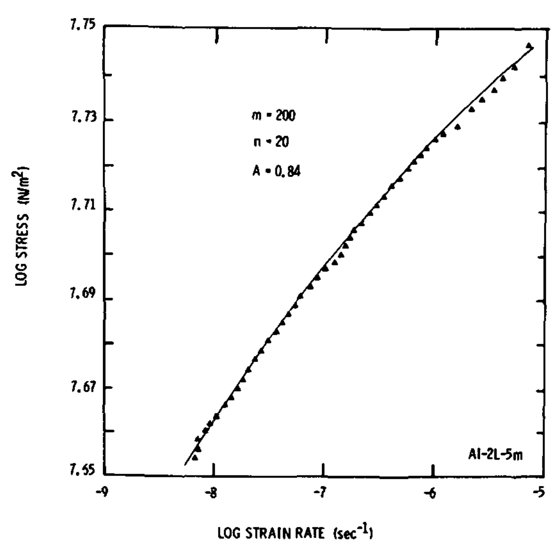

FIG. 2—*Load relaxation behavior of aluminum at 308 K after 1.9 percent strain. The triangles represent the measured data; the solid line is the model fit.*

consistent with the above creep data. For the evolutionary material law to be useful, the materials constants m and n should be unaffected by prior mechanical deformation. Any alterations in the behavior that are a result of history must be accounted for by the variable A.

The value for n ($\cong 20$) was obtained from our steady-state creep measurements. A value for m ($\cong 200$) was estimated from a report of Kocks [*10*]. In the data-fitting procedure, these values were treated as true material constants, and A was adjusted to produce a fit of the model. An example of such a fit to relaxation observed subsequent to monotonic loading is shown as a solid line in Fig. 2. An equally good data fit was obtained with these same m and n values for relaxation events after cyclic deformation. Figure 3 shows relaxation behavior observed in a specimen subsequent to ten cycles of reversed strain at each of the amplitudes ± 0.1, ± 0.2, ± 0.3, and ± 0.4 percent.

Load Relaxation at 373 K

A total of eight relaxation tests subsequent to monotonic deformation and nine tests after cyclic loading were conducted at 373 K. No creep experiments were performed at this temperature, so the value for n ($\cong 12$) was taken from the slopes of the data on log $\dot{\epsilon}$ versus log σ plots at low strain rates. The slopes of the data at high strain rates yielded values for

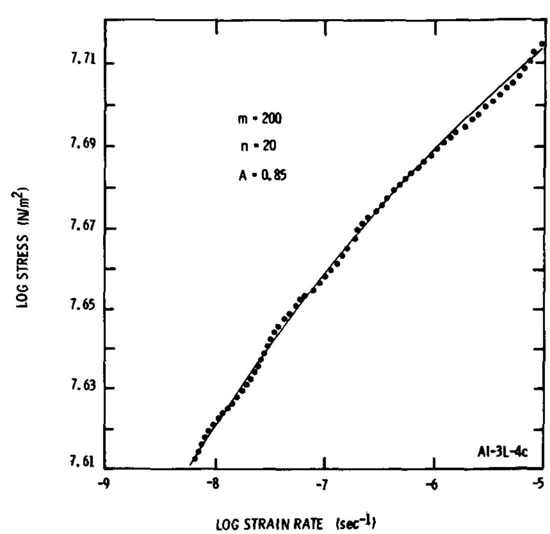

FIG. 3—*Load relaxation observed at 308 K on a specimen subjected to 10 cycles of reversed strain at each of the consecutive amplitudes of ± 0.1, ± 0.2, ± 0.3, and ± 0.4 percent. The circles represent the measurements after the cumulative 40 cycles; the solid line is the calculated fit.*

m of about 100. These numbers agree with those estimated by Kocks [*10*] at this temperature. These values were then used, with *A* as an adjustable parameter, to calculate fits to the relaxation data. An example of measured data and its corresponding fit is shown in Fig. 4 for relaxation after monotonic loading to 2 percent strain. Figure 5 shows data and fit for a relaxation event subsequent to ten cycles of loading at reversed strains at each of the amplitudes ±0.06, ±0.1, ±0.2, ±0.6, and ±0.7 percent. Equally good data fits were obtained for each relaxation event.

The Variable A

It is evident from Eq 3*b* that the magnitude of *A*, which must reflect the state of the microstructure, depends upon several material properties and constants or both, plus the initial stress and strain rate. The parameters in question, namely, *C, S, m,* and *n*, may be temperature dependent, but they must not contain a record *per se* of prior deformation path if the model is to be useful as an evolutionary material law. Any "history dependence" of *A* must result only from the initial conditions at the start of relaxation, that is, strain rate and the stress rate. In the experiments reported here $\dot{\epsilon}_i$ was maintained at a set value ($=10^{-4}$ s^{-1}), so the only

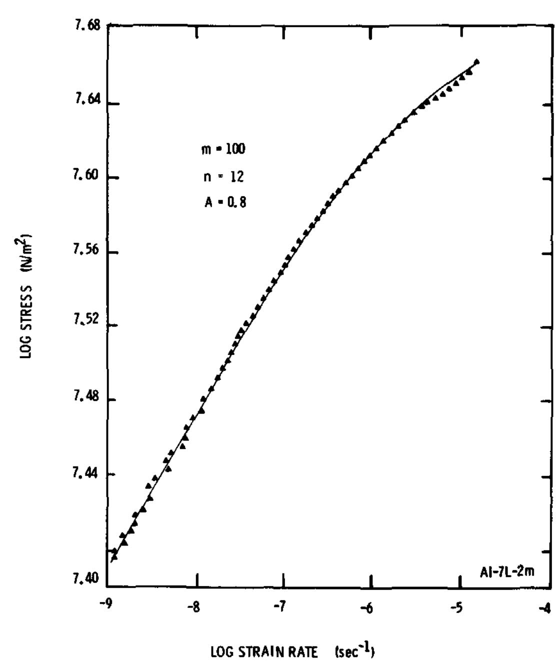

FIG. 4—*Load relaxation observed at 373 K on a specimen monotonically loaded to 2 percent strain. The triangles represent the data; the solid line is the calculated fit.*

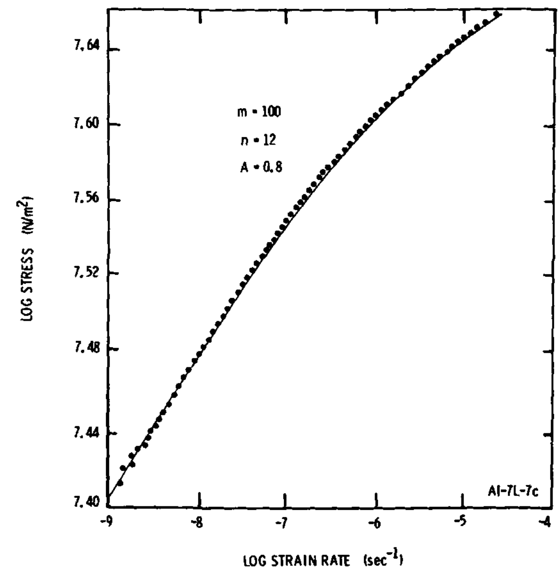

FIG. 5—*Load relaxation observed at 373 K on a specimen cyclicly loaded to ten cycles of reversed strain at each of the consecutive amplitudes of ±0.06, ±0.1, ±0.2, ±0.6, and ±0.7 percent. The circles represent measurements after 50 cumulative cycles; the solid line is the calculated fit.*

remaining mechanical variable in A is the initial stress σ_i, and hence, Eq 3*b* indicates that A should be linearly proportional to σ_i.

In Fig. 6, we have plotted the measured values of A versus the initial stress. Although there is considerable scatter, the data at both temperatures can be represented by straight lines passing through the origin, as required by Eq 3*b*. There is no observable difference between values of A determined from relaxation experiments conducted subsequent to cyclic or monotonic deformation indicating that history effects are determined by only the initial stress and strain rate values for aluminum. This finding is in agreement with the analysis of Hart [*11*], who proposed that only two parameters were needed to specify the state of aluminum. The finding is in contrast however, to our previous work on iron [*9*], where it was determined that the effect of history on state could not be explained by only two state variables.

Model Transient Behavior

The parameters are now sufficiently determined to allow some of the characteristics of the model to be assessed. In particular, we are interested in determining if the model will predict the relaxation behavior reported by Hart and Solomon [*11*] and identified by them as "inelastic transients."

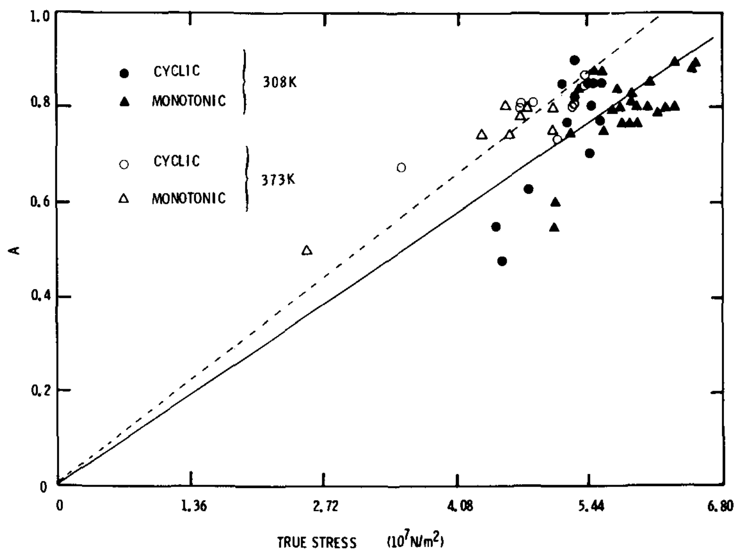

FIG. 6—*A plot demonstrating the dependence of the variable* A *on the stress at the beginning of relaxation.*

In their experiments, Hart and Solomon first recorded relaxation behavior of a specimen extended monotonically at a rate of about 2×10^{-3} s^{-1}. After relaxation, the specimen was elastically reloaded to a stress lower than the initial stress for the first relaxation, and a second relaxation event was imposed. The specimen was then annealed at 423 K, reloaded to a stress intermediate between the initial stresses on the first and second relaxation event, and a third relaxation event was monitored. Hart and Solomon found that while the three relaxation records merged at long times, there was an extended initial region where the relaxations differed considerably (Fig. 7 in Hart and Solomon [*11*]). In these initial regions, Hart and Solomon proposed that the material behavior was dominated by anelastic transients. The present analysis suggests, however, that these results are manifestations of work hardening and recovery during relaxation. In order to demonstrate this result, we used Eqs 3 to simulate the Hart-Solomon experiment. Values of m (=200) and n (=20) determined from our creep and relaxation data at 308 K were used. Our initial hypothetical relaxation was calculated to start from a stress of 5.60×10^7 N/m^2, and two subsequent relaxations were projected starting from reloading stresses of 5.48×10^7 N/m^2 and 5.35×10^7 N/m^2. History effects were accounted for through the variable A, whose values were selected from the line in Fig. 6 as 0.8, 0.77, and 0.75, corresponding to the three initial stresses. The initial strain rate was taken as 4×10^{-4} s^{-1} for each event. This approximates the initial strain rate plotted by Hart and Solomon. The results of computations

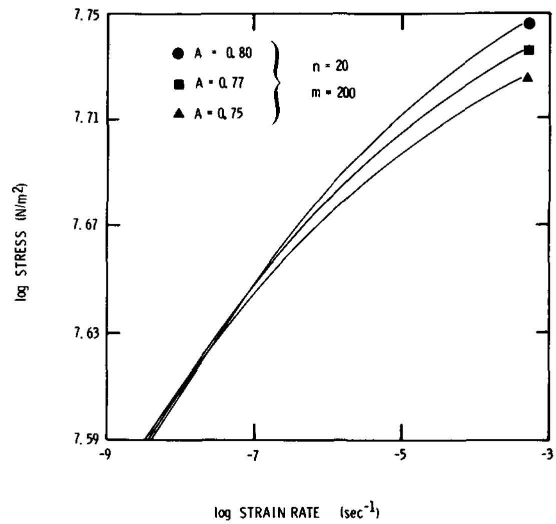

FIG. 7—*Calculated stress relaxation behavior of a sample initially loaded to* 5.60×10^7 N/m^2 (A = *0.80) relaxed, then reloaded to* 5.35×10^7 N/m^2 (A = *0.75) relaxed, then reloaded again to* 5.48×10^7 N/m^2 (A = *0.77*).

based upon these initial values are shown in Fig. 7. These predictions agree with the observations of Hart and Solomon shown in their Fig. 7. However, the physical bases for the behavior differ fundamentally from the explanation offered by them. We suggest that at the larger stresses initially present at short relaxation times, thermally activated dislocation glide controls the behavior; at lower stresses present at long relaxation times, the rates are dominated by microstructural recovery. The observed "transient" behavior is simply a consequence of relaxing from different initial stress levels, combined with the effects of σ_i on the shape of the curve through the parameter A. Initial stress not only affects initial strain rates during relaxation but also influences the transition between regions of glide and recovery-dominated relaxation behavior.

Conclusions

Our observations indicate for stress relaxation and for the limited number of mechanical histories examined that the model proposed by Kocks [*10*] given in Eqs 1 and 2 acts as an evolutionary material law. Stress relaxation can be predicted with good accuracy. Material constants, which by definition must be independent of deformation history, namely, n and m, were found to be so. Examination of the special case of the closed form solution for stress relaxation showed that, as required, the variable A apparently only depends upon stress at the beginning of relaxation for a constant initial strain rate.

The assumption regarding the physical bases of the model was tested. The model assumes that microstructural recovery was an important feature of the relaxation event, becoming the dominant mechanism controlling low strain rate relaxation kinetics. These kinetics should be related to steady-state creep in that the power law exponent n for long time stress relaxation should be nearly equal to the stress exponent n' for steady-state creep. Creep and relaxation experiments at 308 K showed this to be the case, also implying that the recovery mechanisms operating in steady-state creep and relaxation are the same.

In addition to meeting these requirements for internal consistency, the model was also shown capable of predicting the "transient" response observed during relaxation beginning from elastic loading subsequent to previous relaxation [*11*]. In our rationale, this behavior arises because two mechanisms, dislocation glide and microstructural recovery, determine relaxation behavior. Their relative contributions to the strain rate and hence, the shape of the relaxation curve, is dependent upon the initial stress.

Although the proposed model has been shown to be very successful in describing stress relaxation data, it can not yet be considered to have general applicability as an evolutionary material law. The most obvious potential shortcoming lies in the fact that, as proposed by Kocks and utilized here, the model only describes isotropic hardening, that is, the yield surface expands isotropically in stress space. Kinematic hardening behavior, of which the Bauschinger effect is a one-dimensional manifestation, is beyond its scope. Inclusion of a back stress, as we have proposed elsewhere [*14*], will allow the model to describe kinematic as well as isotropic hardening behavior. We feel that eventually both hardening phenomena must be incorporated. Nevertheless, kinematic hardening effects were not discussed in this work, since the experiments were not designed to evaluate the kinematic nature of the material response. The additional complication arising from inclusion of a back stress was unwarranted. Multiaxial and reversed stress experiments must be performed before the present model can be proposed as a useful descriptive-predictive material law. The success of the model in describing monotonic creep and relaxation behavior provides motivation for attempting to extend the description to multiaxial and nonsteady loading conditions.

Acknowledgment

This work was supported by the United States Department of Energy.

References

[*1*] Lagneborg, R., *Metal Science Journal*, Vol. 6, 1972, pp. 127–133.

[2] Kocks, U. F. in *Workshop on Applied Thermovisco Plasticity*, S. Nemat-Nasser, Ed., Technological Institute, Northwestern University, Evanston, Ill., 1975, pp. 244-266.
[3] Swearengen, J. C. and Rohde, R. W., *Metallurgical Transactions*, Vol. 8A, April 1977, pp. 577-582.
[4] Alden, T. S., *Metallurgical Transactions*, Vol. 8A, Nov. 1977, pp. 1675-1679.
[5] *Constitutive Equations in Plasticity*, A. S. Argon, Ed., Massachusetts Institute of Technology Press, Cambridge, Mass., 1975.
[6] Rice, J. R. in *Constitutive Equations in Plasticity*, A. S. Argon, Ed., Massachusetts Institute of Technology Press, Cambridge, Mass., 1975, Chapter 2, pp. 23-80.
[7] Hart, E. W., *Journal of Engineering Materials and Technology, Transactions*, American Society of Mechanical Engineers, July 1976, pp. 193-202.
[8] Hart, E. W., *Acta Metallurgica*, Vol. 18, June 1970, pp. 599-610.
[9] Swearengen, J. C., Rohde, R. W., and Hicks, D. L., *Acta Metallurgica*, Vol. 24, 1976, pp. 969-975.
[10] Kocks, U. F., *Journal of Engineering Materials and Technology, Transactions*, American Society of Mechanical Engineers, Jan. 1976, pp. 77-85.
[11] Hart, E. W. and Solomon, H. D., *Acta Metallurgica*, Vol. 21, March 1973, pp. 295-306.
[12] Rohde, R. W. and Swearengen, J. C., "Mechanical Equation of State Analysis of Elevated Temperature Cyclic Deformation of Austenitic Stainless Steels," in *Transactions of the 4th International Conference on Structural Mechanics in Reactor Technology*, T. A. Jaeger and B. A. Boley, Eds., International Association for Structural Mechanics in Reactor Technology, Aug. 1977, Chapter L 8/5.
[13] Bradley, W. L., Nam, S. W., and Matlock, D. K., *Metallurgical Transactions*, Vol. 8A, March 1976, pp. 425-430.
[14] Swearengen, J. C. and Rohde, R. W., *Journal of Engineering Materials and Technology, Transactions*, American Society of Mechanical Engineers. Vol. 100, April 1978, pp. 221-222.

DISCUSSION

A. Y. C. Lou[1] *(written discussion)*—Since your deformation modeling is to predict long-time response of metal, what is the significance of relating relaxed stress and "strain rate." How do you define strain rate in a stress relaxation test while you keep the strain constant for a long period of time.

R. W. Rohde (authors' closure)—The goal of our deformation modeling is to write inelastic constitutive formulations in terms of variables which describe mechanical behavior as a function of the current microstructural state of an alloy. Toward this end, variables such as strain and time are operationally ill defined. They do not *a priori* reflect current microstructural state. Strain must be traced through material history from some (possibly unknown) reference state, and time must function only in its role as a method of ordering events. Thus, inclusion of strain or time directly as state variables requires knowledge of the entire deformation/time history of a material in order to allow computation of subsequent response. In the current model, time response can simply be determined by integrating the equations which contain the strain rate term.

[1] Central Research Laboratories, The Firestone Tire and Rubber Co., Akron, Ohio, 44317.

It is true for stress relaxation experiments in an infinitely stiff machine—such as utilized for the experiments reported in this paper—that the total strain remains constant. It must be remembered, however, that this total strain ϵ_T is composed of elastic ϵ_e and inelastic ϵ_P components ($\epsilon_T = \epsilon_e + \epsilon_P$). During a relaxation event $\dot{\epsilon}_T = 0$ so inelastic strain accumulates at the expense of elastic strain, allowing simple computation of the strain rate from measurement of the stress-time relaxation curve ($\dot{\epsilon}_P = -\dot{\epsilon}_e = E\dot{\sigma}$).

P. Parikh[1] *and E. Shapiro*[1]

A Phenomenology of Room-Temperature Stress Relaxation in Cold-Rolled Copper Alloys

REFERENCE: Parikh, P. and Shapiro, E., "**A Phenomenology of Room-Temperature Stress Relaxation in Cold-Rolled Copper Alloys,**" *Stress Relaxation Testing, ASTM STP 676,* Alfred Fox, Ed., American Society for Testing and Materials, 1979, pp. 36–41.

ABSTRACT: Room-temperature tension stress relaxation tests on two copper alloys—CDA 510 and CDA 638—were conducted to determine if structural changes accompany stress relaxation. Changes in relaxation rate and in the shape of the tensile stress-strain curves as a result of stress relaxation were analyzed. The results indicate that structural changes during stress relaxation are brought about by a dislocation rearrangement process akin to recovery. Mobile dislocation density was found to change during testing, and work hardening did not contribute in decreasing the relaxation rate.

KEY WORDS: stress relaxation, mechanical properties, copper alloys, dislocations, recovery, thermal activation

Stress relaxation results [*1-4*][2] are often interpreted in terms of thermally activated deformation (TAD) models. TAD models assume that the density of mobile dislocations that surmount short-range obstacles remains constant during stress relaxation and that the short- and long-range obstacle structures remain unchanged. We undertook this study to determine whether these assumptions are valid for stress relaxation in copper alloys. Changes in structure were assessed by repeated stress relaxation testing on the same specimen and by comparing the shape of the elastic-plastic yield transition in tension before and after relaxation tests. In addition, low-temperature recovery annealing treatments and recovery anneal-deformation tests were employed to evaluate the effect of purposeful changes in structure on subsequent relaxation behavior.

[1] Engineering specialist and supervisor, respectively, Mechanical Metallurgy Group, Olin Metals Research Laboratories, New Haven, Conn. 06511.

[2] The italic numbers in brackets refer to the list of references appended to this paper.

Experimental Procedure and Materials

Room-temperature tension stress relaxation tests were conducted either in an Instron machine for 5 to 15 min or in a manually controlled, incrementally unloading type of fixture for longer times. For repeated relaxation tests, specimens were unloaded and then reloaded without removing them from the test rig. All tests were conducted at stress levels below the 0.2 percent offset yield strength. Tension tests were conducted on an Instron machine at a constant cross-head speed of 2.5×10^{-3} m/min.

Alloys used in this study are listed in Table 1 with their nominal compositions in weight percentages. CDA 510 is a phosphor bronze; average grain

TABLE 1—*Nominal compositions.*

Alloy	Weight Percentages
CDA 638	2.8% Al, 1.8% Si, 0.4% Co, balance Cu
CDA 510	5% Sn, 0.2% P, balance Cu

size is 0.015 to 0.020 mm. CDA 638 is a fine-grained silicon-aluminum bronze containing a dispersion of cobalt silicide, which acts as a grain refiner [5]; average grain size is less than 0.005 mm. Both alloys are commercial alloys obtained either in the fully recrystallized condition or in the cold-rolled condition. Necessary additional processing was done in our laboratories. Nominal thickness of test specimens was about 1 mm. Results reported here are from single tests. However, additional tests were conducted on many different conditions to confirm the behavior reported next.

Experimental Results

Effect of Retesting on Stress Relaxation

CDA 510 cold rolled 60 percent was tested for stress relaxation for 2850 h, unloaded, and then reloaded for testing at the same initial stress. Table 2 summarizes the data and shows that the stress relaxation rate decreases on retesting. Yield strength increases only slightly.

TABLE 2—*Stress relaxation of CDA 510 on retesting.*

				First Run	Second Run
Test Temperature, °C	0.2% Yield Strength, MPa	Initial Stress, MPa	Duration of First Run, h	Stress Relaxation, MPa/h	Stress Relaxation, MPa/h
22	710	641	2850	15.2/24	4.1/24

Effect of Stress Relaxation on the Flow Curve Shape

CDA 510 cold rolled 60 percent was tested for stress relaxation for 9500 h at the initial stress of 620 MPa. Figure 1 compares the stress-strain curves before and after stress relaxation. The curve after stress relaxation shows increased stiffness in the preyield region, that is, below the 0.2 percent offset yield strength.

Effect of Recovery Anneal on Stress Relaxation and Flow Curve Shape

Figure 2 compares stress relaxation in 24 h versus initial stress for CDA 638 50 percent cold rolled and 50 percent cold rolled and recovery annealed conditions. The recovery annealed material shows significantly less stress relaxation. Tensile flow curves for both conditions are shown in Fig. 3. There is a significant stiffening of the stress-plastic strain curve in the preyield region, and the yield strength increases slightly.

The effect of cycles of recovery annealing and deformation on stress relaxation were studied in tension at 620 MPa:

1. 30 percent cold rolled + recovery annealed at 310°C/h
2. 30 percent cold rolled + recovery annealed at 310°C/h + 10 percent cold rolled
3. 30 percent cold rolled + recovery annealed at 310°C/h + 10 percent cold rolled + annealed at 310°C/h

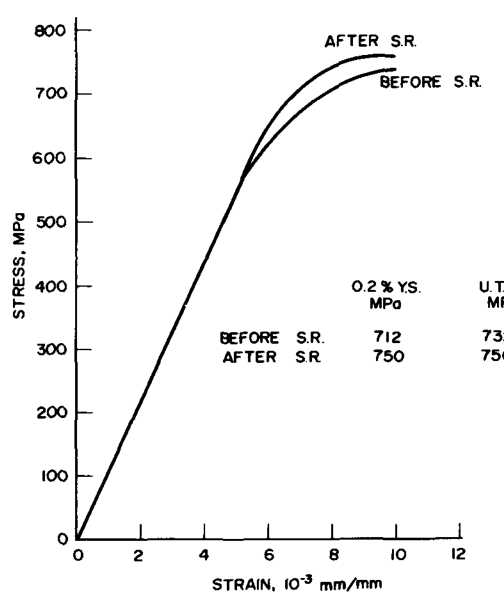

FIG. 1—*Stress-strain curves of CDA 510 before and after stress relaxation.*

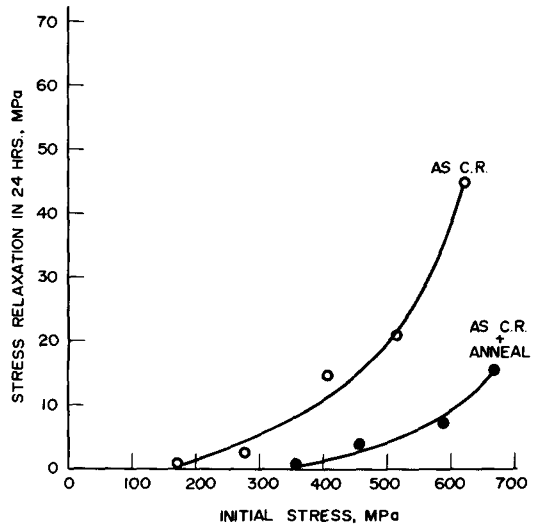

FIG. 2—*Stress relaxation in 24 h versus initial stress for CDA 638.*

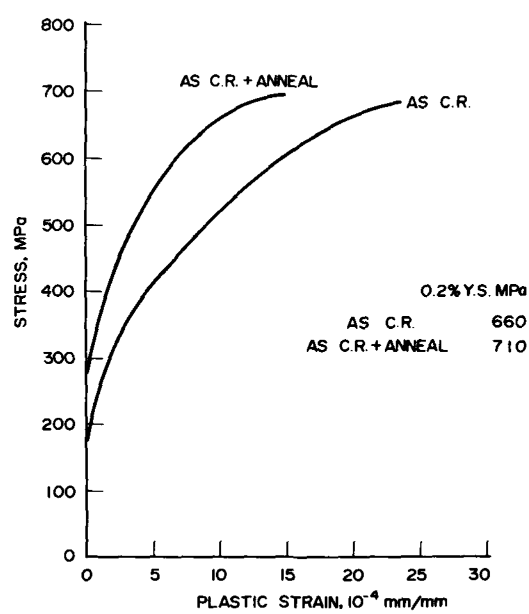

FIG. 3—*Stress-plastic strain curves of CDA 638 as-cold-rolled and after annealing.*

Table 3 lists the tensile properties and summarizes the stress relaxation data. The deformation of recovery annealed material increases the amount of stress relaxation. Reannealing the deformed material restores the lower value comparable to that of the initial recovery annealed state.

Discussion and Conclusions

The results support the view that structure changes during stress relaxation. These changes apparently lead to greater structural stability, as evidenced by stiffening of the stress-strain curves in the preyield region [7].

TABLE 3—*Effect of deformation on recovery anneal alloy 638.*

Condition	0.2% Yield Strength, MPa	Ultimate Tensile Strength, MPa	Stress Relaxation, MPa/min
As annealed	689.50	779.14	8.79/5
As annealed + 10% Cr	703.29	758.45	16.89/5
As annealed + 10% Cr + annealed	717.08	806.72	8.96/5

In addition, the structural changes lead to reduced dislocation mobility, as evidenced by the lower relaxation rate observed in the retesting experiments. Since low-temperature thermal treatments also result in similar flow curve stiffening and reduced relaxation rate, this suggests that the structural changes are brought about by a dislocation rearrangement process akin to recovery.

Yield strength is not changed by stress relaxation or thermal treatment. This implies that the average dislocation density is not decreased, but its distribution is changed [6, 7]. Work hardening cannot be responsible for the reduced stress relaxation rate [8], since deformation after the recovery anneal increases relaxation.

Structural changes during stress relaxation postulated here fall under the broad category of dislocation rearrangement. The specific structural change during stress relaxation will depend on alloy characteristics and homologous test temperature. For example, Alden observed softening during stress relaxation of pure aluminum [9].

References

[1] Guiu, F. and Pratt, P. L., *Physica Status Solidi*, Vol. 6, No. 11, 1964, p. 111.
[2] Li, J. C. M., *Canadian Journal of Physics*, Vol. 45, 1967, p. 493.
[3] Feltham, P., *Journal of Institute of Metals*, Vol. 89, 1961, p. 210.
[4] Gupta, I. and Li, J. C. M., *Metallurgical Transactions*, Vol. 1, 1970, p. 2323.

[5] Butt, S. H. and Crane, J., Technical Report No. P 9-5.1, American Society for Metals, 1969.
[6] Alden, T., *The Philosophical Magazine*, Vol. 25, 1972, p. 785.
[7] Parikh, P. and Shapiro, E., *Metallurgical Transactions*, Vol. 4, 1973, p. 2664.
[8] White, M. G. and Smith, I. O., *Scripta Metallurgica*, Vol. 8, 1974, p. 1153.
[9] Alden, T., *Metallurgical Transactions*, Vol. 8A, 1977, p. 1675.

R. J. Glodowski and G. E. Hoff[1]

Stress Relaxation of Steel Tendons Used in Prestressed Concrete Under Conditions of Changing Applied Stress

---

REFERENCE: Glodowski, R. J. and Hoff, G. E., "**Stress Relaxation of Steel Tendons Used in Prestressed Concrete Under Conditions of Changing Applied Stress,**" *Stress Relaxation Testing, ASTM STP 676.* Alfred Fox, Ed., American Society for Testing and Materials, 1979, pp. 42–58.

ABSTRACT: Several methods have been proposed for predicting the total prestress loss in prestressed concrete structures. Inherent in all of these methods is the concept that the applied elastic strain on the steel tendons changes with time due to creep and shrinkage of concrete. A procedure most often used to determine the steel tendon's stress relaxation contribution to total prestress loss is a time iteration technique. The stress relaxation that occurs in each time interval is predicted from an equation describing stress relaxation as a function of time and initial stress level. This equation is normally derived from data obtained from constant-strain tests as per ASTM E328. During the time iteration program, however, the initial stress level is different for each time interval because of changing elastic strains in the steel tendons due to concrete creep and shrinkage. In some procedures under consideration by the prestressed concrete industry, the actual stress on the tendon at the start of each time interval is assumed to be the correct value for initial stress. Total relaxation is then determined by a summation of the relaxation during each time interval.

The object of the present research is to investigate the effects of variable applied elastic strain on stress relaxation results during a continuous test and to evaluate procedures for assessing these effects. To accomplish this, stress relaxation tests were carried out on 6.35-mm (0.250-in.) diameter prestressing wire. Results of variable elastic strain application during the test were compared with constant-strain stress relaxation data. Based on these results, a new procedure is proposed for predicting the effects of variable elastic strain on the stress relaxation–time relationship. This new procedure incorporates the effect of stress relaxation in prior time intervals on predicted stress relaxation in a given interval. This is accomplished analytically by defining an "effective initial stress" and an "effective time" to be used in the mathematical expression for stress relaxation during each time interval. This new procedure is shown to be more accurate in predicting actual stress relaxation results under conditions of changing applied elastic strain.

[1] Senior research metallurgist and research metallurgist, respectively, Armco, Inc., Middletown, Ohio 45013.

KEY WORDS: stress relaxation, prestressed concrete, steel prestressing tendons (wire), prediction methods, effective time, effective initial stress, variable applied stress (elastic strain)

The prestressed concrete industry has shown considerable interest in the prediction of prestress losses during the lifetime of a structure due to stress relaxation in the steel tendons. The Prestressed Concrete Institute (PCI) recently published [*1*][2] a report by their Committee on Prestress Losses. That report summarized data on creep and shrinkage of concrete and stress relaxation of steel tendons. In addition, design procedures for using these data in estimating loss of prestress after any given time period were presented. It was noted in the committee statement preceding the report that the procedures utilized were not the only satisfactory solution to the complicated problem and were a compromise of diverse opinions. This investigation was initiated to explore one particular area of that design procedure that was not fully agreed upon—specifically, the procedure by which the stress relaxation with time of the steel tendon is predicted under conditions of changing applied stress.

Background

Time-dependent prestress losses are due to steel stress relaxation and creep and shrinkage of concrete. Steel stress relaxation data are normally obtained from tests such as that described in the ASTM Standard for Stress Relaxation Tests (A 328-75) which do not allow significant strain changes during the test. Concrete creep and shrinkage data, on the other hand, are obtained as strain changes with time at essentially constant stress levels. The ASTM Test for Creep of Concrete in Compression (C 512-76) describes the standard procedure for concrete testing. Shrinkage is defined as the strain occurring at zero stress, and creep is the stress-induced time-dependent strain. Thus, the basis of the steel relaxation test—constant strain as stress changes with time—is inconsistent with the test basis used in concrete creep evaluation—constant stress as strain changes with time.

Once the steel tendons are stressed and anchored in the concrete, if a strain change occurs in the concrete, an equivalent strain change must occur in the steel. Also, since a force equilibrium must exist, a load (stress) change in the steel must be balanced by a load (stress) change in the concrete. Since steel stress relaxation is affected by elastic strain (that is, stress) changes and concrete creep is affected by stress (that is, elastic strain) changes, the prediction of both are interdependent.

To account for these changes in stress and strain with time, a step-by-step

[2] The italic numbers in brackets refer to the list of references appended to this paper.

or iteration procedure [2,3] is most often used and is recommended by the Prestressed Concrete Institute (PCI) [1]. Using this approach, the expected service life is divided into small time intervals during which the steel stress relaxation and concrete creep and shrinkage strains are assumed to be independent of each other. In each time interval prestress loss due to stress relaxation and strain changes due to concrete creep and shrinkage can be calculated from the test data. At the end of each time interval, the necessary conditions of force equilibrium and zero strain differential between the concrete and steel must be maintained. An analytical procedure for maintaining equilibrium has been previously described in the literature [2,3].

Prediction of Stress Relaxation

Although the stress relaxation is normally assumed to occur independently during each time interval, the initial stress changes for each different time interval. The stress relaxation data generated under constant strain conditions are normally expressed as functions of initial stress and time by an empirical relationship. The most widely used equation, and that recommended by PCI, is a linear semilog expression proposed by Magura et al [4]:

$$S = \frac{\log t}{10} (R - 0.55) \tag{1}$$

where

S = decimal fraction of initial stress lost due to stress relaxation,
t = test time in hours, and
R = ratio of initial stress (σ_{t0}) to yield stress of tendon (σ_{ys}).

Examples of this equation for various R values are shown in Fig. 1. This equation is only applicable for R values greater than 0.55.

In this expression, the value of R is dependent on the initial stress on the steel tendon at $t = 0$. For initial stresses in the elastic range, this also locks the equation to a constant-strain condition. Then, any elastic strain changes of the steel tendon necessary to maintain equilibrium balance in the structure change the initial stress level. The problem to which this investigation is addressed is to establish a procedure for estimating prestress losses during any time interval from Eq 1 or any other equation when the initial test conditions of constant strain (that is, constant initial stress) no longer apply.

PCI Procedure

The PCI procedure [1] for using Eq 1 during any time interval is as follows

$$\Delta S = \frac{(\log t_2 - \log t_1)}{10} \left(\frac{\sigma_{t1}}{\sigma_{ys}} - 0.55 \right) \tag{2}$$

where

ΔS = decimal fraction of initial stress lost due to stress relaxation during time interval t_1 to t_2,
σ_{t1} = steel stress at $t = t_1$, and
σ_{ys} = yield stress of steel tendon.

In Eq 1, R was defined as the ratio of the initial stress (σ_{t0}), the stress at $t = 0$, to the yield strength (σ_{ys}). For Eq 2, the σ_{t0} value is replaced by the steel stress at the beginning of the time interval σ_{ti}. The problem is that Eq 1 was empirically derived from data where the R ratio was constant at any time t_i. The actual stress on the tendon during the constant strain test on which the equation is based does not stay constant, but decreases with time due to stress relaxation. Assuming that the initial stress (σ_{t0}) is equivalent to the actual stress at any time (σ_{ti}) will then lead to errors in the prediction of the stress relaxation increment.

Effective Initial Stress

These errors can be corrected by defining an "effective initial stress" (σ_{ef}) as the algebraic sum of the initial applied stress (σ_{t0}) and any later changes due to factors other than stress relaxation. These factors include

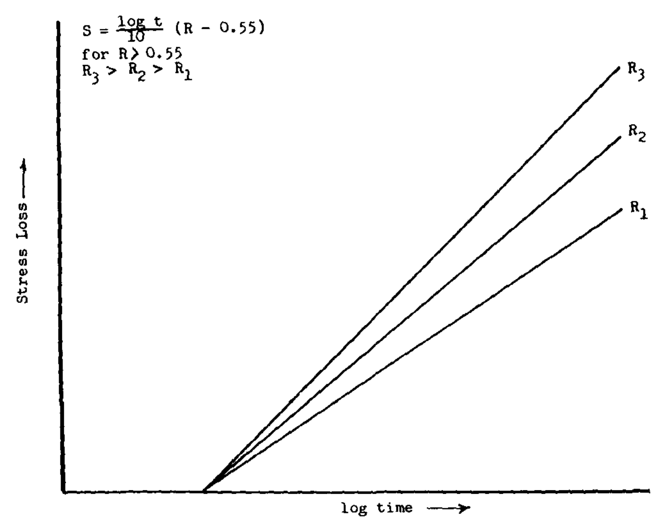

FIG. 1—*Schematic representation of the Magura et al.* [4] *equation for stress relaxation (Eq 1).*

any elastic strain changes in the steel necessary to maintain equilibrium in the structure. This is shown as follows: First, the total stress on the steel tendon at any time t_i (σ_{t_i}) is defined as the initial stress (σ_{t_0}) minus the stress loss due to stress relaxation at t_i (σ_{St_i}) and stress changes due to elastic strain changes ($E\ \Delta\epsilon$).

$$\sigma_{t_i} \equiv \sigma_{t_0} - \sigma_{St_i} + E\ \Delta\epsilon \tag{3}$$

where

σ_{t_i} = actual steel stress at $t = t_i$,
σ_{t_0} = initial steel stress at t_0,
σ_{St_i} = steel stress loss due to stress relaxation at time t_i,
E = elastic modulus of steel tendon, and
$\Delta\epsilon$ = strain change in steel after t_0 (+ for tension, − for compression).

By definition,

$$\sigma_{\text{ef}} \equiv \sigma_{t_0} + E\ \Delta\epsilon \tag{4}$$

Alternately, combining Eqs 3 and 4,

$$\sigma_{\text{ef}} \equiv \sigma_{t_i} + \sigma_{St_i} \tag{5}$$

Constant Time Curve Transfer Procedure

If σ_{ef} is substituted for σ_{t_0} in Eq 1, the stress relaxation versus time curve shown in Fig. 1 can be defined during any time interval. The next question is where on that curve does one start that time interval. Modifying Eq 2 by replacing σ_{t_1} with σ_{ef} results in the following equation:

$$S = \frac{\log t_2 - \log t_1}{10} \left(\frac{\sigma_{\text{ef}}}{\sigma_{\text{ys}}} - 0.55 \right) \tag{6}$$

This equation predicts that the stress relaxation from t_1 to t_2 is independent of stress relaxation that occurred prior to t_1.

To illustrate this, Fig. 2 shows an example of this constant time curve transfer procedure where two steel tendons are initially loaded to different initial stress levels R_2 and R_3. At time t_1, the effective initial stresses were reduced to the same effective initial stress level σ_{ef}. Equation 6 would predict that both tendons would relax at the same rate beyond t_1 and would follow the predicted curve R_1 for that σ_{ef}. The predicted stress relaxation beyond t_1 on curve R_1 is independent of the path to that point; that is, R_2 or R_3. This is the premise that the authors investigated using actual steel wire tendons in a controlled stress relaxation test situation.

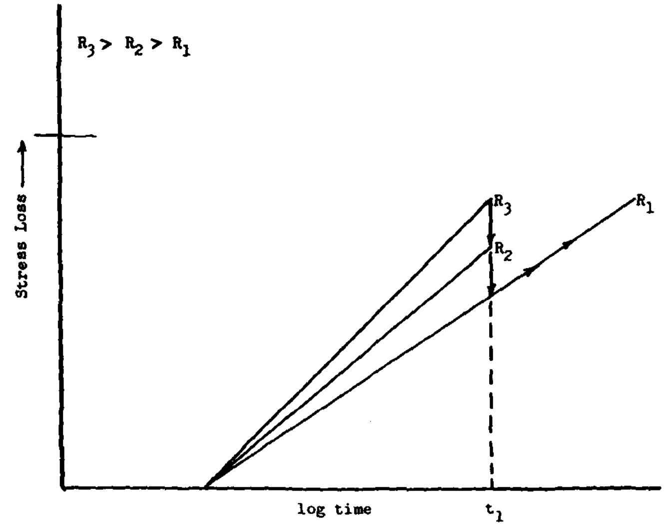

FIG. 2—*Schematic representation of the procedure for constant time curve transfer using Eq 6.* $R_3 > R_2 > R_1$.

Experimental Procedure

Test Material

The steel wire tendons used for this investigation were a nominal 0.80C-0.80Mn composition. Processing included cold drawing of controlled cooled rod (Stelmor process) to 6.35-mm (0.250-in.) diameter wire (total draft of 67 percent) followed by stress relieving at about 370°C (700°F). Final wire properties met all ASTM Specifications for Uncoated Stress Relieved Wire for Prestressed Concrete (A 421-76).

All samples used in the stress relaxation tests were obtained from the same coil to minimize sample variations. Duplicate tensile specimens were taken from opposite ends of each stress relaxation specimen. Average tensile properties for the eleven stress relaxation test specimens were 1540 MPa (223 ksi) yield strength and 1700 MPa (246 ksi) tensile strength. Maximum variation among all specimens for yield and tensile strength was 1.7 and 2.3 percent, respectively. All specimens were stored in a temperature-controlled room at 20°C (68°F) prior to testing to minimize any static aging effects on the stress relaxation results.

Testing Procedure

Stress relaxation testing was carried out on two Denison Model T55R stress relaxation testing machines illustrated in Fig. 3. Each has the

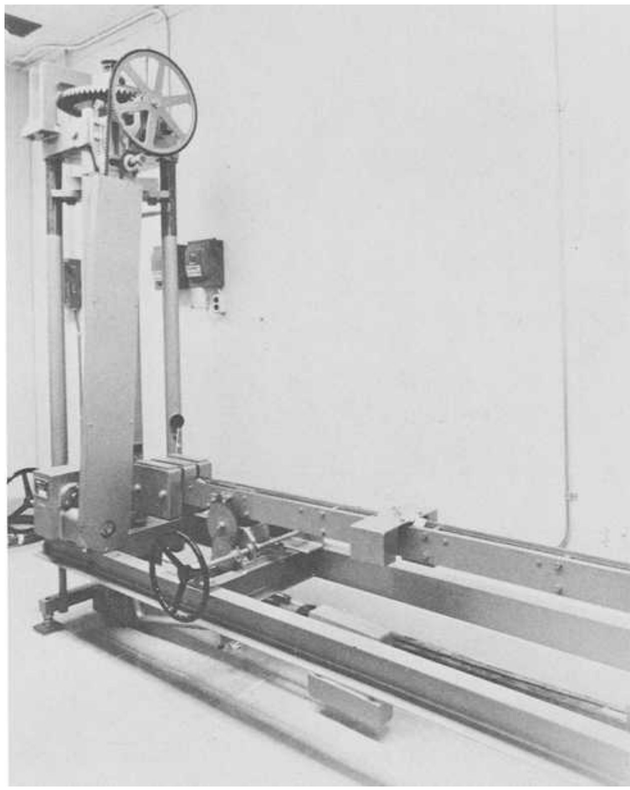

FIG. 3—*Overall view of Denison stress relaxation machine.*

capability of applying 160 kN (36000 lb) to a 1350-mm (54-in.) long specimen using a leverage loading system. The load is applied manually by a mechanical screw system that transmits the strain to the specimen until the lever system is balanced. The lever arm has a vernier scale that is divided into 9-N (2-lb) increments so that load loss can be measured each time the poise weight moves.

Immediately after the proper lever balance is achieved, a 1000-mm (40-in.) extensometer is attached to the specimen as shown in Fig. 4. The extensometer includes a microswitch, which is tripped when the specimen elongates approximately 0.0063 mm (0.00025 in.), which is equivalent to 6.3 microstrain. The tripped microswitch activates a motor that moves the poise weight on the lever arm, reducing the load until the specimen elastically contracts the same amount of strain. Thus, while the strain is not constant, as defined for pure stress relaxation, it is restricted within a small range as allowed by ASTM E 328-75 to approximate a continuously relaxing condition.

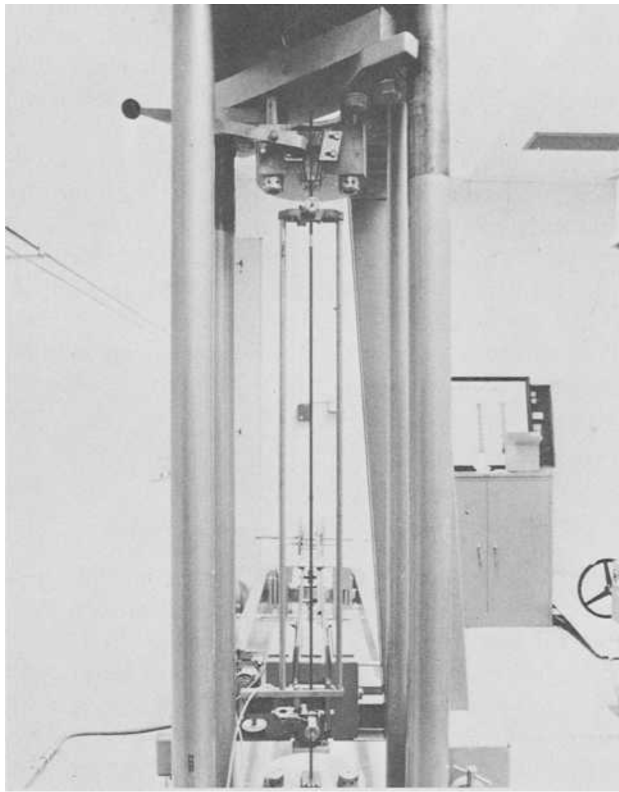

FIG. 4—*View of Sample* (center) *with 1000-mm (40-in.) extensometer attached.*

The two stress relaxation machines are in a controlled-environment room that is maintained at a constant temperature of 20°C (68°F). All of the test data reported and the discussion resulting from that data are based on the assumption of a constant ambient temperature of 20°C (68°F).

The time at which an individual load reduction occurs is automatically indicated on an event recorder connected to both machines. Associated new loads are then read directly from the balance beam. The stress relaxation data for an individual specimen can then be plotted from the total test time and cumulative load loss.

To investigate the effects of elastic strain changes during a stress relaxation test, individual wires were loaded initially to either 79.5 or 83 percent of their actual yield strength. The wires were tested at constant strain for times of 1, 6, 24, or 72 h and then manually unloaded so that the effective stress, the sum of the actual stress and the stress lost due to stress relaxation, was 77 percent of the actual yield strength of that test wire. The resulting stress relaxation was compared to the "base" curve, which was obtained by a constant-strain stress relaxation test initially loaded to 77 percent of the actual yield strength. This base curve test was run beyond 900 h.

The effects of multiple strain changes were assessed by loading duplicate specimens to 83 percent of the actual yield strength for 6 h. The loads were then manually reduced to an equivalent initial stress of 79.5 percent of the actual yield strength. These tests were then continued for 48 h, whereupon the load was further reduced to the effective initial stress level of 77 percent of the actual yield strength. The resulting stress relaxation data were then compared to the base curve run at an initial stress of 77 percent of the actual yield strength.

Results and Discussion

Results Using Constant Time Curve Transfer Procedure

Figure 5 shows the results of the two tests run at 79.5 percent and 83 percent of actual yield strength for 72 h. The relaxation data are shown after changing the load to an effective initial stress level of 77 percent of the actual yield strength. These relaxation data are compared to the base curve, which was run at an initial stress level of 77 percent of the actual yield strength without any applied load changes. The constant time curve transfer procedure to the base curve is done on a constant time basis (that

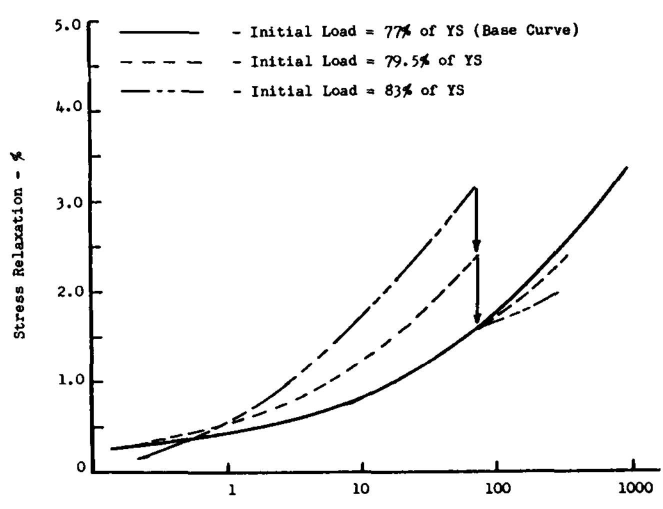

FIG. 5—*Seventy-two-hour results of constant time curve transfer procedure.*

is, $t_1 = 72$ h). This is necessary to comply with Eq 6. As discussed earlier, this procedure implies that both tests should follow the base curve after t_1. As can be seen in Fig. 5, the 79.5 percent initial stress test falls slightly below the base curve, and the 83 percent initial stress test falls substantially further below the base curve.

It is apparent in Fig. 5 and in subsequent figures that the base stress relaxation curve, as well as the other higher-stress level relaxation curves, do not follow a linear semilog relationship as would be expected from Eq 1. Previous experience with a large number of unpublished stress relaxation tests on prestressing wire has indicated that the linear semilog description is not accurate for times up to 1000 h. Equation 1 was originally derived from a large number of test results, of which only the stress at a completion of the test—sometimes as much as 10 000 to 20 000 h—was known [*4*]. The semilog expression worked quite well for that case where little or no data were available in the shorter time region. Subsequent results indicate that a quadratic equation of the form

$$\%S = A + B(\log t) + C(\log t)^2 \tag{7}$$

will describe the actual data very well in the short time region and will extrapolate to values consistent with Eq 1 for long-time stress relaxation losses. The constants A, B, and C can be described as functions of the stress level ratio resulting in a standard expression for stress relaxation as a function of time and initial stress. It is not the purpose of this discussion to evaluate the form of the stress relaxation equation. In fact, the form of the equation is of no consequence to the conclusions expressed as a result of this investigation.

Figures 6, 7, and 8 show similar test results for the 24-h, 6-h, and 1-h stress change tests. In all cases, the results are the same as shown in Fig. 5 in that the actual stress relaxation is less than would be predicted by a constant time transfer to the base 77 percent stress level curve. Also, the relaxation occurring after t_1, the time at which the load is changed, is dependent on the prior stress level. The higher initial stress level before t_1 causes more stress relaxation to occur. The higher initial stress level tests had consistently lower relaxation rates (slope of the stress relaxation-time curve) after the load change to the same *effective* initial stress level at t_1.

The results of the tests as shown in Figs. 5 through 8 have demonstrated that Eq 6 will not accurately describe the effect of changing elastic strain (that is, stress or load) on subsequent stress relaxation during any time interval. This result was anticipated from a previous discussion [5] about the mechanical equation of state that assumes, as does Eq 6, a unique functional relationship between stress, strain (or effective initial stress), strain rate (relaxation), and temperature (constant). This concept was not expected to hold for situations where metallurgical structure (that is,

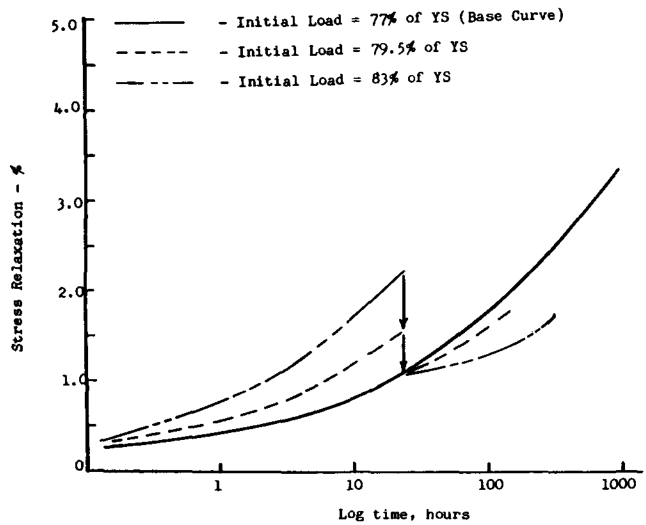

FIG. 6—*Twenty-four-hour results of constant time curve transfer procedure.*

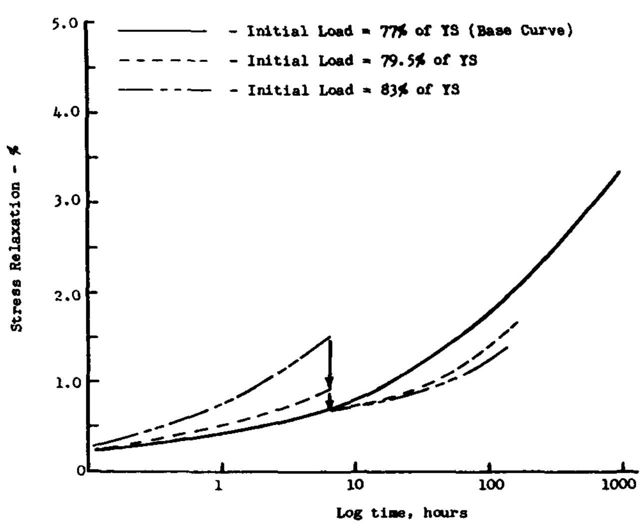

FIG. 7—*Six-hour results of constant time curve transfer procedure.*

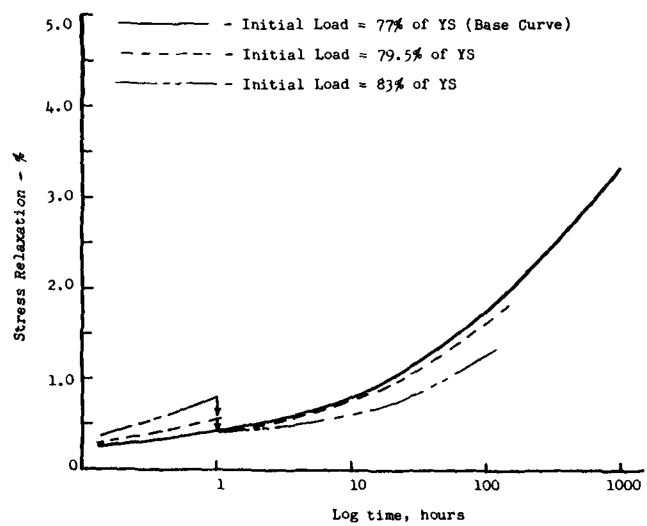

FIG. 8—*One-hour results of constant time curve transfer procedure.*

dislocation substructure) changes are expected to occur and to affect these relationships.

Constant-Stress Loss Curve Transfer

If one assumes that changes in the dislocation substructure do control relaxation and that no significant recovery occurs at the temperature of interest, then a second solution to the problem of stress relaxation prediction after elastic strain changes is suggested. Under these assumptions, the amount of stress relaxation that has occurred in a steel specimen is directly related to a particular dislocation substructure. The rate of stress relaxation is known to be a function of the applied stress as shown in Figs. 5 through 8. However, if the amount of stress relaxation is known prior to the start of a time interval at t_1, then the rate of stress relaxation after the applied stress adjustment at t_1 can be predicted from the effective initial stress at t_1 and the amount of prior stress relaxation. The amount of prior stress relaxation defines a particular state of dislocation substructure. That particular state of dislocation substructure would exist at the point on the effective initial stress relaxation curve where the total relaxation is equivalent to the prior stress relaxation. This would not be the point on the curve at $t = t_1$, but a point where the stress relaxation level is equivalent to the prior stress relaxation. This is shown schematically in Fig. 9. As shown in this figure, two different initial stress level ratios R_2 and R_3 are each reduced at time t_1 to the same effective initial stress level ratio R_1. Subse-

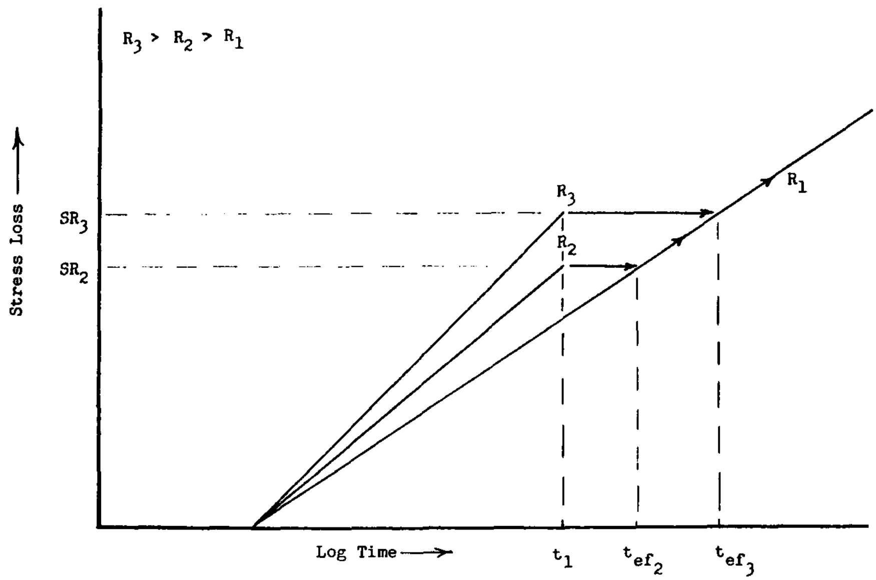

FIG. 9—*Schematic representation of the procedure for constant stress loss curve transfer using Eq 9. At time* t_1, *stress level ratios* R_2 *and* R_3 *are changed to an effective initial stress level ratio* R_1. *Subsequent relaxation is predicted from the initial stress level ratio* R_1 *at equivalent stress loss values* S_2 *and* S_3.

quent relaxation is predicted from the relaxation curve of that effective initial stress level ratio R_1 at an equivalent stress loss value S_2 and S_3, respectively. Because of the nature of this plotting convention, the procedure to be described is called the constant-stress loss curve transfer procedure. The example in Fig. 9 is shown for conditions of decreasing applied stress, because that is the normal situation for steel tendons in prestressed concrete. The concept should also be applicable for situations of increasing applied stress.

The constant-stress loss curve transfer procedure is done as follows:

1. Define the effective initial stress level σ_{ef} at t_1 as described previously.
2. Solve the stress relaxation equation used (for example, Eq 1) for the effective time t at these values of effective initial stress level and amount of prior relaxation.

Note that now the effective time (t_{ef}) is defined as the time at which the amount of stress relaxation prior to t_1 would have occurred during a constant-strain test with an initial stress level equivalent to the effective initial stress level at t_1.

In equation form, the procedure is accomplished as follows, assuming Eq 1 as the stress relaxation equation:

$$\log t_{ef} = \frac{10S}{(\sigma_{ef}/\sigma_{ys}) - 0.55} \tag{8}$$

then

$$\Delta S = \frac{\log(t_{ef} + \Delta t) - \log t_{ef}}{10} \left(\frac{\sigma_{ef}}{\sigma_{ys}} - 0.55\right) \tag{9}$$

where

$$\Delta t = t_2 - t_1 \tag{10}$$

Because the assumption for this procedure is that a particular state of dislocation substructure is the key to defining the subsequent relaxation rate, a slight adjustment in the value of prior-stress relaxation ratio S in Eq 8 is necessary. Dislocation substructure, for the case of stress relaxation, is expected to be a function of the plastic strain. The plastic strain is directly related to the relaxation stress loss by the elastic modulus. Therefore, the S value, which is a ratio of steel stress relaxation stress loss to initial stress, must be adjusted to accommodate the changing effective initial stress level. This is done by redefining the S value using the actual steel stress relaxation stress loss and the effective initial stress level at the time of interest.

Results Using Constant-Stress Loss Curve Transfer Procedure

Using this constant-stress loss curve transfer procedure, all of the relaxation data previously shown in Figs. 5 through 8 have been replotted and are shown in Figs. 10 through 13. As these figures show, the constant-stress loss curve transfer procedure does an acceptable job of predicting the actual data. Remember that the base curve would be the predicted curve, assuming an empirical equation describing actual stress relaxation as a function of initial stress level. The actual data are shown as the dashed lines around the base curve.

To demonstrate the effect of two stress changes prior to t_1, duplicate specimens were tested at an initial stress level of 83 percent of actual yield strength for 6 h, reduced to an effective initial stress of 79.5 percent of actual yield strength and run to 72 h, and then reduced to an effective initial stress of 77 percent of actual yield strength. These results are shown in Fig. 14. Again, the constant-stress loss curve transfer procedure predicts stress relaxation (base curve) very close to the actual data—certainly within the scatter expected from these tests.

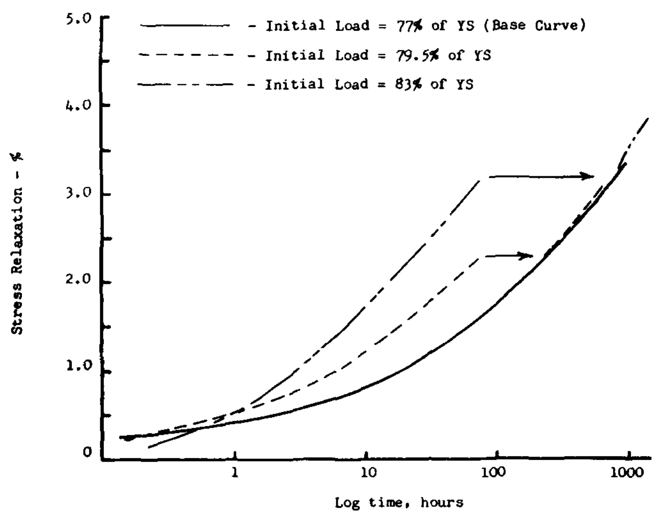

FIG. 10—*Seventy-two-hour results of constant stress loss curve transfer procedure.*

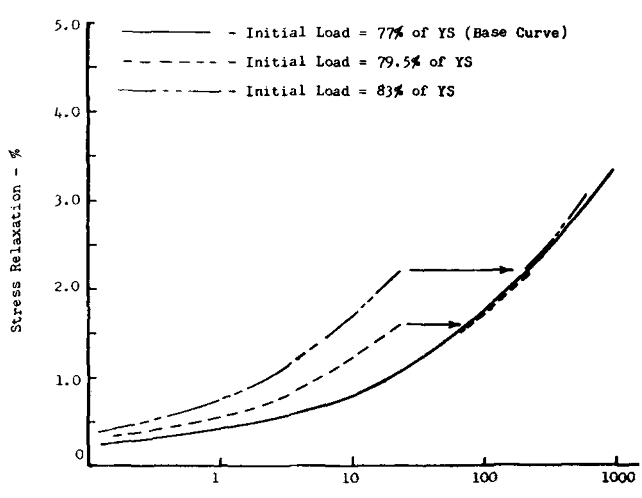

FIG. 11—*Twenty-four-hour results of constant stress loss curve transfer procedure.*

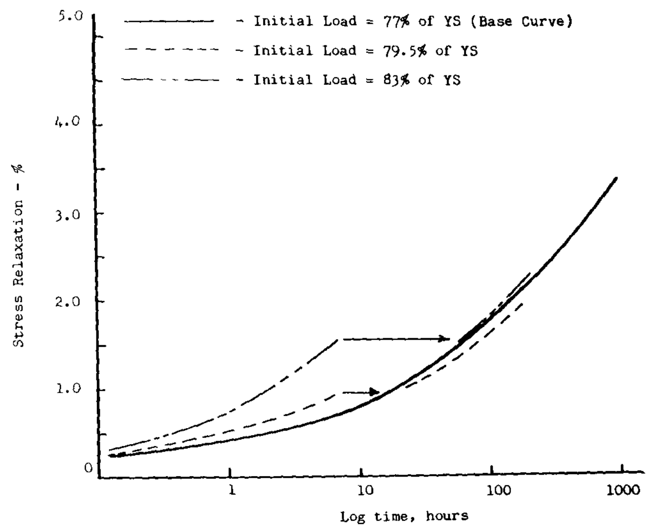

FIG. 12—*Six-hour results of constant stress loss curve transfer procedure.*

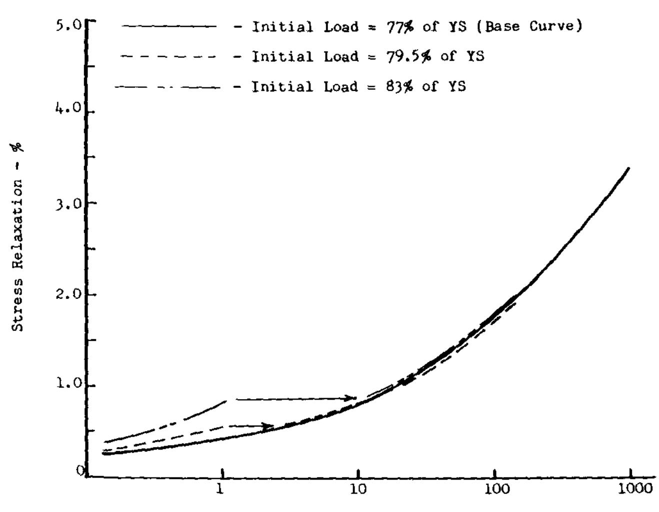

FIG. 13—*One-hour results of constant stress loss curve transfer procedure.*

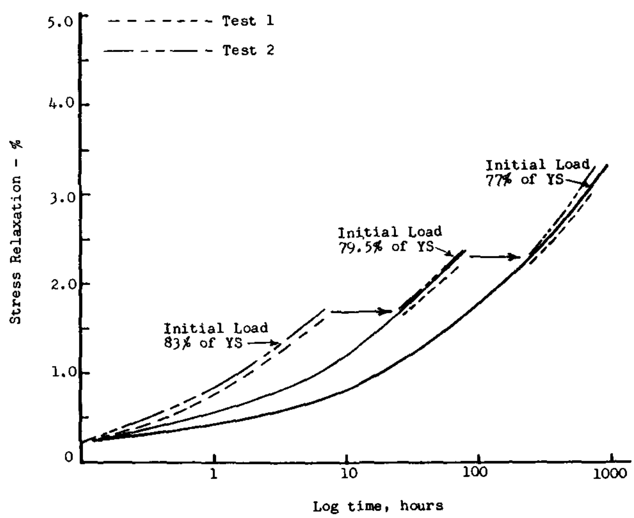

FIG. 14—*Results of constant stress loss curve transfer after multiple stress changes.*

Conclusions

Results from a series of stress relaxation tests at 20°C (68°F) have indicated that stress relaxation of a cold-drawn and stress-relieved 0.80C prestressing wire at stress levels in the elastic range is apparently controlled by the dislocation substructure with very little recovery occurring. A constant-stress loss curve transfer procedure is proposed that incorporates the effect of prior-stress relaxation in previous time intervals on predicted stress relaxation in subsequent time intervals. Using this procedure, the effects of changing applied elastic strain on the stress relaxation rate can be predicted. This is accomplished analytically by defining an "effective initial stress" and an "effective time" to be used in the mathematical expression for stress relaxation during each time interval. This procedure should be applicable to any empirical expression for stress relaxation as a function of time and initial stress level.

References

[1] Preston, H. K., *Journal of the Prestressed Concrete Institute*, July/Aug. 1975, pp. 44-75.

[2] Glodowski, R. J. and Lorenzetti, J. J., *Journal of the Prestressed Concrete Institute*, March/April 1972, pp. 17-32.

[3] Ghali, A. and Dilger, W. H., *American Concrete Institute Journal*, Nov. 1973, pp. 759-763.

[4] Magura, D. D., Sozen, M. A., and Siess, C. P., *Journal of the Prestressed Concrete Institute*, April 1964, pp. 13-57.

[5] McClintock, F. A. and Argon, A. S., *Mechanical Behavior of Materials*, Addison-Wesley, Reading, Mass., p. 194.

Material and Product Application and Test Methods

S. U. V. Idermark[1] *and E. R. Johansson*[1]

Room-Temperature Stress Relaxation of High-Strength Strip and Wire Spring Steels—Procedures and Data

REFERENCE: Idermark, S. U. V. and Johansson, E. R., "**Room-Temperature Stress Relaxation of High-Strength Strip and Wire Spring Steels—Procedures and Data,**" *Stress Relaxation Testing, ASTM STP 676,* Alfred Fox, Ed., American Society for Testing and Materials, 1979, pp. 61-77.

ABSTRACT: Stress relaxation of strip spring steels was investigated with the vibrating string technique. The modified AISI 301 austenitic stainless steel had the lowest relaxation rate up to 170 h followed by a standard AISI 301 stainless steel, a martensitic stainless chromium steel (Type 420), a texture rolled carbon steel (Type 1078), and a hardened and tempered carbon steel (Type 1074). A high elastic limit had a beneficial effect in lowering the stress relaxation rate. The stress relaxation rate for the carbon steels was accelerated after an initial period. The specimens that had an acceleration in stress relaxation also exhibited a simultaneous change in stress-strain behavior as proved by tension testing.

Helical extension wire springs were tested at constant length in a test rig. The modified AISI 301 austenitic stainless steel had the best relaxation properties, followed by a 17-7 precipitation hardenable steel and a standard AISI 302 austenitic stainless steel. An increase in prestress level decreased the stress relaxation as measured at the same testing stress. Springs coiled from wire with the highest values of yield and tensile strength gave the lowest relaxation rate.

KEY WORDS: stress relaxation, springs, strip steels, wire, test equipment, mechanical properties, residual stresses

The behavior of spring steels under load is of great interest to the designer of springs. Few data are available on room-temperature stress relaxation for high-strength spring steels. This paper presents such data for stainless and carbon strip spring steels and for stainless helical extension wire springs. The paper also describes the use of the vibrating string technique for stress relaxation testing of strip spring steels and a method for testing of helical extension wire springs under constant constraint.

[1] Research engineer and manager, respectively, Mechanical Metallurgy, Steel Research Centre, Sandvik AB, Sandviken, Sweden.

Testing Equipment

Strip Spring Steels

The stress relaxation tests were performed in two special rigs. In order to maintain constant constraint on the specimens during testing, the load frame construction must be stiff compared to the specimen. The load frame (approximately 1.75 m in height and 0.5 m in width) consists of four U-bars, with a cross-sectional area of 7 cm^2 each, between two fixed platens. The compression of the testing equipment was less than 0.01 mm when loading with 10 kN, corresponding to a strain variation in the test specimen of less than ± 0.00001 mm/mm. The upper specimen grip is vertically adjustable by a screw.

The two rigs were placed in a temperature chamber, where the temperature was controlled by a thermostat. The fluctuation of temperature during a test was less than $\pm 1°C$ (24 to 26°C), corresponding to a maximum strain variation of ± 0.000005 when testing stainless steels.

The initial stress on the specimen was applied by a pneumatic cylinder attached to the lower grip. The maximum allowable tensile force for the cylinder was 10 kN.

In order to excite and record the frequency of vibration in the strip, a pair of electromagnetic transducers was used. In Fig. 1, a block diagram shows the principle of the measurement method. The distance between two well-defined nodal points achieved by spring-loaded edges on the specimen determined the gage length, which was 1.000 m in this case.

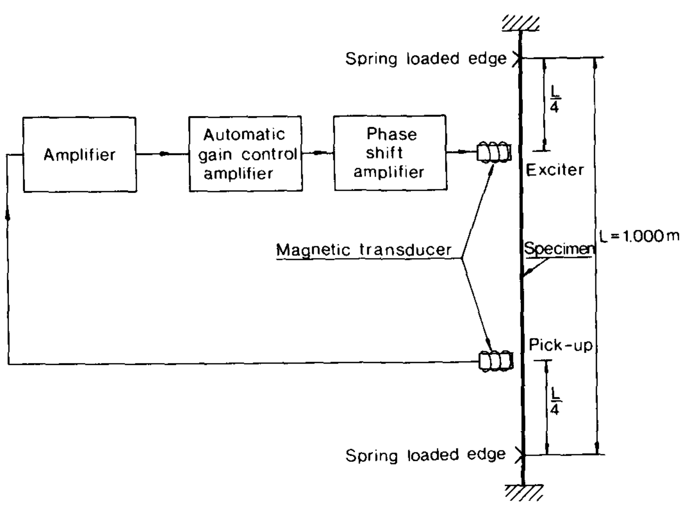

FIG. 1—*Block diagram of the relaxation test setup for strip spring steels.*

Wire Spring Steels

Four test rigs were built (total height approximately 0.6 m) for testing of ten helical extension springs in each test rig (Fig. 2). When testing the springs at the highest stress, the maximum deflection of the test rig was less than 0.015 mm. This corresponds to an error in the measured stress during relaxation of less than 0.01 percent. The temperature fluctuations in the testing room were ±2°C (22 to 26°C), corresponding to an error in the measured stress of less than ±0.005 percent. The test load was measured by strain gages fixed to a ram. This measuring device could be unloaded and attached to any one of the springs. The springs, however, were never unloaded during the relaxation test. Difficulties in keeping constant constraint, when shifting the measuring device from spring to spring, gave an error in the stress reading that was estimated to be a maximum of ±0.5 percent.

Material Tested and Specimen Types

Different strip and wire spring steels have been tested. Chemical com-

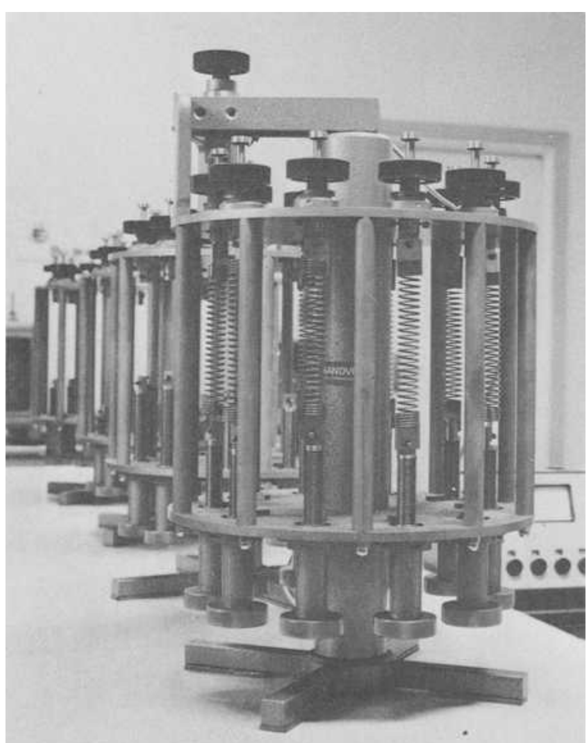

FIG. 2—*Test equipment for helical extension springs.*

positions are given in Table 1, sizes and mechanical properties in Table 2. The variation of width and thickness along the strip specimens (length = 1.2 m) was less than ±0.2 and ±1.0 percent, respectively, for all strips.

Helical extension springs were coiled from 1.0, 1.5, 2.0, and 2.5-mm-diameter wire. The mean diameter D_m of the coils equaled ten times the wire diameter. In order to be able to measure the relaxation in the coils only, the springs were fabricated without any hooks. A pitch of 1 mm plus the wire diameter was selected for all springs, and the number of active coils was chosen to give a spring length of about 150 mm in the extended condition. The variation in wire diameter was less than ±0.1 percent and the variation in coil diameter less than ±1.0 percent. After coiling, the springs were tempered as shown in Table 2.

Testing Procedure

Strip Spring Steels

The technique used is based upon the fact that the frequency of a vibrating string fixed at both ends is a function of the tension in the string.[2]

$$f_n = \frac{n}{2l}\left(\frac{\sigma}{\rho}\right)^{1/2} \qquad (1)$$

where

f_n = frequency of harmonic number n in hertz,
l = gage length in metres,
n = number of the harmonic (second harmonic is used),
σ = tensile stress in the string in newtons per square metre, and
ρ = density in kilograms per cubic metre.

The accuracy in frequency reading was within 0.1 Hz, the variation in gage length and density were negligible. Logarithmic differentiation of the formula above gives a maximum error of ±0.3 N/mm^2.

The relaxation test consisted in loading the specimen to an extension corresponding to a predetermined stress level, followed by a recording of the stress-time curve while maintaining the total strain on the specimen constant.

The initial extension of the specimen was determined by a special preloading technique in which the frequency method was used to get a value of the elastic modulus of the strip. This preloading technique (loading from, for example, 200 to 400 N/mm^2, that is, less than the testing load)

[2] Gohn, G. R. and Fox, A., *Material Research and Standards*, Vol. 1, Dec. 1961, pp. 957-966.

TABLE 1—*Chemical composition (nominal).*

Grade			Element Content (percent by weight)						
AISI	Sandvik	Product	C	Si	Mn	Cr	Ni	Mo	Al
1074	15LM	strip	0.75	0.2	0.75	...	...	...	
1078, modified	16 Texture	strip	0.80	0.25	0.4	...	...	...	
420, modified	7C27Mo2	strip	0.38	0.4	0.6	13.5	...	1.0	
301	12R11	strip	0.10	0.6	1.3	17.5	7.5	...	
301, modified	11R51	strip and wire	0.09	1.2	1.3	17	8	0.7	
302	12R10	wire	0.10	0.6	1.2	18	9	...	
17-7 PH	9RU10	wire	0.07	0.45	0.8	16.5	7.5	...	1.0

TABLE 2—*Mechanical properties of the tested steels.*

Grade AISI	Size (mm)	$R_{p0.01}$ (N/mm^2)[a]	$R_{p0.2}$ (N/mm^2)[b]	R_m (N/mm^2)[c]	$\tau_{0.2}$ for Springs (N/mm^2)[d]	Treatment
301M	20 × 0.198	1370	2140	2280		cold worked and tempered 425°C/4 h
301	14 × 0.20	1320	2020	2040		cold worked and tempered 350°C/3 h
	3.5 × 0.20	1110	1750	1780		cold worked and tempered 350°C/3 h
	7.6 × 0.40	1010	1630	1730		cold worked and tempered 350°C/3 h
	10 × 0.20	1030	1550	1600		cold worked and tempered 350°C/3 h
420M	10 × 0.20	1190	1400	1770		hardened and tempered
1078M	7.95 × 0.22		2300	2320		texture rolled (patented, cold worked) and tempered 250°C/0.5 h
1074	10 × 0.20	1560	1650	1800		hardened and tempered
	10 × 0.25	1380	1575	1770		hardened and tempered
301M	ϕ1.5	1560	2370	2600	1477	cold worked and tempered 425°C/4 h
	ϕ2.0		2200	2400		cold worked and tempered 425°C/4 h
	ϕ2.5	1880	2300	2500	1598	cold worked and tempered 425°C/4 h
17-7 PH	ϕ0.99		2280	2320		cold worked and tempered 480°C/1 h
	ϕ1.0	1620	2100	2150	1538	cold worked and tempered 480°C/1 h
	ϕ2.0	1230	2020	2070	1250	cold worked and tempered 480°C/1 h
302	ϕ1.0	1310	1950	2160	1153	cold worked and tempered 350°C/3 h
	ϕ2.0	1040	1890	2090	1076	cold worked and tempered 350°C/3 h

[a] $R_{p0.01}$ = elastic limit, 0.01 percent offset yield strength.
[b] $R_{p0.2}$ = 0.2 percent offset yield strength.
[c] R_m = tensile strength.
[d] $\tau_{0.2}$ = 0.2 percent offset shear yield strength.

was carried out without the pneumatic cylinder. The upper specimen grip, attached to the screw, was adjusted upward, and the displacement was recorded. The initial extension, corresponding to an initial stress in the relaxation test, could then be calculated from this preloading displacement.

The method has two main advantages—settings in the grips and other parts of the rig will not affect the test, and a more accurate value of the initial stress can be determined.

The test was started with the activation of the pneumatic cylinder. It took approximately 2 s to reach the testing load. The time elapsed between loading and first reading was less than 30 s, depending on the time required to get a stable resonant frequency in the specimen and to measure the frequency. A constant-amplitude amplifier ensured that every reading was done with the same amplitude, regardless of the variations in stress and specimen size. The amplitude was chosen as low as possible in order to avoid nonlinear effects in the test system and heating of the strip.

Wire Spring Steels

The stiffness and the shear strength of the different springs were determined by a load-deflection test using a tension testing machine. The following formula was used to calculate the spring shear stress.[3]

$$\tau = \frac{8P D_m K}{\pi d^3} \tag{2}$$

where

P = load on spring,
d = wire diameter,
D_m = mean diameter of the spring, and
K = curvature correction factor.[3]

The springs were preset five times to a shear stress value equal to a certain percentage of the ultimate tensile strength of the wire or to a shear stress value equal to the shear yield strength ($\tau_{0.2}$) as determined from the load deflection test of the springs.

After presetting, the springs were tested at constant constraint. Initial shear stress levels between 800 and 1400 N/mm^2 were chosen for the test. To achieve the initial stress, the springs were strained with the aid of a screw mechanism. The time to reach the initial stress was 1 min in every test. The initial stress was measured at zero time, at 6 min, and at different times up to about 120 h. The mean value of the remaining stress

[3] Wahl, A. M., *Mechanical Springs*, McGraw-Hill, New York, 1963, pp. 56–58.

for ten springs in every test was calculated, and a regression line for the remaining stress as a function of log time was determined.

Results

Strip Spring Steels

Examples of the stress relaxation curves for the different grades are shown in Fig. 3. The experimental points for the stainless steels follow a straight line in the remaining stress versus log time diagram. It appears from the figure that the stress relaxation rate for carbon steels increased after about 40 min. The results from all the tests are presented in Table 3, where the initial slope $\Delta\sigma/\Delta \log t$, the break point, the secondary slope, and percentage of relaxation after 170 h are calculated.

The modified AISI 301 steel had the lowest relaxation rate up to 170 h followed by AISI 301, 420M, 1078M, and 1074. When comparing AISI 301 at different tensile strengths, the lowest stress relaxation was measured for the material with the highest tensile strength (Table 3). Testing AISI 1074 at different initial stress levels showed that the stress relaxation rate increased with increasing initial stress (Fig. 4). To get a simple comparison between the different grades, interpolated and extrapolated stress relaxation values for different initial stresses and times have been calculated in Table 4.

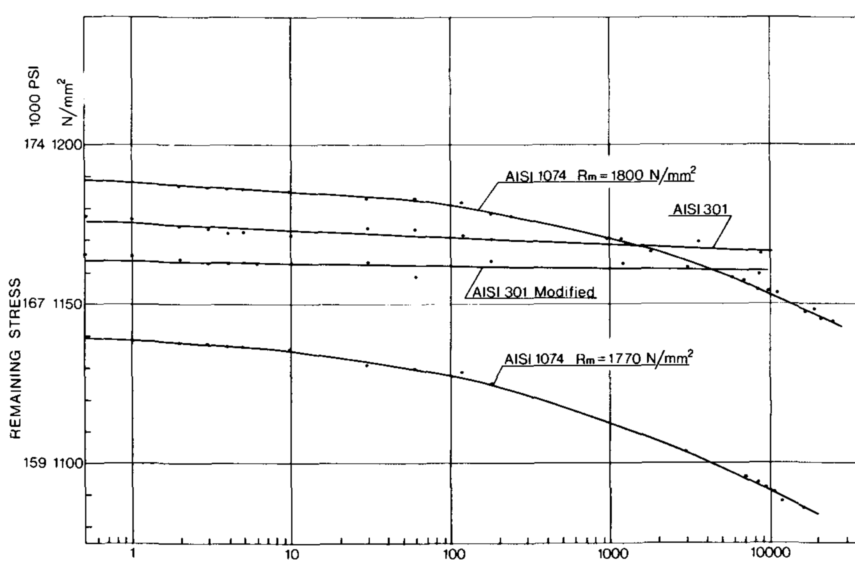

FIG. 3—*Stress relaxation curves for strip spring steels. Remaining stress versus log time.*

TABLE 3—*Stress relaxation data for strip spring steels.*

Grade AISI	R_m (N/mm^2)	Initial Stress (N/mm^2)	Initial Slope $-\Delta\sigma/\Delta \log t$ (σ, N/mm^2)	Breakpoint (min)	Secondary Slope $-\Delta\sigma/\Delta \log t$ (σ, N/mm^2)	Percentage of Relaxation up to 170 h
301M	2280	1217	1.0			0.34
	2280	1165	0.5			0.25
301	2040	1184	1.2			0.50
	2040	1176	1.8			0.60
	1780	1204	2.2			0.75
	1780	1192	2.2			0.85
	1730	1089	3.0			1.2
	1730	1079	2.2			1.0
	1600	1185	4.3			1.5
	1600	1074	2.5			1.1
	1600	868	0.8			0.9
420M	1770	1161	5.5			2.1
	1770	1137	5.3			2.0
1078M	2320	1206	6.7			2.4
	2320	1150	3.0	3000	12	1.6
	2320	1127	8.3	1000	21	3.2
1074	1800	1217	3.5	40	17	3.7
	1800	1190	2.5	100	23	2.8
	1800	1110	3.5	300	22	3.5
	1770	1638	42.0			10.9
	1770	1260	7.7	500	(50)	6.9
	1770	1162	4.5	200	26	4.0
	1770	1140	4.1	200	24	4.3
	1770	1060	3.9	500	16	3.5
	1770	922	1.0	1000	4	0.6

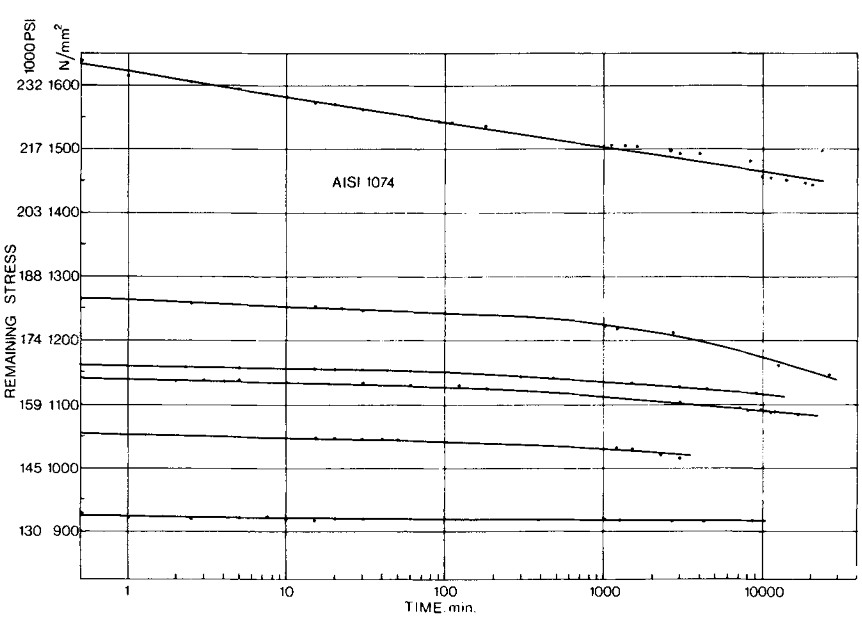

FIG. 4—*Stress relaxation curves for AISI 1074 carbon steel tested at different initial stress levels.*

Wire Spring Steels

The stress relaxation for one type of spring is presented in Fig. 5. Each point in the diagram is a mean value of ten springs. The slope $\Delta\sigma/\Delta \log t$ has been calculated in Table 5, where also the percentage of relaxation up to 100 h is shown. When comparing all the data, it is evident that the modified AISI 301 grade had the lowest relaxation rate, followed by the 17-7 PH grade and AISI 302. This can also be seen in Table 6, where the stress relaxation of the different grades are compared at approximately the same prestress level. When springs manufactured from one and the same material were prestressed to different levels, the highest prestress level gave the lowest amount of relaxation. (Compare the values in Table 5 for AISI 301M and AISI 302.)

Discussion

Strip Spring Steels

With the testing procedure used, it has been possible to record even small changes in stress. The behavior during the loading period up to the initial stress level has not been investigated. It might have been done

TABLE 4—*Interpolated and extrapolated (in parentheses) remaining stresses after different times—strip spring steels.*

Grade AISI	Initial Stress (N/mm^2)	Remaining Stress (N/mm^2) up to				
		1 Hour	1 Day	1 Week	1 Month	1 Year
301M	1200	1198	1197	1196	(1196)	(1195)
	1100	1099	1098	1097	(1097)	(1096)
301						
$R_m = 2040\ N/mm^2$	1200	1197	1195	1193	(1192)	(1191)
$R_m = 1600\ N/mm^2$	1200	1191	1186	1182	(1180)	(1175)
	1100	1094	1090	1088	(1086)	(1084)
420M	1100	1090	1082	1079	(1075)	(1070)
1078M	1100	1094	1090	1082	(1073)	(1060)
1074						
$R_m = 1800\ N/mm^2$	1200	1195	1182	1165	(1150)	(1125)
	1100	1095	1082	1065	(1050)	(1025)
$R_m = 1770\ N/mm^2$	1200	1187	1165	1135	(1100)	(1060)
	1100	1091	1075	1058	(1045)	(1020)
	1000	994	982	975	(965)	(950)
	900	898	897	895	(890)	(885)

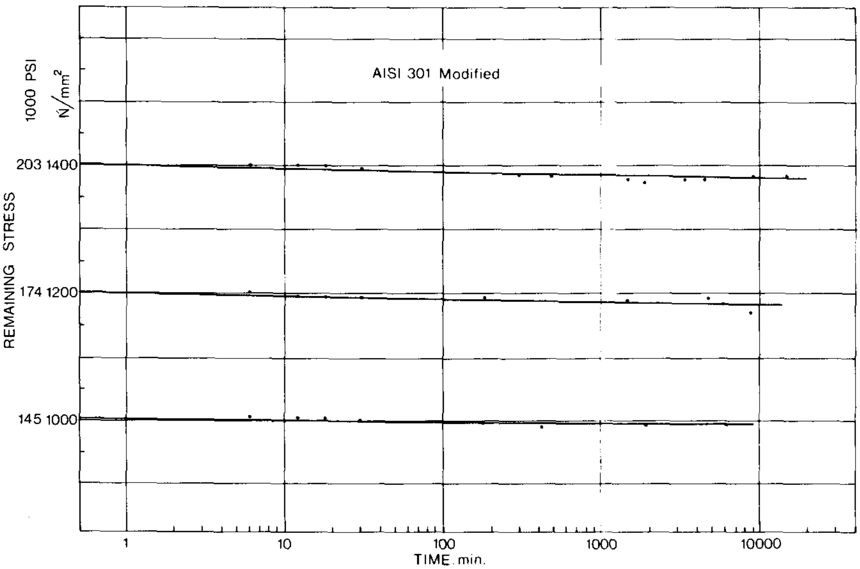

FIG. 5—*Stress relaxation curves for AISI 301M springs (wire diameter 1.5 mm) at different initial stress levels.*

with the aid of load cells. However, a tested load cell was not rigid enough to continuously record the true stress relaxation values.

The increased stress relaxation rates for the carbon steels were first considered as being an effect of grip slippage. However, tension tests on reference specimens, and on specimens that had been stress relaxed, showed different stress-strain behaviors. An example of this is given in Fig. 6 for the AISI 1074 steel. The two specimens showed an obvious difference from the elastic limit up to $R_{p0.2}$. In addition, tension testing of carbon steel specimens after different stress relaxation times indicated no such change in stress-strain behavior unless they were relaxed beyond the point where the increased relaxation began. This increased relaxation occurred even at relaxation stresses below $R_{p0.01}$. The tension testing of the stainless steels did not indicate any difference in stress-strain behavior before and after stress relaxation.

Stainless steels with a high elastic limit had a comparatively low relaxation rate. However, carbon steels with even higher elastic limits than the stainless steels had a higher relaxation rate, mainly due to the increased relaxation after the break point. Testing carbon steel at an initial stress of 1600 N/mm^2 showed that the stress relaxation rate was high from the first second. The elastic limit ($R_{p0.01}$ = 1380 N/mm^2) for this specimen was lower than the initial stress level.

The residual stresses and the martensite content were measured for some of the test specimens (see Table 7). The residual stresses were deter-

TABLE 5—*Stress relaxation data for wire spring steels.*

Grade	Wire Diameter (mm)	Presetting (N/mm^2)	Initial Stress (N/mm^2)	$-\Delta\sigma/\Delta \log t$ (σ, N/mm^2)	Percentage of Relaxation up to 100 h	Presetting (N/mm^2)	Initial Stress (N/mm^2)	$-\Delta\sigma/\Delta \log t$ (σ, N/mm^2)	Percentage of Relaxation up to 100 h
AISI 301M	1.5	1236	1000	0.9	0.5	1600	1000	0.5	0.2
	1.5	1236	1330	6.8	1.8	1600	1200	3.2	0.8
	1.5					1600	1400	5.1	2.0
	2.0					1520	1000	1.7	1.0
	2.0					1520	1200	5.1	2.0
	2.0					1520	1400	5.8	2.0
	2.5	1520	1000	3.2	1.5	1600	1000	2.2	0.9
	2.5	1520	1200	2.5	1.0	1600	1200	4.1	1.2
	2.5	1520	1400	4.9	1.7	1600	1400	5.4	1.4
17-7 PH	0.99 to 1.0	1320 (0.99)	1000	1.7	1.2	1540 (1.0)	1000	3.8	1.7
	0.99 to 1.0	1320 (0.99)	1200	5.4	2.2	1540 (1.0)	1200	10.7	3.9
	0.99 to 1.0	1320 (0.99)	1400	21.8	7.7	1540 (1.0)	1400	11.5	4.3
	2.0	1230	1000	2.8	1.4	1250	1000	4.8	2.0
	2.0	1230	1200	3.6	1.5	1250	1200	5.5	2.5
AISI 302	1.0	1153	800	4.5	2.5	1320	800	2.2	1.4
	1.0	1153	1000	5.0	2.7	1320	1000	4.7	2.5
	1.0					1320	1200	10.4	4.0
	2.0	1076	1000	3.9	1.5	1230	1000	2.8	1.4
	2.0	1008	1200	11.1	4.1				
	2.0	1140	1200	9.2	3.6	1230	1200	7.4	3.1

TABLE 6—*Stress relaxation for wire spring steels compared at approximately the same prestress level.*

Wire Diameter (mm)	Prestress (N/mm^2)	Grade	Percent Relaxation up to 100 h at the Following Initial Stresses			
			1000 N/mm^2	1200 N/mm^2	1330 N/mm^2	1400 N/mm^2
1.5	1230	AISI 301M	0.5		1.8	
1.0	1320	17-7 PH	1.2	2.1		
1.0	1320	AISI 302	2.5	4.0		
1.5	1230	AISI 301M	0.5		1.8	
2.0	1230	17-7 PH	1.4	1.5		
2.0	1230	AISI 302	1.4	3.1		
1.5	1600	AISI 301M	0.2	0.8		2.0
1.0	1540	17-7 PH	1.7	3.9		4.3

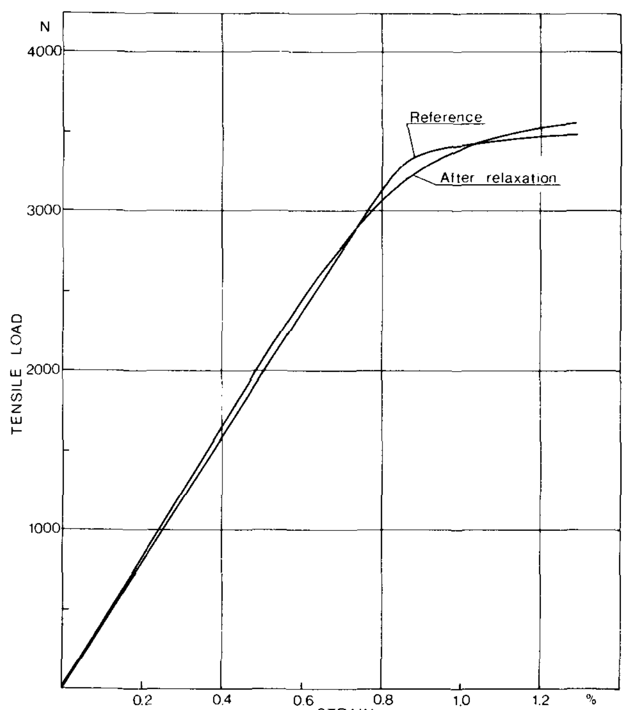

FIG. 6—*Tension testing curves—reference specimen and a specimen that has been stress relaxed. AISI 1074 carbon steel,* R_m *= 1800 N/mm^2.*

TABLE 7—*Residual stress and martensite content before and after stress relaxation of strip spring steels.*

Grade	Specimen		Residual Stress (N/mm^2)		Martensite Content (%)
			α-phase	γ-phase	
AISI 301M	reference	Side 1	−183 ± 85	−145 ± 70	50.6
		Side 2	−148 ± 60		
	relaxed	Side 1	−171 ± 75	−220 ± 43	49.5
		Side 2	−138 ± 61		
AISI 301	reference	Side 1	−195 ± 140		51.3
R_m = 2040 N/mm^2		Side 2	−189 ± 146		
	relaxed	Side 1	−209 ± 125		50.7
		Side 2	−181 ± 125		
AISI 301	reference	Side 1	−75 ± 8		27.1
R_m = 1730 N/mm^2		Side 2	−80 ± 7		
	relaxed	Side 1	−84 ± 4		27.1
		Side 2	−29 ± 7		
AISI 1074	reference	Side 1	−229 ± 16		
R_m = 1800 N/mm^2					
	relaxed	Side 1	−205 ± 11		

mined with $CrK\alpha_1$ radiation on (211) line and with ψ angles of 0, 33, and 50°, respectively ($\sin \psi^2$ method). The martensite content was determined with a magnetic balance. There was no significant change in martensite content for the austenitic stainless steels due to stress relaxation. It was difficult to see any change in the amount of residual stresses. However, the carbon steel AISI 1074 might have a decrease in compressive residual stresses due to the stress relaxation.

The extrapolated values for the remaining stresses given in Table 4 were calculated with the assumption that the accelerated relaxation rate for the carbon steels had a constant slope in the stress versus log time diagram up to one year. Further investigations will clarify whether this was true or not.

Wire Spring Steels

Due to the relatively long loading time, some stress relaxation occurred before the initial stress level was reached. The way of loading could therefore influence the amount of stress relaxation, especially for specimens tested at the highest initial stress levels. The results have shown that an increased prestress level lowers the relaxation rate. To achieve a high prestress level without deforming the spring too much, the elastic limit, the tensile strength, and the shear strength must be sufficiently high. According to the results, the springs coiled from wires with the highest values of $R_{p0.2}$ and R_m gave the lowest relaxation rate.

Conclusions

The stainless spring steel strips tested had a lower stress relaxation rate than the carbon steel strips. A high elastic limit had a beneficial effect for both types of steel. The stress relaxation rate for the carbon steels was accelerated after an initial period. This led to a considerable total stress relaxation in spite of the relatively low relaxation rate during the first hours. The specimens that had an acceleration in stress relaxation also exhibited a different stress-strain behavior compared to reference specimens.

Helical extension wire springs were preset to different levels. A high prestress level had a beneficial effect on the relaxation rate. Springs coiled from high-strength wire had the lowest relaxation rates.

DISCUSSION

Alfred Fox[1] *(written discussion)*—

1. In your vibrating string technique. The time dependent decrease in the tension of the string is measured by determining the resonant frequency of the string. This measurement surpasses an alternating bending stress component. What was the magnitude of this component as compared to the tensile stress?
2. How does the load relaxation rate found in a complex helical spring compare with that found in wire in uniaxial tension?
3. What was the modification of Type 301 steel?
4. What mechanism do you attribute the nonlinear behavior of the stress-strain curve for carbon steel after stress relaxation to?

S. U. V. Idermark and E. R. Johansson (authors' closure)—

1. The lateral displacement of the string was less than 0.1 mm corresponding to a bending stress less than 0.1 N/mm^2.
2. We have not yet tested the stress relaxation of wires in uniaxial tension.
3. The silicon content was higher in the modified than in normal Type 301 steel. Furthermore, molybdenum was added to the modified steel, see Table 1.

We believe that the mechanism behind this behavior is microcreep (see for example, C. W. Marschall, R. E. Maringer, *Dimensional Instability,* Pergamon Press, New York, 1977).

[1] Bell Laboratories, Murray Hill, N. J. 07974.

Alfred Fox[1]

Stress Relaxation in Bending of AISI 301 Type Corrosion-Resistant Steel Strip*

REFERENCE: Fox, Alfred, "**Stress Relaxation in Bending of AISI 301 Type Corrosion-Resistant Steel Strip,**" *Stress Relaxation Testing, ASTM STP 676*, Alfred Fox, Ed., American Society for Testing and Materials, 1979, pp. 78-88.

ABSTRACT: Bending stress relaxation experiments were made on AISI 301 type corrosion-resistant steel strip. Test data obtained on standard, tapered cantilever beam test specimens at temperatures ranging from 23 to 93°C (73 to 200°F)[2] over a time period of 20 000 h (2 years, 4 months) are compared with force relaxation data obtained on two complex clamp spring designs made from this material. Good correlation is obtained between the two sets of data. The effects of stress relief heat treatment and anisotropy on stress relaxation were also studied. Finally, the stress relaxation behavior of 301 type corrosion-resistant steel strip is compared to that of CA762 (12 percent nickel-silver). Both materials, if properly heat treated, retain better than 98 percent of the initial stress value after 20 000 h at 93°C (200°F) in the "elastic" range.

KEY WORDS: corrosion-resistant steel, creep (metals), mechanical properties (metals), nickel-silver, springs, stainless steels, strip, stress relaxation (metals)

Various type of flat springs are used for clamping small-size relays, transformer cores, and like items. The following material requirements are desired:

1. Good corrosion resistance
2. Good formability
3. Good resistance to stress relaxation
4. Easy welding and soldering
5. Low cost

*All measurements in these experiments were made in English customary units.

[1] Associate member of technical staff, Metallurgical Engineering Department, Bell Laboratories, Murray Hill, N. J. 07974.

Corrosion-resistant AISI 301 type steel (18 percent chromium and 8 percent nickel) meets many of these requirements and therefore increasingly attracts spring designers. While design data for this alloy are available for many of the properties enumerated[2], very little data can be found in the literature on the stress relaxation behavior of 301 steel strip. A knowledge of the stress relaxation behavior is requisite, however, for ensuring long time reliability.

The present study was initiated as a consequence of a cost reduction proposal for changing the clamp spring material for one of the miniature relays shown in Fig. 1 from CA762 (12 percent nickel-silver), hard temper, to corrosion resistant steel of the 301 type (18 percent chromium, 8 percent nickel), half-hard temper. The contact gaging stability in the relay shown is critical and can be significantly improved by use of a pileup clamp shown on one of the relays in Fig. 1. Another application for this material

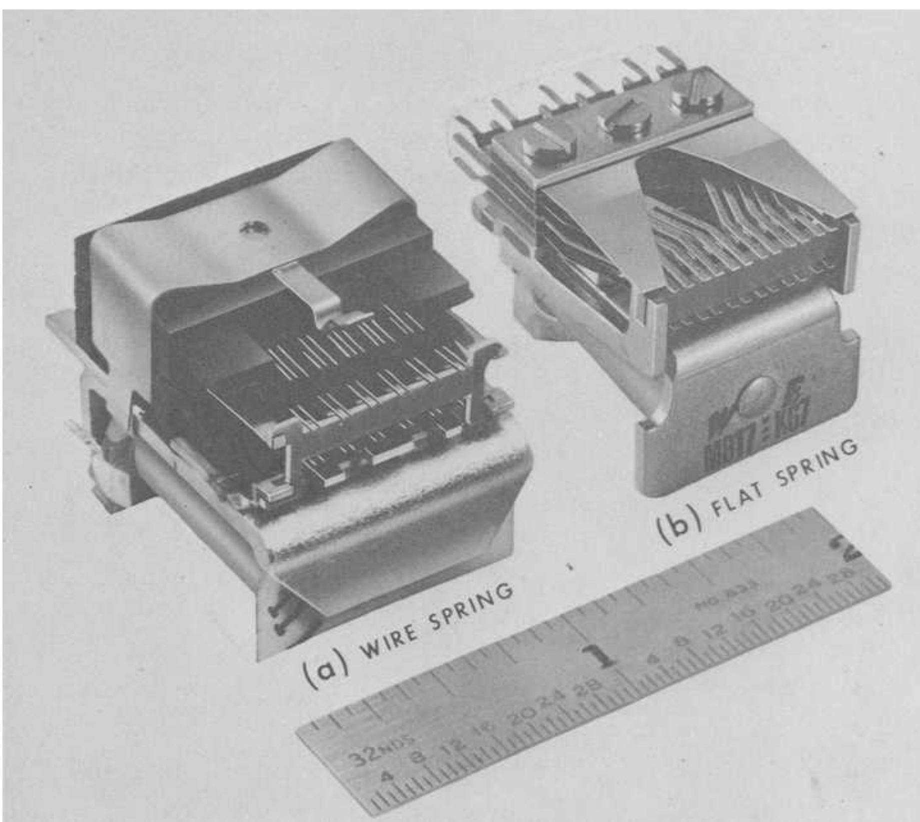

FIG. 1—*Miniature relays.*

[2]Takamura, M. et al, *Review of the Electrical Communication Laboratory,* Vol. 18, Nos. 1-2, Jan./Feb. 1970, pp. 27-46.

are clips used to hold the transformer cores together in Touch-Tone[3] dials as shown in Fig. 2. After a study of the stress relaxation behavior of the pileup clamp shown in Fig. 1 was initiated, it became immediately apparent that fundamental stress relaxation data were required that could be applied to many other types of spring designs.

This paper summarizes the results of stress relaxation studies in bending on 301 type corrosion-resistant steel and CA762 (12 percent nickel-silver) strip at temperatures ranging from 23 to 93°C (73 to 200°F). Tests were carried out over a 20 000 h time period. To see how applicable such fundamental data are to complex spring designs, they are compared with force relaxation data obtained on relay pileup clamps (Fig. 1) made from both materials and on transformer core clamps (Fig. 2) made from 301 stainless steel only.

Materials Tested

The materials tested were 0.51-mm (0.020-in.) thick strips of:

1. AISI Type 301 corrosion resistant steel, half-hard temper having a tensile strength of 910 MPa (132 ksi) in the sheet-rolling direction.
2. CA762 (12 percent nickel-silver), hard temper having a tensile strength of 710 MPa (103 ksi) and a 0.01 percent offset yield strength of 414 MPa (60 ksi) in the sheet-rolling direction.

The chemical composition of the materials tested is shown in Table 1.

In addition to the tapered cantilever beam stress relaxation test specimens that were made from Items 1 and 2 (Table 1), relay clamp springs were made from both materials. These springs are punched and formed so

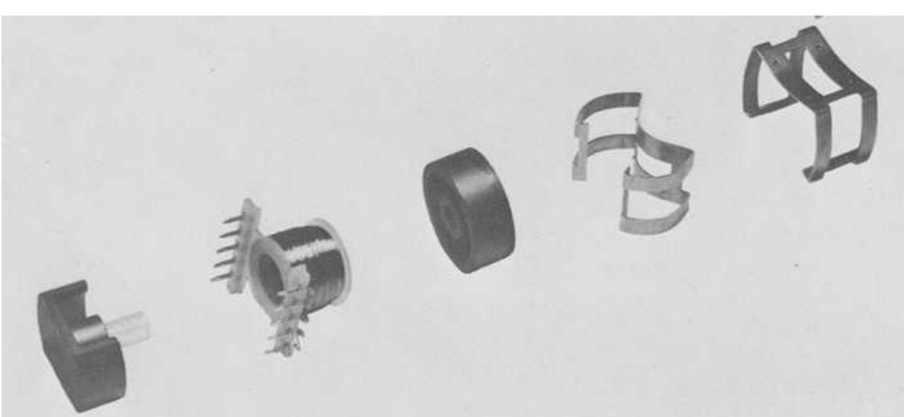

FIG. 2—*Exploded view of Touch-Tone transformer parts.*

[3] Trademark of the American Telephone and Telegraph Co.

TABLE 1—*Chemical composition of materials tested.*

Item	Material	Element	Content (percent by weight)
1	301 corrosion-resistant steel	chromium	17.49
		nickel	7.82
		manganese	1.40
		silicon	0.56
		carbon	0.044
2	CA762	copper	57.58
		nickel	12.27
		manganese	0.23
		iron	0.16
		lead	0.04
		zinc	29.61

that the normal stress is applied within ±7.5 deg in the sheet-rolling direction. In addition, transformer core springs made from 0.33-mm (0.013-in.) thick, half-hard temper AISI 301 type steel were tested. These springs are punched and formed so that the normal stress is applied parallel to the rolling direction. We did not check the chemical composition of the 0.33-mm (0.013-in.) thick stainless steel.

Tests were made on both as-received and stress relief heat-treated material. The corrosion-resistant steel was tested in the "as-received" condition and after stress relief heat treatment at 316°C (600°F) for periods ranging from ½ to 48 h. The corrosion-resistant steel test specimens were taken parallel and at 90 deg to the rolling direction. The stress-strain curve for this material was practically nonlinear over the entire load range; therefore, meaningful values of yield strength could not be obtained. Instead, the stress relaxation tests on this material were made at a maximum bending stress equal to 40 percent of the ultimate tensile strength, a value commonly used at the "elastic limit" for this type of stainless steel. The CA762 strip was tested in the "as-received" condition and after stress relief heat treatment at 191°C (375°F) for periods ranging from 2 to 48 h. The nickel-silver test specimens were initially stressed to a maximum bending stress corresponding to their 0.01 percent offset, room temperature tensile yield strength [414 MPa (60 ksi)] and were tested only with the normal stress in the rolling direction.

Methods of Test

Stress relaxation tests were made on tapered beam, constant moment, cantilever beam specimens as described by Fox.[4] This method is one of

[4] Fox, A., *Journal of Materials,* Vol. 6, No. 2, June 1971, p. 428.

those described in ASTM Standard Recommended Practice for Stress-Relaxation Tests for Materials and Structures, Part C, Conducting Stress Relaxation Tests of Materials (E 328-78) as Method C—elastic springback upon unloading at the end of the test period. To establish whether or not we could utilize the same test specimen for obtaining more than one point on the stress-time curve, we cycled one specimen from each material, both in the as-received and in the heat-treated conditions at the test temperature within the maximum displacement range of the stress relaxation test. We found the specimens to follow the same load versus displacement curve after 20 successive reloadings. On the basis of these observations, our measurements were made on the same specimen by unloading, measuring the permanent set, then reloading after the various time intervals. The relations used for calculating the stress from elastic springback are given by Spotts.[5] The stress remaining, reported in this paper, is the bending stress produced by the elastic moment on the outer fiber immediately prior to the release of the load. This is the value mainly of interest to spring designers who are concerned with loss in spring force as reflected by the elastic moment.

In addition to the tests made on standard tapered beam cantilever test specimens, we made tests on relay pileup clamp springs using the fixture shown in Fig. 3. The method used corresponds to Method B described in ASTM E 328 " . . . measurement of the force required to lift the specimen just free of one or more constraints during the test period." The clamp springs were inserted into the fixture shown in Fig. 3. The plunger, which simulates the force exerted on the spring by the pileup is depressed and then twisted so that its top shoulder rests against the shoulder of the fixture. At this time, electrical contact is made between the plunger and grounded through a spring-loaded contact that normally protrudes 0.05 mm (0.002 in.) from the shoulder and fixture. It should be noted that both plunger and fixture are relatively very stiff compared to the spring. The plunger can now be depressed by means of a universal testing machine (a table model TMS Instron was used), and the force required to break the electrical contact can be measured using a compression load cell. This force equals that which the spring exerts on the pileup and vice versa if no compressive flow were to occur in the pileup. This force is then measured at room temperature after various loading periods at elevated temperature, and the decrease in force as a function of time and temperature is determined.

It should be noted that in the actual relay pileup assembly, the loss in clamping force is governed not only by relaxation of the clamp spring,

[5] Spotts, M. F., *Mechanical Design Analysis*, Prentice Hall, Englewood Cliffs, N. J., 1964, p. 334.

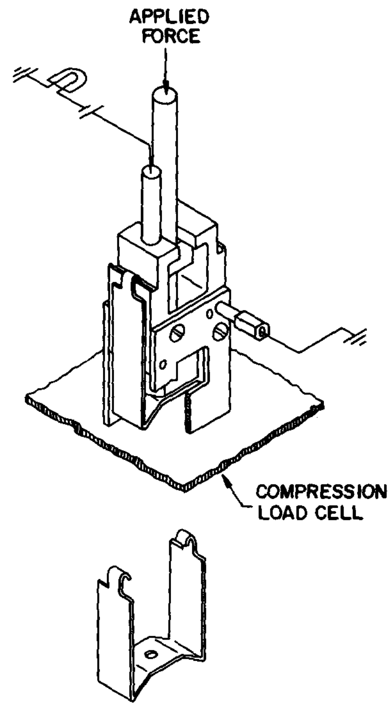

FIG. 3—*Pile-up clamp stress relaxation test fixture.*

but also by cold flow of the plastic pileup. This, however, was the subject of a separate study.

To measure the change in clamping force in stainless steel clips used with transformer cores, a similar method was used, except that a tensile load cell was used to determine the force required to lift the spring just off the transformer core. The test setup is shown in Fig. 4.

Test Data

Stress relaxation data for the 301 type corrosion-resistant steel strip tested are shown in Fig. 5 in the form of a plot of remaining bending stress versus log time. Test data are shown for a period of about 20 000 h for test temperatures ranging from 23 to 93°C (73 to 200°F), for specimens oriented so that the normal stress was applied parallel and transverse to the strip-rolling direction, respectively. The effect of anisotropy and heat-treating times at 316°C (600°F) on stress relaxation at 93°C (200°F) are shown in Fig. 6.

Stress relaxation data for as-received and stress relief heat-treated CA762

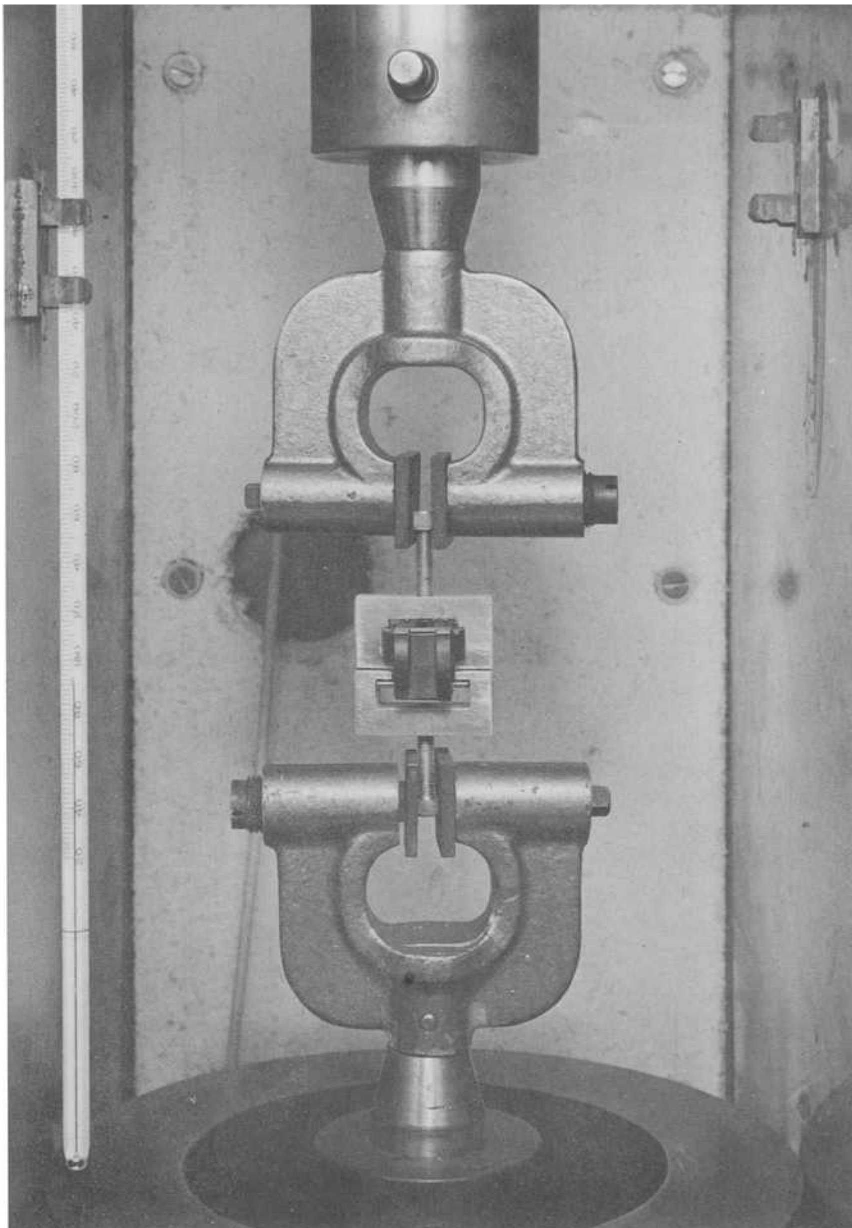

FIG. 4—*Transformer clamp relaxation test setup.*

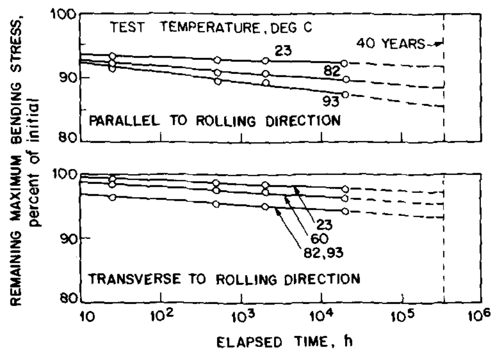

FIG. 5—*Stress relaxation test data for "as-received" AISI type 301 stainless steel strip. Temper: half-hard; initial stress: 364 MPa (52.8 ksi).*

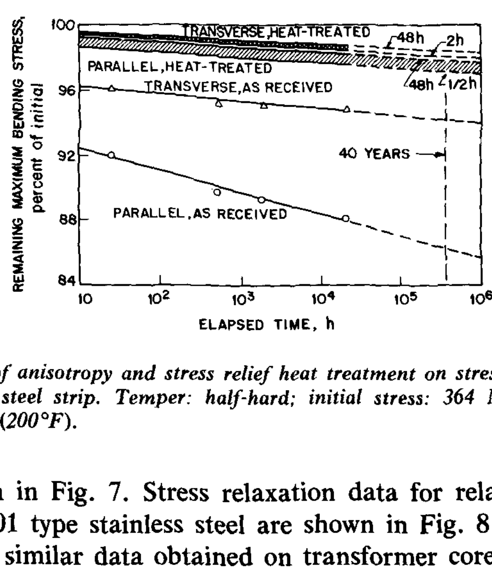

FIG. 6—*Effect of anisotropy and stress relief heat treatment on stress relaxation of AISI type 301 stainless steel strip. Temper: half-hard; initial stress: 364 MPa (52.8 ksi); test temperature: 93°C (200°F).*

strip are shown in Fig. 7. Stress relaxation data for relay pileup clamps formed from 301 type stainless steel are shown in Fig. 8. These data are compared with similar data obtained on transformer core clamps and the basic specimen relaxation data in Table 2. Figure 9 summarizes the stress relaxation values after 20 000 h as a function of test temperature, grain orientation, and stress relief heat treatment for the 301 type stainless steel strip.

Discussion

From Figs. 6 and 9 it is seen that for the 301 type stainless steel, the loss in stress is greater when the applied normal stress is in the strip-rolling direction. This effect is believed due to residual stress present from the cold rolling. Similar observations were made on heavily cold-rolled phos-

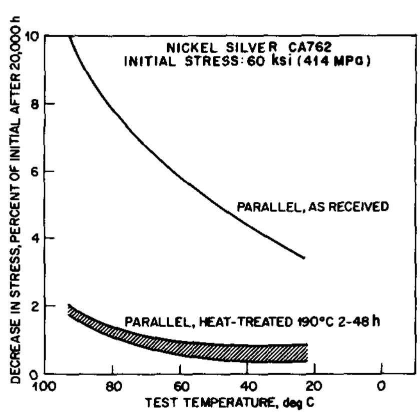

FIG. 7—*Effect of test temperature on stress relaxation of CA 762 strip (12 percent nickel-silver). Temper: hard; initial stress: 414 MPa (60 ksi, 0.01 percent offset yield strength).*

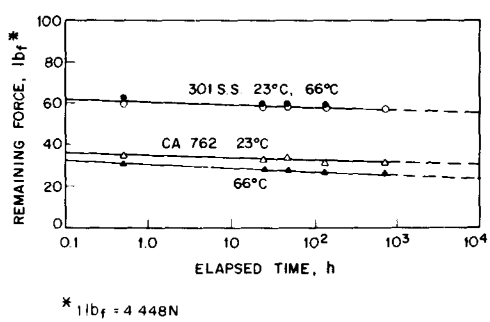

FIG. 8—*Force relaxation of relay pileup clamps made from AISI type 301 stainless steel and CA762 strips.*

TABLE 2—*Comparison of fundamental stress relaxation data with load relaxation in complex springs.*

Type of Spring and Material[a]	Heat Treatment Time, h	Temperature	Force Retained After 1500 h at 66°C (150°F), percent of 1-h value
Tapered cantilever specimen, 301 stainless steel	0.5	316°C (600°F)	99.2
Pile-up clamp 301 stainless steel	0.5	316°C (600°F)	93.3
Transformer core clamp, 301 stainless steel	1	316°C (600°F)	96.5

[a] All material taken so that normal stress was in the direction of rolling.

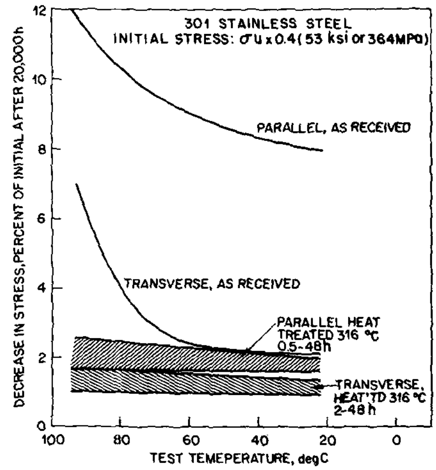

FIG. 9—*Effect of test temperature on stress relaxation of AISI type 301 stainless steel strip. Temper: half-hard; initial stress: 364 MPa (52.8 ksi).*

phor bronze (CA510) and copper-nickel-tin alloy (CA725) (97.3 and 98 percent reduction in area by cold rolling).[4]

The maximum decrease in stress to be expected after 40 years at 93°C is less than 15 percent of the initial value in the rolling direction and less than 6 percent in the direction transverse to rolling for unheat-treated 301 stainless steel. After stress relief heat treating, these values are reduced to less than 3 percent, as shown in Fig. 6. A similar improvement in the stress relaxation behavior of cold-rolled copper alloys following a stress relief heat treatment was noted by Fox.[4]

As shown in Figs. 6 and 9, the half-hour heat treatment at 316°C (600°F) adequately relieves residual stresses. Further increases in the heat-treating time for periods from 1 to 48 h did not produce significant additional improvement in stress relaxation behavior. From a production point of view, the half-hour treatment is also economically more attractive. It may also be noted from Fig. 6 that the material anisotropy is significantly reduced as a consequence of the heat treatment. If the spring can be punched without need for a given grain orientation, this may result in significant material economy.

From Fig. 7, it is seen that after stress relief heat treatment, the loss in stress in the nickel-silver is reduced from 10 to less than 2 percent after 20 000 h at 93°C (200°F) and that increasing further the heat-treating time produces no additional benefit. From Table 2 it may be seen that the data obtained using force relaxation measurements on complex springs agree quite well with relaxation measurements using the springback technique and a tapered cantilever beam test specimen, the difference being no more than 6 percent of the force retained expressed as a percentage of the 1-h value. Both the pileup clamp and transformer core clamp are heat treated after the initial forming but are subject to significant plastic deformation after clamping. The standard test specimen, however, is tested in the "elastic" range of the material. Irrespective of the differences in the initial loading conditions, however, the data obtained from both types of test are in reasonable agreement.

Conclusions

The bending stress relaxation behavior of AISI 301 type corrosion-resistant steel strip and of CA762 (12 percent nickel-silver) was characterized in the temperature range 23 to 93°C (73 to 200°F). Test data were taken over a 20 000-h period. Stress relief heat treatment was found to significantly reduce anisotropic behavior present in "as-rolled" sheet and reduce the loss in stress in those two materials to less than 2 percent after 20 000 h at 93°C (200°F), provided the initial stress is in the "elastic range." Good correlation was obtained between data obtained on standard tapered beam cantilever beam specimens using the elastic springback method and data obtained on complex springs using a force liftoff technique.

Acknowledgments

I would like to thank Bell Labs, Columbus, for supplying the materials and relay clamps used in this study; M. V. Rao for the photographs and test data pertaining to the transformer core clamps; and P. R. White, P. L. Key, and T. D. Schlabach for reviewing the manuscript.

DISCUSSION

R. A. Piscitelli[1] (*written discussion*)—Would you expect to get the same stress relaxation data on the same material using your cantilever test as using Bill Filer's mandrel test?

Alfred Fox (*author's closure*)—The two tests should give identical results. We like the constant moment cantilever because it is smaller and hence permits us to test a greater number of specimens in a relatively small oven.

[1] The Bendix Corp., Electrical Components Division, Sidney, N. Y. 13838.

E. W. Filer[1] *and C. R. Scorey*[2]

Stress Relaxation in Beryllium Copper Strip

REFERENCE: Filer, E. W. and Scorey, C. R., "**Stress Relaxation in Beryllium Copper Strip,**" *Stress Relaxation Testing, ASTM STP 676,* Alfred Fox, Ed., American Society for Testing and Materials, 1979, pp. 89-111.

ABSTRACT: A study was made of the stress relaxation of three beryllium copper alloys in strip form at temperatures between 20 and 200°C. The work was undertaken to obtain comprehensive stress relaxation data that would be useful in engineering design. A mandrel test method was chosen because many of the commercial applications in which stress relaxation is important concern strip material. Materials were stressed at levels of 50, 75, and 100 percent of the 0.2 percent offset yield strength for a total of 40 days. The results showed that aging greatly reduced the stress relaxation in beryllium copper alloys. There was no apparent dependence of stress relaxation on strip orientation. For comparative purposes, a number of tests were run on other copper spring alloys.

KEY WORDS: mechanical tests, bend tests, beryllium copper alloys, deformation, elastic properties, stress relaxation, yielding

Beryllium copper is widely used for conducting spring applications, because it has an excellent combination of mechanical strength, fatigue strength, electrical conductivity, and corrosion resistance. The demand for maximum performance has increased because of the closer packaging and miniaturization of electrical components operating at higher temperatures. Materials must remain stable under these operating conditions, especially when they are under stress for long periods of time. A conducting spring must retain its properties during service. Thus, it is important that the spring designer know the stress relaxation characteristics of the alloy he uses.

This study was undertaken for the purpose of obtaining comprehensive stress relaxation data, which would be useful in engineering design, for three beryllium copper alloys. The alloys studied were C17000, C17200, and C17500.

[1]Supervisor, Research and Development Laboratory, Kawecki Berylco Industries, Inc., Reading, Pa. 19603.

[2]Senior research metallurgist, formerly of Kawecki Berylco Industries, Inc., Pfizer Co. Metal and Composite Products, Wallingford, Conn. 06492.

Stress relaxation was measured as a function of initial stress at temperatures from 20 to 200°C for material in the age-hardenable and aged conditions. A test procedure applicable to strip samples was chosen.

A mandrel test method was used for stressing the strips to a desired outer fiber stress and exposing it to the test temperature. Tests were run on each material for a total of 1000 h (40 days) at stress levels of 50, 75, and 100 percent of the 0.2 percent offset yield strength.

A comparison was made to determine the dependence of stress relaxation on strip orientation, parallel or normal to the rolling direction. The effects of restressing the strips during the test were also studied. For comparative purposes, stress relaxation tests were run on five copper spring alloys.

Test Method

The material used in these experiments was in the form of strip 0.25 to 0.64 mm (0.010 to 0.025 in.) thick. Test strips were cut 100 mm (4 in.) long by 12.7 mm (0.5 in.) wide. A cylindrical mandrel was used for stressing the strip by wrapping the strip around the mandrel and holding at temperature for specified times. The experimental procedure is illustrated in Fig. 1. The diameter of the cylindrical mandrel was determined from the stress to be applied to the strip. The equations used for the calculation were derived from the elastic flexure equation and the bending moment of a spring.

The radius of curvature of the strip was determined using an optical comparator for measuring the chord height h and the chord length $2L$, as shown in Fig. 2. The radius of curvature was calculated from the mathematical formula

$$R = (L^2 + h^2) / 2h \tag{1}$$

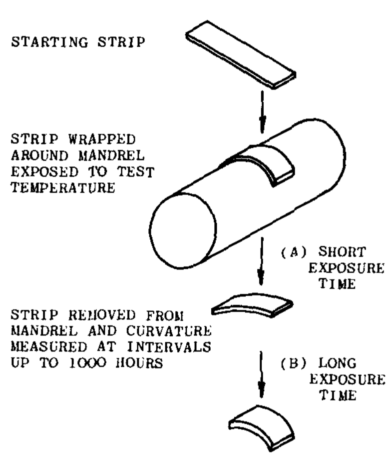

FIG. 1—*Experimental procedure for determining stress relaxation.*

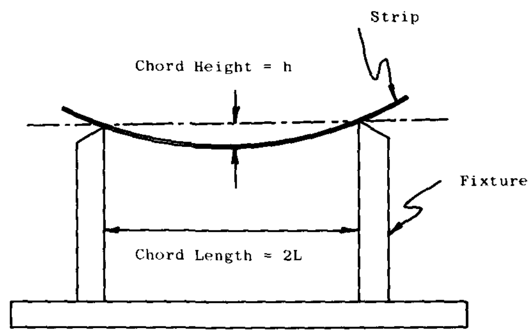

FIG. 2—*Fixture for strip curvature measurement.*

The equation for calculating the mandrel diameter was derived from the elastic flexure equation given in ASTM Recommended Practice for Stress-Relaxation Tests for Materials and Structures (E 328-175) paragraph 32.9.1

$$\sigma = Mc/I \tag{2}$$

where

σ = nominal flexure stress at the outer fiber,
M = the bending moment,
c = distance from outer fiber to centroid axis of the cross section, and
I = moment of inertia about the centroid axis of the cross section.

For rectangular cross sections

$$c/I = 6/bt^2 \tag{3}$$

where

b = width of strip and
t = thickness of strip.

Combining Eqs 2 and 3,

$$\sigma = 6M/bt^2$$

Since the load required to form the strip around the mandrel is directly proportional to the bending moment of the spring, this bending moment is calculated directly from the bend radius using elastic theory with the following equation[3]

[3]Austen, A. R. and Taylor, W., "Stress Relaxation in Beryllium Copper and Beryllium Nickel Springs," in *Proceedings,* 1971 Fourth Annual Connector Symposium, Electronic Connector Study Group, Inc., Cherry Hill, N. J., Oct. 1971.

$$M = \frac{bt^3E}{12}\left(\frac{1}{R_m} - \frac{1}{R}\right) \quad (4)$$

where

M = bending moment,
b = strip width,
t = strip thickness,
E = modulus of elasticity,
R_m = mandrel radius, and
R = strip radius of curvature.

Combining Eqs 3 and 4 and simplifying, we obtain the equation used for calculating the mandrel size required for a certain stress or the stress remaining after testing

$$\sigma = \frac{Et}{2}\left(\frac{1}{R_m} - \frac{1}{R}\right) \quad (5)$$

Three mandrel diameters were calculated for each alloy temper to be tested. These corresponded to outer fiber stresses of 50, 75, and 100 percent of the 0.2 percent offset yield strength. The room-temperature modulus was used for calculating the mandrel diameter for elevated temperature tests. Since the elastic modulus for beryllium copper alloys decreases with increasing temperature, the actual stress on the specimen would be higher than calculated, and the strip would be subjected to a more severe test. There is less than a 10 percent difference in modulus in this temperature range. The test strip was clamped to the mandrel, and after 1 h at 22°C, the strip was removed and a measurement made of the stress remaining in this strip using Eqs 1 and 5. This stress was taken to be the initial stress for the test. Tests were run at 22°C (72°F), 100°C (212°F), 150°C (302°F), and 200°C (392°F). The mounted strip was then placed in an oven at the test temperature and removed for measurement after approximately 20, 100, 300, and 1000 h and the remaining stress calculated. After each measurement, the same strip was replaced on the mandrel. In the 200°C, one extra measurement was made after only 1 h at temperature. This was done because some materials showed a rapid initial relaxation at this temperature.

This test method does not conform to ASTM E 328-75, because single strips were used instead of multiple strips. Data indicate that it does not make any difference if single or multiple strips are used.

A test was run in which the mandrel diameter was reduced so that about 2 percent strain could be introduced into the specimen. Additional tests were run with the strips cut normal to the rolling direction so that a comparison could be made with the strips taken parallel to the rolling direction. Tests were run using separate strips for each period of time at temperature to see if this affected the results compared to the standard method of restressing the strip after each measurement.

The chemical compositions of the various alloys tested are shown in Table 1. All of the specimens tested for a particular alloy were within these specifications. The mechanical properties for these alloys, including the different tempers, were determined, and the results are summarized in Table 2. The 0.2 percent offset yield strength reported is the value used to determine the required bending stress. Table 3 gives the amount of cold reduction required to produce the various tempers of beryllium copper alloys and the aging conditions required to produce the optimum properties.

Results

C17000 (Berylco 165) was tested as described, and the results are summarized in Tables 4 through 7. The age-hardenable materials were tested at 22 and 100°C, except for the ½H temper material, which was also tested at 150°C. The age-hardenable materials relaxed more with increased testing temperature and time, and the relaxation was greatest at the highest stress levels of testing. This material is not normally used in the age-hardenable condition, but the upper temperature limits of use had to be established. The ½H material was tested at 150°C to verify that there would be a significant drop in the remaining stress. The maximum loss after testing for 1000 h was 20 percent more than in the 100°C tests at all levels of testing.

The C17000 (Berylco 165) alloy is normally used in the aged condition, and the results of the stress relaxation tests are summarized in Tables 4 through 7. The stresses remaining, for all practical purposes, were the same after testing at all times up to 1000 h at 22 and 100°C and at all stress levels. After testing at 150°C, the specimens tested at 50 percent of the 0.2 percent offset yield strength showed a loss in stress of 5 to 8 percent over specimens tested at 100°C. This loss increased to 10 to 16 percent over the specimens tested at 100°C at 100 percent of 0.2 percent offset yield strength. There was considerable loss in the remaining stress after testing at 200°C with the greatest loss being on the strongest material, HT temper, and naturally at the highest stress level. The C17000 (Berylco 165) alloy performed better at this temperature than the copper spring temper alloys.

TABLE 1—*Chemical composition of materials tested.*

Alloy	Trade Name	Nominal Composition, percent
C17000	Berylco 165	1.60 to 1.79 Be, 0.20 min Co, balance Cu
C17200	Berylco 25	1.80 to 2.00 Be, 0.20 min Co, balance Cu
C17500	Berylco 10	0.40 to 0.70 Be, 2.40-2.70 Co, balance Cu
C26000	Cartridge brass, 70%	68.5 to 71.5 Cu, balance Zn
C51000	Phosphor bronze 5% A	4.2 to 5.8 Sn, 0.03 to 0.35 P, balance Cu
C52100	Phosphor bronze 8% C	7.0 to 9.0 Sn, 0.03 to 0.35 P, balance Cu
C72500		8.5 to 10.5 Ni, 1.8 to 2.8 Sn, balance Cu
C77000	Nickel-silver 55-18	53.5 to 56.5 Cu, 16.5 to 19.5 Ni, balance Zn

TABLE 2—*Tensile properties of test material.*

Alloy	Temper	Strip Thickness, in.	Tensile Strength MPa	Tensile Strength ksi	0.2% Offset Yield Strength MPa	0.2% Offset Yield Strength ksi	Percent Elongation in 2 in.	Modulus GPa	Modulus Msi
C17000	A	0.0120	469	68	200	29	53	127.6	18.5
	AT	0.0122	1165	169	1020	148	10	127.6	18.5
	¼H	0.0110	545	79	469	68	31	127.6	18.5
	¼HT	0.0110	1179	171	1000	145	10	127.6	18.5
	½H	0.0246	669	97	634	92	13	127.6	18.5
	½HT	0.0095	1255	182	1138	165	6	127.6	18.5
	H	0.0190	807	117	772	112	2	127.6	18.5
	HT	0.0190	1331	193	1200	174	3	127.6	18.5
C17200	A	0.0183	503	73	255	37	49	124.8	18.1
	AT	0.0126	1282	186	1027	149	7	131.0	19.0
	¼H	0.0123	593	86	510	74	30	126.9	18.4
	¼HT	0.0196	1227	178	1076	156	8	133.1	19.3
	½H	0.0220	662	96	614	89	16	129.6	18.8
	½HT	0.0220	1317	191	1165	169	5	133.1	19.3
	H	0.0125	800	116	758	110	3	120.0	17.4
	HT	0.0127	1372	199	1220	177	2	131.7	19.1
C17500	AT	0.0123	745	108	648	94	15	135.8	19.7
	½H	0.0243	462	67	434	63	5	128.9	18.7
	½HT	0.0140	862	125	779	113	12	135.1	19.6
	H	0.0200	552	80	524	76	3	130.3	18.9
	HT	0.0217	869	126	772	112	13	135.8	19.7
C26000	spring	0.0100	662	96	634	92	2	104.1	15.1
C51000	spring	0.0100	717	104	703	102	2	115.8	16.8
C52100	spring	0.0100	786	114	745	108	3	111.7	16.2
C72500	spring	0.0100	621	90	614	89	1	143.4	20.8
C77000	spring	0.0100	786	114	779	113	1	131.7	19.1

NOTE—1 in. = 2.54 cm.

TABLE 3—*Amount of cold reduction required to produce the various tempers of beryllium copper alloys and aging conditions for optimum properties.*

Alloy	Designation	Percent Cold Reduction	Aging Conditions: Designation	Aging Conditions: Temperature [°C (°F)]	Aging Conditions: Time, h
C17000	A	0	AT	316 (600)	3
	¼H	11	¼HT	316 (600)	2
	½H	21	½HT	316 (600)	2
	H	37	HT	316 (600)	2
C17200	A	0	AT	316 (600)	3
	¼H	11	¼HT	316 (600)	2
	½H	21	½HT	316 (600)	2
	H	37	HT	316 (600)	2
C17500	A	0	AT	482 (900)	3
	½H	21	½HT	482 (900)	2
	H	37	HT	482 (900)	2

TABLE 4—*Stress relaxation in C17000 (Berylco 165) alloy—test temperature 22°C.*

Temper	Remaining Stress After Hours Indicated, percent: 20 h	100 h	300 h	1000 h
	INITIAL STRESS 50% OF 0.2% OFFSET YIELD STRENGTH			
HT	100	99	99	100
½HT	99	99	99	98
¼HT	99	99	99	99
AT	100	99	99	99
H	100	100	100	99
½H	100	100	100	100
¼H	100	100	100	100
A	100	100	100	100
	INITIAL STRESS 75% OF 0.2% OFFSET YIELD STRENGTH			
HT	100	100	99	99
½HT	100	100	100	100
¼HT	99	99	99	98
AT	99	99	98	98
H	99	99	99	98
½H	100	100	99	99
¼H	99	98	98	97
A	100	98	98	96
	INITIAL STRESS 100% OF 0.2% OFFSET YIELD STRENGTH			
HT	99	98	96	96
½HT	100	99	98	98
¼HT	97	97	96	96
AT	99	99	96	95
H	99	98	97	96
½H	99	99	98	98
¼H	96	95	94	92
A	97	97	95	93

TABLE 5—*Stress relaxation in C17000 (Berylco 165) alloy—test temperature 100°C.*

Temper	Remaining Stress After Hours Indicated, percent			
	20 h	100 h	300 h	1000 h
	INITIAL STRESS 50% OF 0.2% OFFSET YIELD STRENGTH			
HT	99	98	98	96
½HT	99	99	98	97
¼HT	100	99	99	98
AT	99	98	98	97
H	89	87	83	81
½H	90	86	84	80
¼H	90	87	82	79
A	92	86	77	75
	INITIAL STRESS 75% OF 0.2% OFFSET YIELD STRENGTH			
HT	99	98	96	96
½HT	97	96	96	96
¼HT	99	99	97	97
AT	98	98	97	97
H	88	85	82	80
½H	85	83	79	77
¼H	88	84	80	77
A	80	74	66	61
	INITIAL STRESS 100% OF 0.2% OFFSET YIELD STRENGTH			
HT	98	97	95	94
½HT	98	97	96	96
¼HT	95	95	94	94
AT	98	97	94	95
H	84	80	78	75
½H	86	86	79	77
¼H	87	85	81	79
A	90	83	75	62

The C17200 (Berylco 25) alloy contains more beryllium than the C17000 (Berylco 165) alloy, resulting in higher mechanical properties in both the age-hardenable and the aged tempers. The results of the stress relaxation tests are summarized in Tables 8 through 11.

The age-hardenable C17200 (Berylco 25) alloy showed the remaining stress to be similar to the C17000 (Berylco 165) alloy when tested at 22 and 100°C except for the A temper. Here, the remaining stresses in the A temper were higher than the C17000 (Berylco 165) alloy at 100°C. Only the ½H temper strip was tested at 150°C, and the stresses remaining were 22 to 27 percent less than those of the strip tested at 100°C. There was no significant difference in the stresses remaining after testing at 150°C for the three test levels.

The C17200 (Berylco 25) alloy is used in the aged condition because of the higher mechanical properties and the better stress relaxation properties. The remaining stresses are a few percentage points lower in the material tested at

TABLE 6—*Stress relaxation in C17000 (Berylco 165) alloy—test temperature 150°C.*

Temper	Remaining Stress After Hours Indicated, percent			
	20 h	100 h	300 h	1000 h
	INITIAL STRESS 50% OF 0.2% OFFSET YIELD STRENGTH			
HT	95	93	91	88
½HT	97	95	93	91
¼HT	99	97	96	93
AT	98	95	94	92
½H	77	71	66	58
	INITIAL STRESS 75% OF 0.2% OFFSET YIELD STRENGTH			
HT	95	91	89	85
½HT	96	94	92	90
¼HT	96	95	93	91
AT	96	95	93	92
½H	80	72	67	60
	INITIAL STRESS 100% OF 0.2% OFFSET YIELD STRENGTH			
HT	93	90	87	84
½HT	91	89	86	82
¼HT	96	93	93	91
AT	95	94	91	87
½H	76	72	65	58

TABLE 7—*Stress relaxation in C17000 (Berylco 165) alloy—test temperature 200°C.*

Temper	Remaining Stress After Hours Indicated, percent				
	1 h	20 h	100 h	300 h	1000 h
	INITIAL STRESS 50% OF 0.2% OFFSET YIELD STRENGTH				
HT	95	85	77	70	61
½HT	95	89	83	76	65
¼HT	98	91	85	78	69
AT	97	93	89	84	78
	INITIAL STRESS 75% OF 0.2% OFFSET YIELD STRENGTH				
HT	91	82	74	65	56
½HT	95	88	82	74	64
¼HT	96	90	84	77	67
AT	94	89	84	79	70
	INITIAL STRESS 100% OF 0.2% OFFSET YIELD STRENGTH				
HT	89	79	70	62	54
½HT	93	85	79	70	61
¼HT	96	89	84	76	67
AT	94	88	82	77	70

TABLE 8—*Stress relaxation in C17200 (Berylco 25) alloy—test temperature 22°C.*

Temper	Remaining Stress After Hours Indicated, percent			
	20 h	100 h	300 h	1000 h
	INITIAL STRESS 50% OF 0.2% OFFSET YIELD STRENGTH			
HT	99	100	99	99
½HT	99	100	100	99
¼HT	99	100	99	100
AT	100	100	100	99
H	99	99	99	99
½H	100	100	100	100
¼H	100	99	99	99
A	100	100	100	100
	INITIAL STRESS 75% OF 0.2% OFFSET YIELD STRENGTH			
HT	99	99	98	98
½HT	100	100	99	99
¼HT	99	99	99	99
AT	100	98	98	97
H	100	98	98	97
½H	100	100	100	100
¼H	99	99	99	98
A	100	100	100	98
	INITIAL STRESS 100% OF 0.2% OFFSET YIELD STRENGTH			
HT	99	98	97	97
½HT	99	98	98	99
¼HT	99	99	99	99
AT	97	97	92	91
H	96	94	89	91
½H	99	99	98	98
¼H	99	99	98	96
A	98	98	96	98

100°C when compared to the 22°C tests, but nothing really significant. At 150°C, there is more of a loss, with the largest being on the material tested at 100 percent of the 0.2 percent offset yield strength. The stress remaining was 6 to 16 percent lower than the material tested at 100°C at all levels of testing. At 200°C, there was a significant loss in the remaining stress, with the losses increasing with time. There was approximately 60 percent of the initial stress remaining in all specimens when tested at 50, 75, and 100 percent of the 0.2 percent offset yield strength at 200°C.

The C17500 (Berylco 10) alloy contains only 0.5 percent beryllium, and as a result, the mechanical properties are less than those of the C17000 (Berylco 165) and C17200 (Berylco 25) alloys. Since the aging temperature is higher, this material can be used at a higher temperature. The results of the stress relaxation tests are summarized in Tables 12 through 15.

The age-hardenable material shows an increase in the stress loss at the

TABLE 9—*Stress relaxation in C17200 (Berylco 25) alloy—test temperature 100°C.*

Temper	Remaining Stress After Hours Indicated, percent			
	20 h	100 h	300 h	1000 h
	INITIAL STRESS 50% OF 0.2% OFFSET YIELD STRENGTH			
HT	99	98	97	96
½HT	99	98	97	97
¼HT	99	98	97	96
AT	99	99	99	98
H	89	85	82	80
½H	90	86	81	79
¼H	90	86	82	80
A	89	83	80	75
	INITIAL STRESS 75% OF 0.2% OFFSET YIELD STRENGTH			
HT	99	98	97	95
½HT	99	98	97	95
¼HT	98	98	96	96
AT	98	98	97	96
H	88	85	81	78
½H	89	86	82	80
¼H	90	85	82	80
A	87	83	79	77
	INITIAL STRESS 100% OF 0.2% OFFSET YIELD STRENGTH			
HT	97	95	94	93
½HT	98	97	95	95
¼HT	96	95	93	93
AT	98	97	95	95
H	87	84	79	77
½H	89	85	82	79
¼H	84	80	76	71
A	84	81	76	69

higher stress levels of testing at ambient temperature. There was a significant loss in the remaining stress when testing at 100°C over the 22°C tests, with the loss varying from 22 to 30 percent of the initial stress. Again, only the ½H temper strip was tested at the higher temperatures. At 150°C, the remaining stress was 65 to 70 percent of the initial stress, with the lower value being for the strip tested at the higher load levels. At 200°C, the remaining stresses had decreased to 51 to 55 percent of the initial stress.

The aged C17500 (Berylco 10) alloy showed no significant stress relaxation when testing at ambient temperature. The percentage of remaining stresses were less at 100°C than the ambient temperature tests with the same trend continuing when testing at 150°C. At 200°C, the increase in loss was significant, with the greatest loss being in the materials tested at 100 percent of the 0.2 percent offset yield strength.

TABLE 10—*Stress relaxation in C17200 (Berylco 25) Alloy—test temperature 150°C.*

Temper	Remaining Stress After Hours Indicated, percent			
	20 h	100 h	300 h	1000 h
	INITIAL STRESS 50% OF 0.2% OFFSET YIELD STRENGTH			
HT	95	92	89	86
½HT	95	93	91	89
¼HT	96	95	91	88
AT	97	94	93	90
½H	80	73	65	57
	INITIAL STRESS 75% OF 0.2% OFFSET YIELD STRENGTH			
HT	92	89	86	82
½HT	95	93	91	88
¼HT	97	95	91	89
AT	96	94	92	90
½H	78	71	64	53
	INITIAL STRESS 100% OF 0.2% OFFSET YIELD STRENGTH			
HT	89	85	81	77
½HT	94	90	88	85
¼HT	94	93	89	87
AT	95	93	90	88
½H	77	71	65	56

TABLE 11—*Stress relaxation in C17200 (Berylco 25) alloy—test temperature 200°C.*

Temper	Remaining Stress After Hours Indicated, percent				
	1 h	20 h	100 h	300 h	1000 h
	INITIAL STRESS 50% OF 0.2% OFFSET YIELD STRENGTH				
HT	96	87	80	71	61
½HT	95	88	80	73	65
¼HT	96	88	82	75	64
AT	95	89	82	72	63
	INITIAL STRESS 75% OF 0.2% OFFSET YIELD STRENGTH				
HT	93	85	77	69	58
½HT	93	85	78	69	61
¼HT	93	85	78	69	58
AT	95	87	79	71	61
	INITIAL STRESS 100% OF 0.2% OFFSET YIELD STRENGTH				
HT	93	83	75	66	55
½HT	92	83	76	67	58
¼HT	92	84	77	69	58
AT	94	86	81	73	63

TABLE 12—*Stress relaxation in C17500 (Berylco 10) alloy—test temperature 22°C.*

	Remaining Stress After Hours Indicated, percent			
Temper	20 h	100 h	300 h	1000 h
	INITIAL STRESS 50% OF 0.2% OFFSET YIELD STRENGTH			
HT	100	100	100	100
½HT	100	100	100	99
AT	99	99	99	98
H	100	98	96	96
½H	100	100	100	97
	INITIAL STRESS 75% OF 0.2% OFFSET YIELD STRENGTH			
HT	100	100	99	99
½HT	100	99	99	99
AT	100	99	96	95
H	97	96	95	94
½H	98	96	94	94
	INITIAL STRESS 100% OF 0.2% OFFSET YIELD STRENGTH			
HT	100	99	99	98
½H	100	99	99	99
AT	100	100	99	98
H	96	95	93	92
½H	98	98	97	95

TABLE 13—*Stress relaxation in C17500 (Berylco 10) alloy—test temperature 100°C.*

	Remaining Stress After Hours Indicated, percent			
Temper	20 h	100 h	300 h	1000 h
	INITIAL STRESS 50% OF 0.2% OFFSET YIELD STRENGTH			
HT	97	97	96	94
½HT	97	95	93	89
AT	98	97	96	95
H	79	75	73	71
½H	86	84	81	78
	INITIAL STRESS 75% OF 0.2% OFFSET YIELD STRENGTH			
HT	97	96	96	95
½HT	94	92	89	87
AT	98	97	95	93
H	79	76	73	71
½H	85	83	81	77
	INITIAL STRESS 100% OF 0.2% OFFSET YIELD STRENGTH			
HT	96	96	94	94
½HT	92	90	87	85
AT	97	95	96	93
H	79	76	72	70
½H	82	79	77	74

TABLE 14—*Stress relaxation in C17500 (Berylco 10) alloy—test temperature 150°C.*

Temper	Remaining Stress After Hours Indicated, percent			
	20 h	100 h	300 h	1000 h
	INITIAL STRESS 50% OF 0.2% OFFSET YIELD STRENGTH			
HT	97	94	94	92
½HT	96	96	91	90
AT	96	92	93	90
½H	78	75	70	70
	INITIAL STRESS 75% OF 0.2% OFFSET YIELD STRENGTH			
HT	97	94	94	93
½HT	96	93	90	87
AT	95	92	89	86
½H	76	72	70	68
	INITIAL STRESS 100% OF 0.2% OFFSET YIELD STRENGTH			
HT	95	93	91	90
½HT	94	92	87	86
AT	93	89	86	84
½H	74	70	67	65

TABLE 15—*Stress relaxation in C17500 (Berylco 10) alloy—test temperature 200°C.*

Temper	Remaining Stress After Hours Indicated, percent				
	1 h	20 h	100 h	300 h	1000 h
	INITIAL STRESS 50% OF 0.2% OFFSET YIELD STRENGTH				
HT	94	90	87	86	83
½HT	94	89	84	81	77
AT	93	89	83	79	75
½H	75	66	63	58	55
	INITIAL STRESS 75% OF 0.2% OFFSET YIELD STRENGTH				
HT	95	90	88	86	83
½HT	92	86	80	77	71
AT	91	85	80	75	69
½H	71	64	58	56	52
	INITIAL STRESS 100% OF 0.2% OFFSET YIELD STRENGTH				
HT	94	88	85	82	79
½HT	89	83	78	73	67
AT	90	84	78	73	67
½H	70	63	55	52	51

Five other copper spring temper alloys were run at the same time for comparison purposes. The chemical composition and the mechanical properties of C26000, C51000, C52100, C72500, and C77000 alloys are given in Tables 1 and 2. These materials were tested at the same relative stress levels based on their 0.2 percent offset yield strength and temperature as the beryllium copper alloys. The C26000 alloy lost 7 to 20 percent at ambient temperature depending on the amount of stress to which the strip was subjected. At 100°C, there was a 45 percent loss, which increased to over 60 percent at 150°C. The C51000 and C52000 alloys were very similar in that there was up to 9 percent loss at 100 percent of the yield strength at ambient temperature. This loss increased to 25 percent at 100°C and 60 percent at 150°C. The C72500 and C77000 spring alloys were similar to the C51000 and C52100 alloys at ambient temperature and 100°C. These alloys were considerably better than the C51000 and C52100 alloys at 150°C, but not as good as the beryllium copper alloys. At 200°C, the C72500 alloy had a loss of 40 to 45 percent, while the C77000 alloy loss was 46 to 53 percent. Tables 16, through 19 show the percentage of the remaining stress for these alloys. No tests were run at 200°C on the C26000, C51000, and C52500 alloys, because the losses at 150°C were too high.

To study the effects of higher initial stress levels on the relaxation of

TABLE 16—*Stress relaxation in copper spring temper alloys—test temperature 22°C.*

Alloy	Remaining Stress After Hours Indicated, percent			
	20 h	100 h	300 h	1000 h
	INITIAL STRESS 50% OF 0.2% OFFSET YIELD STRENGTH			
C26000	96	94	92	93
C51000	99	99	99	99
C52100	99	97	97	98
C72500	100	99	99	99
C77000	100	100	99	99
	INITIAL STRESS 75% OF 0.2% OFFSET YIELD STRENGTH			
C26000	98	94	89	88
C51000	97	97	96	96
C52100	99	97	96	94
C72500	99	99	98	98
C77000	100	99	98	97
	INITIAL STRESS 100% OF 0.2% OFFSET YIELD STRENGTH			
C26000	91	88	81	80
C51000	97	94	92	92
C52100	96	93	93	91
C72500	99	96	90	88
C77000	96	94	93	90

TABLE 17—*Stress relaxation in copper spring temper alloys—test temperature 100°C.*

Alloy	Remaining Stress After Hours Indicated, percent			
	20 h	100 h	300 h	1000 h
	INITIAL STRESS 50% OF 0.2% OFFSET YIELD STRENGTH			
C26000	69	63	59	55
C51000	88	82	78	74
C52100	89	83	79	75
C72500	91	87	85	85
C77000	91	87	86	84
	INITIAL STRESS 75% OF 0.2% OFFSET YIELD STRENGTH			
C26000	71	65	58	55
C51000	85	80	75	72
C52100	86	83	80	77
C72500	86	83	80	79
C77000	85	84	81	79
	INITIAL STRESS 100% OF 0.2% OFFSET YIELD STRENGTH			
C26000	74	64	60	58
C51000	85	84	78	75
C52100	86	80	76	75
C72500	85	82	80	78
C77000	84	82	78	77

TABLE 18—*Stress relaxation in copper spring temper alloys—test temperature 150°C.*

Alloy	Remaining Stress After Hours Indicated, percent			
	20 h	100 h	300 h	1000 h
	INITIAL STRESS 50% OF 0.2% OFFSET YIELD STRENGTH			
C26000	54	45	41	36
C51000	70	58	52	44
C52100	73	60	53	45
C72500	81	77	76	74
C77000	83	79	76	73
	INITIAL STRESS 75% OF 0.2% OFFSET YIELD STRENGTH			
C26000	52	46	39	36
C51000	69	57	50	42
C52100	69	61	51	42
C72500	78	74	72	70
C77000	79	73	71	69
	INITIAL STRESS 100% OF 0.2% OFFSET YIELD STRENGTH			
C26000	54	47	41	38
C51000	65	58	52	44
C52100	68	59	48	40
C72500	74	72	69	67
C77000	74	71	69	66

TABLE 19—*Stress relaxation in copper spring temper alloys—test temperature 200°C.*

	Remaining Stress After Hours Indicated, percent				
Alloy	1 h	20 h	100 h	300 h	1000 h
	INITIAL STRESS 50% OF 0.2% OFFSET YIELD STRENGTH				
C72500	79	71	67	65	61
C77000	78	70	64	59	54
	INITIAL STRESS 75% OF 0.2% OFFSET YIELD STRENGTH				
C72500	79	68	64	61	58
C77000	73	65	59	54	50
	INITIAL STRESS 100% OF 0.2% OFFSET YIELD STRENGTH				
C72500	71	64	61	58	55
C77000	69	61	55	51	47

C17200, the material was tested at four different stress levels—50, 75, and 100 percent of the 0.2 percent offset yield strength—and with an initial plastic strain of about 2 percent at 200°C. The results of these tests are shown in Fig. 3 for ¼HT temper. It was apparent that as the initial stress level was raised, some plastic deformation was introduced at the start of the test, but there was no pronounced increase in stress relaxation. At lower temperatures, where the relaxation was not as great, the difference between the curves for temperatures for different initial stresses also was less.

All of the strip specimens used to obtain the data presented were cut with the length of the strip in the rolling direction. Accordingly, the axis of bending when mounted on a mandrel was normal to the strip-rolling direction. In

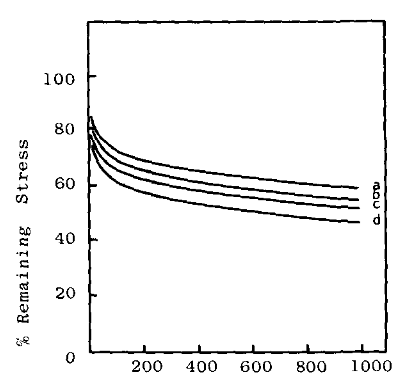

FIG. 3—*Stress relaxation in C17200 (Berylco 25), ¼HT temper, at 200°C with an initial strain of* (a) *50 percent of the 0.2 percent offset yield strength,* (b) *75 percent of the 0.2 percent offset yield strength,* (c) *100 percent of the 0.2 percent offset yield strength, and* (d) *a stress corresponding to 2 percent plastic strain.*

practice, strip may be bent in many directions other than normal to the rolling direction when a spring is formed. It is therefore of interest to know whether the stress relaxation characteristics are related to the rolling direction. To determine this effect, a test was conducted in which ¼HT temper C17200 alloy strip specimens were bent along an axis parallel to the rolling direction. Results for strip in the two orientations are shown in Fig. 4. At 22°C, there was no significant amount of relaxation in either specimen. At 200°C, there was a significant amount of relaxation, but the amount of relaxation was similar for both strip orientations. Any difference between the two would most likely be seen at 200°C. From these data, it appears that strip orientation was not important in determining stress relaxation.

Several tests were also run in which a separate test strip was used for each measurement during the 40-day period. This was done to determine whether restressing the strip after each measurement affected the results. This testing was performed using ¼HT and ½HT C17200 alloy at 150°C. The ¼HT material was tested at the yield strength, while the ½HT material was tested at 50 percent of the yield strength. Table 20 shows there was no significant difference between the single and multiple strip tests.

Summary

A study has been made of stress relaxation in three beryllium-copper alloys in strip form at temperatures between 20 and 200°C. The alloys studied were C17000, C17200, and C17500. The work was undertaken with the purpose of obtaining comprehensive stress relaxation data that would be useful in engineering design. Stress relaxation was measured as a function of temperature and initial stress for material in the AT, ¼HT, ½HT, and HT aged

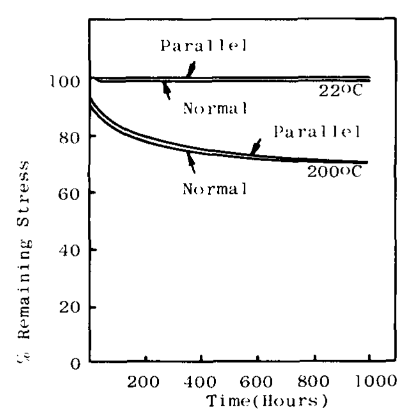

FIG. 4—*Comparison of the stress relaxation in C17200 alloy, ¼HT temper, when testing parallel and normal to the rolling direction at a stress level of 50 percent of the 0.2 percent offset yield strength.*

TABLE 20—*Stress relaxation in C17200 (Berylco 25) alloy—multiple and single strip test, test temperature 150°C.*

Temper	Strip Test	Remaining Stress After Hours Indicated, percent				
		1 h	20 h	100 h	300 h	1000 h
		INITIAL STRESS 100% OF 0.2% OFFSET YIELD STRENGTH				
¼HT	single	97	95	94	90	87
¼HT	multiple	99	94	95	91	90
		INITIAL STRESS 50% OF 0.2% OFFSET YIELD STRENGTH				
½HT	single	98	96	94	92	89
¼HT	multiple	96	94	94	92	89

tempers and in the age-hardenable condition. A test procedure applicable to strip specimens was chosen, because many of the commercial applications for beryllium copper in which stress relaxation is important concern strip material.

The mandrel test method was used. In this test, a strip specimen is stressed by wrapping it around a cylindrical mandrel to produce a desired initial outer fiber stress and exposing it to the test temperature. The change in the natural curvature of the strip when it is removed from the mandrel after a period of time at test temperature was used to calculate the relaxation of the initial outer fiber stress. Tests were run on each material for a total of 40 days. During this period, the strip specimen was removed periodically for a curvature measurement and then replaced on the mandrel. Three initial stress levels were employed for each material tested. These were 50, 75, and approximately 100 percent of the 0.2 percent offset yield strength.

The results show that aging greatly reduces stress relaxation in beryllium copper alloys. The annealed and aged tempers also show less relaxation than the cold-worked and aged tempers. Increasing the initial outer fiber stress from 50 to 100 percent of the 0.2 percent offset yield strength increased the measured relaxation, but the effect was not pronounced. For example, C17200 alloy, ½HT temper tested at 150°C, showed 89 percent of the initial outer fiber stress remaining after testing 40 days at 50 percent of the 0.2 percent offset yield strength. At 100 percent of the 0.2 percent offset yield strength, the remaining stress was 85 percent. A test in which the mandrel diameter was reduced so that about 2 percent strain was introduced into the sample showed a further increase in stress relaxation, but the increase was not pronounced. A number of tests run with strip cut parallel and normal to the rolling direction showed no apparent dependence of stress relaxation on strip orientation. Several tests were also run in which a separate test strip was used for each measurement during the 40-day period. This was done to determine whether restressing a strip after each measurement affected the results. Within the limits of experimental accuracy, no such effect was observed. For comparative purposes, a number of tests were also run on some other copper spring temper alloys. These included C26000, C51000, C52100, C72500, and C77000.

DISCUSSION

R. A. Piscitelli[1] (*written discussion*)—In mandrel test, how soon after removing the load on specimen must radius of curvature be measured? Will the radius of curvature measured depend on the length of time elapsed after removing the load? Have you checked this with the beryllium-copper alloys specifically Berylco 10, ½HT.

E. W. Filer and C. R. Scorey (*authors' closure*)—

It is, first of all, important that the specimen be cooled to room temperature before the load is removed. The authors' practice was to make radius of curvature measurements within 5 to 60 min of unloading. Reloading followed the measurement immediately. Tests on some heat-treated 25 alloy showed no difference in radius of curvature over a 5 to 60-min period. This was not checked on 10 alloy.

Because the rate of relaxation at room temperature is very slow, and the rapid initial relaxation occurring at elevated temperatures is not observed, no significant relaxation is expected in a period of minutes. Creep under the influence of residual stresses at room temperature could change the strip curvature. If this did occur, it would mean also that individual specimens would have to be used for each measurement.

Alfred Fox[2] (*written discussion*)—

1. In a recent paper, published in the *Journal for Testing and Evaluation*, May 1978 issue, we showed that for CA 172, one of the alloys discussed in your paper, the relaxation rate increases drastically at temperatures above 121°C (250°F) so that for higher operating temperatures we would not want to use this material for long time spring applications. In addition we found that material that had an initially higher degree of cold work and bending yield strength such as CA 172 condition TH04 (HT) relaxed more than solution annealed and precipitation heat treated material such as CA 172 condition TF00 (AT) so that the advantages of the higher initial maximum permissible working stress level for TH04 disappears as illustrated in the attached table. Do you have any comments on these observations?

[1] The Bendix Corporation, Electrical Components Division, Sidney, N. Y. 13838.
[2] Bell Laboratories, Murray Hill, N. J. 07974.

Estimated stress remaining after 40 years at 121°C (250°F) for CA 172 and Alloy 9244 (initial stress at approximately 80% of bending yield strength).

Alloy	Temper	Orientation	Initial Stress ksi	Initial Stress MPa	Estimated Stress Remaining After 40 Years at 121°C (250°F) ksi	MPa	Percent of Initial Value
CA 172	TF00 (AT)	parallel RD[a]	107	738	98	676	92
CA 172	TH01 (¼ HT)	parallel RD	104	717	94	648	90
CA 172	TH02 (½ HT)	parallel RD	128	882	102	703	80
CA 172	TH04 (HT)	parallel RD	138	951	96	662	70

[a] RD = rolling direction.

2. We also found that the stress relaxation behavior of solution annealed material is considerably improved with the precipitation heat treatment.

The following table obtained for material tested at an initial stress corresponding to 80 percent of the bending yield strength illustrates the point. Solution annealed material is generally not used since springs are generally formed from such material which has good formability and then precipitation heat-treated to obtain high resistance to stress relaxation (at temperatures below 121°C).

Effect of precipitation heat treatment on stress relaxation of CA 172 TD01 (¼H).

Test Temperature °F	Test Temperature °C	Stress Remaining, % of Initial After 4 h at Temperature Shown ($\sigma_0/\sigma_y = 0.8$) Solution Annealed (TD01)	Precipitation Heat-Treated (TH01)
73	23	92.5	99.2
250	121	84.1	97.0
350	177	65.3	93.3
450	232	20.6	79.6

In view of this observation, however, do you have any comments relative to the use of mill hardened copper-beryllium alloy for springs?

E. W. Filer and C. R. Scorey (authors' closure)—

1. The increase in relaxation above 121°C referred to is shown also by our results at 100, 150, and 200°C. For critical application requiring a

40 year service life, it may not be possible to use temperatures above 120°C. With other less stringent applications requiring perhaps less than a 40 year service life, temperatures up to 150°C or even higher may be possible.

We also find HT tempers relax more than AT material, and that where possible AT is preferred over HT. Since the tensile property ranges of AT and HT overlap to some extent, it may be possible to select AT material at the high end of the property range for stress relaxation applications.

The short time or initial relaxation may often be engineered out of a part. This is done by exposing the formed part to the service temperature for a few hours prior to installation. The initial spring deflection must be such that after the first stage of relaxation has taken place the remaining spring force is at the high end of the required operating range. Since the initial relaxation is larger with ½HT and HT tempers than it is with AT and ¼HT tempers, some advantage can be regained for the higher initial maximum permissible working stress level for TH04.

2. We do not recommend that the unheat-treated tempers be used for applications where stress relaxation is important. The mill-hardened tempers of beryllium copper are normally heat-treated after cold working (exceptions may be 10 HTC or 10 HTR) but the heat treatment is not always optimum for stress relaxation performance. Normal heat-treated tempers are preferred for applications requiring the best possible stress relaxation behavior.

K. Amin[3] (*written discussion*)—You showed, in ¼HT alloy (Berylco 25), no effect of specimen orientation on stress relaxation is observed. Have you done any testing on ½HT, HT, or even only cold-rolled strips to see that effect? We believe that different temper conditions like HT, H, etc. would definitely show a dependence on orientation, specially knowing that residual stresses (measured) on H condition along the rolling direction at our laboratories show values as high as 300 MPa. Would you please comment on that?

E. W. Filer and C. R. Scorey (*authors' closure*)—I think I recall testing two 25 alloy tempers for orientation dependence. I doubt that the other would have been unheat-treated. An HT-temper might well show a greater effect than a ¼HT because of the greater cold work.

An unheat-treated H temper strip will certainly contain high residual stresses which would vary with orientation. No tests were conducted on such material because it is not a temper normally used in beryllium copper spring applications. Insofar as the stress relaxation in heat-treated beryllium copper has been found not to show a pronounced dependence on the

[3] Bendix Research Laboratories, Southfield, Mich. 48076.

initial stress, changes in relaxation with orientation because of residual stresses likewise, would not be expected to be pronounced. Residual stresses may be important sometimes with heat-treated strip as a result of slitting stresses.

P. Parikh[1]

Report on Bending Stress Relaxation Round Robin

REFERENCE: Parikh, P., "**Report on Bending Stress Relaxation Round Robin,**" *Stress Relaxation Testing, ASTM STP 676*, Alfred Fox, Ed., American Society for Testing and Materials, 1979, pp. 112–125.

ABSTRACT: Three laboratories participated in a bending stress relaxation, round robin, test program. Elastic springback, continuous force measurement, and lift-off methods were used to determine stress remaining. Cold-rolled copper alloys CDA 110 (ETP copper) and CDA 260 (70-30 brass) at thicknesses of 0.05, 0.1, and 0.25 cm were utilized. All tests were conducted at 105°C up to about 200 h according to the ASTM Recommended Practice for Stress Relaxation Tests for Materials and Structures (E 328-75). The results show that the agreement among the three methods is quite good.

KEY WORDS: mechanical tests, bending, stress relaxation, elastic springback, lift-off method, continuous force measurement, round robin, copper alloys

The ASTM Recommended Practice for Stress Relaxation Tests for Materials and Structures (E 328-75) consists of three parts, covering testing in tension, compression, and bending. Of these three, the recommended practice for bending was recently introduced. This practice allows for three different ways of determining stress relaxation data. These are:

1. Continuously reading force indicator.
2. Force required to lift the specimen free of one or more constraints during the test period.
3. Elastic springback upon unloading at the end of the test period.

No comparative data for these different test methods are published. Therefore a task group was set up at the meeting of Subcommittee E28.11 held in Philadelphia on 2 Dec. 1975, to conduct a bending stress relaxation

[1] Engineering specialist, Mechanical Metallurgy Group, Olin Metals Research Laboratories, New Haven, Conn. 06511.

round robin. Three laboratories—Bell Laboratories, General Electric, and Olin Metals Research Laboratories—participated in the round robin using materials supplied from the same source. Bell Laboratories used the elastic springback method, General Electric used the continuous force measurement method, and Olin used the lift-off method. This paper summarizes the results of the bending stress relaxation round robin.

Test Materials

Alloys CDA 110 (ETP copper) and CDA 260 (70-30 brass) were processed from commercial hot rolled plate at Olin Metals Research Laboratories to final thicknesses of 0.05, 0.1, and 0.25 cm. The final cold reduction for all thicknesses was 40 percent. The grain size after final annealing was 0.020 to 0.030 mm. Cold rolling between earlier annealing treatments was varied in order to achieve the same final cold reduction at different final thicknesses. The recrystallization anneal prior to final cold rolling was the same for all thicknesses. Tension tests were done on duplicate specimens at room temperature. Table 1 summarizes the tension test data, which show no significant thickness dependence.

Test Procedure

The initial test conditions for all three test methods were aimed at stress or strain levels corresponding to 80 percent of the 0.02 percent offset yield strength (low stress) and 80 percent of the 0.2 percent offset yield strength (high stress). The duration of the test was about 200 h. Test temperature was 105°C.

Bell Laboratories

The details of the elastic springback method has been described previously.[2] The test specimen is a tapered cantilever loaded at the vertex of an equilateral triangle. In order to study the thickness effect, 0.05 and 0.1-cm-thick specimens were used. The test specimen is loaded at room temperature by means of a wedge to the desired deflection and inserted into the oven at the test temperature. After a preselected time has elapsed, the test specimen block assembly is removed from the oven and allowed to come to room temperature. The wedge is removed, and the permanent set at the vertex of the triangle is measured. The same specimen is reloaded and the test continued. Since the Recommended Practice E 328-75 does not allow the use of the same specimen, a few tests were conducted utilizing

[2] Fox, A., *Journal of Materials*, Vol. 6, No. 2, June 1971, pp. 422–435.

TABLE 1—*Tension test data.*

Alloy	Thickness, cm	0.02% Yield Strength, MPa (ksi)	0.2% Yield Strength, MPa (ksi)	Ultimate Tensile Strength, MPa (ksi)
CDA 110[a]	0.05	245.5 (35.6)	313.7 (45.5)	332.3 (48.2)
	0.10	227.5 (33.0)	320.6 (46.5)	331.6 (48.1)
	0.25	227.5 (33.0)	308.2 (44.7)	322.7 (46.8)
CDA 260[b]	0.05	322.7 (46.8)	533.0 (77.3)	568.8 (82.5)
	0.10	328.9 (47.7)	534.4 (77.5)	578.5 (83.9)
	0.25	327.5 (47.5)	515.7 (74.8)	563.3 (81.7)

[a] Tensile modulus = 117.2×10^3 MPa (17×10^6 psi).
[b] Tensile modulus = 112.4×10^3 MPa (16.3×10^6 psi).

different specimens. The following formulas are used for determining initial condition and stress remaining:

1. Initial strain ϵ_0 is calculated by dividing the desired stress by the modulus of elasticity.
2. Initial radius of curvature is then $R_0 = \frac{1}{2}t(1/\epsilon_0 + 1)$, where t is the thickness.
3. Angle included between the normals to the fixed and free specimen ends is $\theta_0 = l_0/R_0$, where l_0 is the specimen length.
4. Initial deflection, $Y_0 = R_0\,(1 - \cos\theta_0)$.
5. Springback is $(Y_0 - \Delta Y)/Y_0$, where ΔY is the permanent deflection of the free end at any time. Springback is assumed to measure percent stress remaining.
6. In order to compare stress remaining values obtained by the springback method with those obtained by the other two methods, a correction in the springback due to initial permanent deflection is required. The initial permanent deflection at room temperature is subtracted from both Y_0 and ΔY to obtain Y_0' and $\Delta Y'$, respectively. Corrected springback is $(Y_0' - \Delta Y')/Y_0'$. This correction is negligible for stress levels near 80 percent of the 0.02 percent yield strength.

General Electric

A four-point loading system with a continuously load-monitoring system at test temperature was used. The outer supports are 16.5 cm apart, and the inner loading points are 11.4 cm apart. In order to keep the moment arms constant, the knife edges should be prevented from slipping. This was accomplished by allowing them to rest against seats that were glued onto the specimen at the four locations. The specimen is nominally 1.27 cm wide and 0.25 cm thick. A spherometer is used to monitor and thus maintain the bending strain constant (E 328-75) during the test. The spherometer was calibrated with the use of a brass specimen instrumented with strain gages. The specimen is loaded to the desired strain level when at test temperature. The loading is manually controlled to achieve a constant strain rate. A continuous record of load remaining is obtained at the test temperature.

Load curves are determined using a three-point loading geometry to establish the initial conditions. An extensometer is used to measure deflection from which the strain could be calculated. Strain is given by $\epsilon = t/2R$, and R is calculated from the equation

$$(R + t/2 + \Delta Y)^2 + a^2 = (R + t/2)^2$$

where

a = distance between the central and outer loading points,
t = thickness, and
ΔY = deflection at the center.

Load values are used to calculate stress with the use of the flexure formula. The initial strain ϵ_0 is calculated with the formula $\epsilon_0 = t/2R$.

Bell Laboratories and Olin measure springback and load remaining, respectively, at room temperature after the exposure at test temperature, and General Electric measures load remaining at the test temperature. For comparison purposes, General Electric's data are corrected for the modulus differences at 105°C and room temperature. Accordingly, the percent stress remaining values are reduced by about 3.5 percent.[3]

Olin Metals Research Laboratories

The details of the lift-off method are described in a recent publication.[4] A double-triangle-shaped specimen is loaded at the specimen center via a plunger, while the specimen is held at both ends. The specimen is nominally 0.1 cm thick. The initial load corresponding to the desired initial stress is calculated using the elastic flexure formula. When the desired load is reached, the loading plunger is locked in place for the duration of the test. This assures a constant specimen curvature at all times. The fixture is then put into the furnace at test temperature. Periodically, the fixture is taken out of the furnace and allowed to come to room temperature. The load remaining in the specimen is determined at room temperature using the lift-off method. The initial strain ϵ_0 is calculated from the deflection of the specimen and the specimen geometry.

[3] Wawra, H. H., *Metallurgy*, Vol. 28, Dec. 1974, pp. 1168-1175.
[4] Parikh, P. and Shapiro, E., *Recent Developments in Mechanical Testing, ASTM STP 608*, American Society for Testing and Materials, Sept. 1976, pp. 106-117.

Results and Discussion

Stress relaxation data for CDA 110 are summarized in Tables 2 through 4, and those for CDA 260 are summarized in Tables 5 through 7. Data from duplicate tests on CDA 260 (initial stress level at 80 percent of the 0.2 percent yield strength) are shown in Tables 6 through 8. The data in Tables 2 through 7 are plotted in Figs. 1 through 4 as percent stress remaining versus time. Bell Laboratories and General Electric data plotted are corrected for initial permanent deflection and modulus differences, respectively.

Initial stress σ_0 reported in Tables 2 through 7 is the tensile stress at a strain equal to the outer fiber strain ϵ_0 and is obtained from the tensile stress-strain curve. This method of defining the initial condition is suitable here because all three methods provide strain data. The comparison of initial condition is thus on the same basis.

The differences among the three laboratories in the initial strain and stress conditions at both stress levels are significant. However, percent stress remaining at both stress levels for each alloy (Fig. 1 versus Fig. 2 and Fig. 3 versus Fig. 4) is about the same. Therefore, the comparison of stress relaxation data at each stress level is acceptable in spite of such large spread in the initial conditions. For materials that do not show stress independence of percent stress remaining, stress relaxation data should only be compared for a narrow range of the initial conditions.

The curves in Figs. 1 through 4 show similar slopes, indicating that the data from different methods are in good agreement. All data lie within a band of ± 5 percent stress remaining. Duplicate results in Tables 6 through 8 indicate that the reproducibility in different test methods is of the same order.

Bell Laboratories' data show that within 0.05 to 0.1 cm thickness, springback is not thickness dependent. The comparison of springback data from single specimen and different specimens in Table 9 suggests that, in the case of copper alloys, the error from using a single specimen to determine the entire stress relaxation curve is not large.

Springback test method, in contrast with the lift-off method and the continuous load measurement method, requires that proper correction due to initial permanent deflection be made. This correction is expected to depend upon the alloy, the processing, and the initial stress level.

Conclusion

The agreement between the springback, the lift-off, and the continuous load recording methods is quite good—± 5 percent stress remaining.

In order to compare stress remaining determined by an indirect method such as the springback with that determined by direct methods such as the

TABLE 2—*Bell Laboratories—CDA 110 stress relaxation data.*

	Percent Springback			
	Low Stress[a]		High Stress[b]	
Time, h	t = 0.0523 cm Y_0 = 0.208 cm ϵ_0 = 0.00192 σ_0 = 210.5 MPa (30.5 ksi)	t = 0.1036 cm Y_0 = 0.094 cm ϵ_0 = 0.00174 σ_0 = 195.3 MPa (28.3 ksi)	t = 0.0531 cm Y_0 = 0.239 cm Y_0' = 0.213 cm ϵ_0 = 0.00225 σ_0 = 242.9 MPa (35.2 ksi)	t = 0.1036 cm Y_0 = 0.163 cm Y_0' = 0.145 cm ϵ_0 = 0.00297 σ_0 = 286.4 MPa (41.5 ksi)
0	100	100	100	100
2	74	75	71 (80)	66 (78)
6	70	68	67 (75)	62 (74)
25	63	59	61 (68)	58 (70)
71	59	54	56 (60)	52 (64)
216	51	48	53 (58)	48 (60)

[a] Percent springback not corrected for initial permanent deflection.
[b] Parentheses show values corrected for initial permanent deflection.

TABLE 3—*General Electric—CDA 110 stress relaxation data.*

Time, h	Percent Stress Remaining[a]: Low Stress, t = 0.254 cm, ϵ_0 = 0.00193, σ_0 = 210.5 MPa (30.5 ksi)	Percent Stress Remaining[a]: High Stress, t = 0.254 cm, ϵ_0 = 0.00374, σ_0 = 323.6 MPa (46.9 ksi)
0	100	100
1	84 (81)	81 (78)
2	80 (77)	...
6	77 (74)	71 (70)
10	75 (72)	71 (69)
30	71 (69)	64 (62)
70	65 (63)	60 (58)
90	64 (62)	...

[a] Parentheses show values corrected for modulus differences between room temperature and 105°C.

TABLE 4—*Olin—CDA 110 stress relaxation data.*

Low Stress, t = 0.1031 cm, ϵ_0 = 0.00168, σ_0 = 187.7 MPa (27.2 ksi)		High Stress, t = 0.1031 cm, ϵ_0 = 0.00249, σ_0 = 257.4 MPa (37.3 ksi)	
Time, h	Percent Stress Remaining	Time, h	Percent Stress Remaining
0	100	0	100
1	73	1	73
6	68	6	67
24	61	24	60
49	59	49	57
103	54	100	52
175	51	172	49
247	50	244	47

TABLE 5—*Bell Laboratories—CDA 260 stress relaxation data.*

	Percent Springback			
	Low Stress[a]		High Stress[b]	
Time, h	$t = 0.0526$ cm $Y_0 = 0.259$ cm $\epsilon_0 = 0.00241$ $\sigma_0 = 246.3$ MPa (35.7 ksi)	$t = 0.1036$ cm $Y_0 = 0.142$ cm $\epsilon_0 = 0.00260$ $\sigma_0 = 267.7$ MPa (38.8 ksi)	$t = 0.0521$ cm $Y_0 = 0.511$ cm $Y_0' = 0.427$ cm $\epsilon_0 = 0.00475$ $\sigma_0 = 433.3$ MPa (62.8 ksi)	$t = 0.1041$ cm $Y_0 = 0.249$ cm $Y_0' = 0.218$ cm $\epsilon_0 = 0.0046$ $\sigma_0 = 422.3$ MPa (61.2 ksi)
0	100	100	100	100
2	81	85	68 (82)	76 (86)
6	76	82	64 (78)	73 (83)
25	72	77	60 (72)	68 (77)
71	69	74	57 (69)	65 (74)
216	65	71	54 (64)	62 (70)

[a] Percent springback not corrected for initial permanent deflection.
[b] Parentheses show values corrected for initial permanent deflection.

TABLE 6—*General Electric—CDA 260 stress relaxation data.*

Time, h	Percent Stress Remaining[a]		
	Low Stress	High Stress	
	t = 0.254 cm ϵ_0 = 0.00235 σ_0 = 240.8 MPa (34.9 ksi)	t = 0.254 cm ϵ_0 = 0.00525 σ_0 = 460.2 MPa (66.7 ksi)	t = 0.254 cm ϵ_0 = 0.00530 σ_0 = 465.0 MPa (67.4 ksi)
0	100	100	100
1	93 (90)	87 (84)	88 (85)
2	91 (88)	85 (82)	...
6	87 (84)	82 (79)	80 (77)
20	82 (79)	76 (73)	76 (73)
70	75 (72)	73 (70)	71 (69)
90	75 (72)	71 (69)	...
100	74 (71)	71 (69)	...

[a] Parentheses show values corrected for modulus differences between room temperature and 105°C.

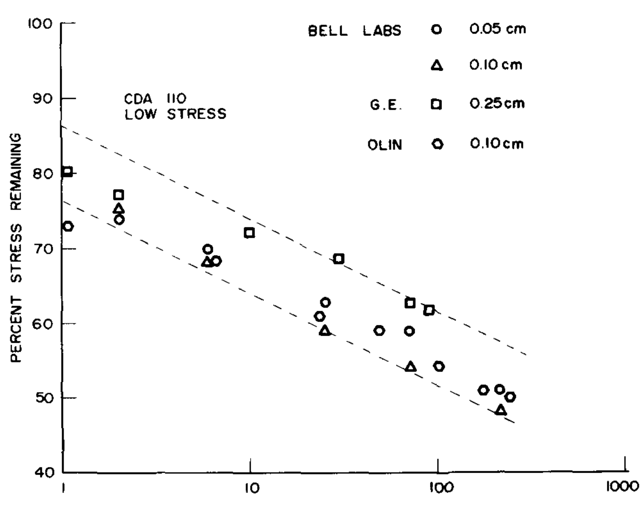

FIG. 1—*Percent stress remaining versus time for CDA 110 (ETP copper); initial stress equals 80 percent of 0.02 percent yield strength.*

TABLE 7—*Olin—CDA 260 stress relaxation data.*

Low Stress		High Stress			
$t = 0.1034$ cm, $\epsilon_0 = 0.00233$, $\sigma_0 = 240.8$ MPa (34.9 ksi)		$t = 0.1024$ cm, $\epsilon_0 = 0.00474$, $\sigma_0 = 433.3$ MPa (62.8 ksi)		$t = 0.1034$ cm, $\sigma_0 = 433.3$ MPa (62.8 ksi)	
Time, h	Percent Stress Remaining	Time, h	Percent Stress Remaining	Time, h	Percent Stress Remaining
0	100	0	100	0	100
1	84	1	82	1	81
6	78	5	81	6	78
24	75	25	76	24	75
49	72	73	71	49	74
99	70	193	69	98	71
171	68	265	68	170	71
243	67			218	70
				242	69

TABLE 8—*Bell Laboratories—duplicate test results for CDA 260—high stress.* [a]

	Percent Springback			
Time, h	$t = 0.0521$ cm $Y_0 = 0.511$ cm $\epsilon_0 = 0.00475$	$t = 0.0523$ cm $Y_0 = 0.500$ cm $\epsilon_0 = 0.00470$	$t = 0.1041$ cm $Y_0 = 0.249$ cm $\epsilon_0 = 0.00460$	$t = 0.1034$ cm $Y_0 = 0.252$ cm $\epsilon_0 = 0.00460$
0	100	100	100	100
2	68	71	76	76
6	64	67	73	72
25	60	62	68	68
71	57	59	65	64
216	54	56	62	61

[a] Not corrected for initial permanent deflection.

TABLE 9—*Bell Laboratories—stress relaxation data using virgin specimens*[a] *for each time period.*

	Percent Springback			
	CDA 110		CDA 260	
Time, h	Low Stress t = 0.0530 cm Y_0 = 0.218 cm ϵ_0 = 0.002115 σ_0 = 227.7 MPa (33.0 ksi)	High Stress t = 0.1041 cm Y_0 = 0.160 cm ϵ_0 = 0.00297 σ_0 = 286.4 MPa (41.5 ksi)	Low Stress t = 0.0526 cm Y_0 = 0.0239 cm ϵ_0 = 0.002214 σ_0 = 224.9 MPa (32.6 ksi)	High Stress t = 0.1041 cm Y_0 = 0.251 cm ϵ_0 = 0.0046 σ_0 = 422.3 MPa (61.2 ksi)
0	100	100	100	100
25	62 (61)	55 (58)	77 (72)	64 (68)
216	56 (53)	42 (48)	61 (65)	62 (62)

[a] Values in the parentheses are measured when the same specimen is used throughout the relaxation test.

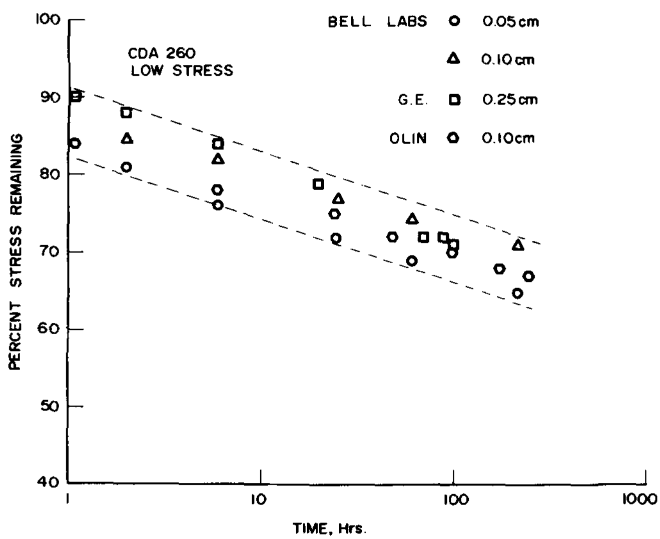

FIG. 2—*Percent stress remaining versus time for CDA 110 (ETP copper); initial stress equals 80 percent of 0.2 percent yield strength.*

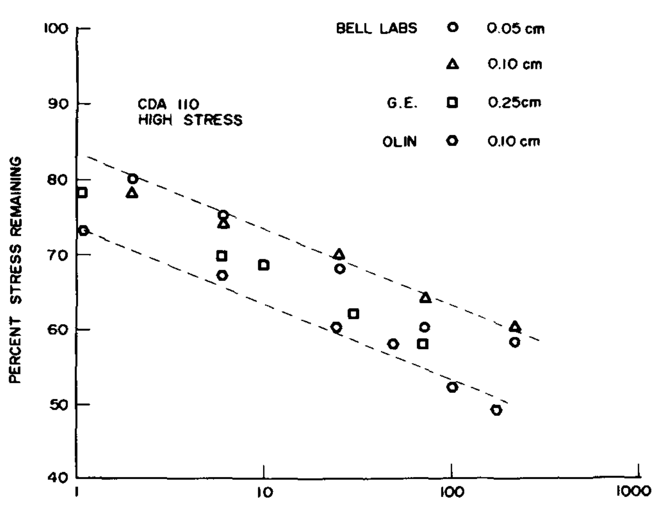

FIG. 3—*Percent stress remaining versus time for CDA 260 (70-30 brass); initial stres equals 80 percent of 0.02 percent yield strength.*

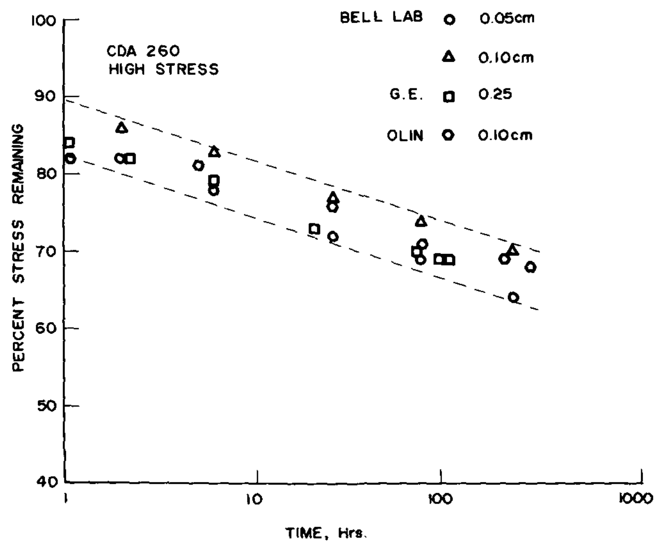

FIG. 4—*Percent stress remaining versus time for CDA 260 (70-30 brass); initial stress equals 80 percent of 0.2 percent yield strength.*

continuous load measurement or the lift-off, the correction due to differences in the initial condition should be made.

Acknowledgments

Discussions with A. Fox and A. K. Schmieder are acknowledged.

A. Y. C. Lou[1]

Negative Stress Relaxation in Polyurethane Induced by Volume Shrinkage

REFERENCE: Lou, A. Y. C., "**Negative Stress Relaxation in Polyurethane Induced by Volume Shrinkage,**" *Stress Relaxation Testing, ASTM STP 676*, Alfred Fox, Ed., American Society for Testing and Materials, 1979, pp. 126-139.

ABSTRACT: An unusual increase in stress due to volume shrinkage under constant constraint conditions was observed when a Caytur 21 extended Adiprene polyurethane specimen was tested at 121°C (250°F) and 1 percent constant strain. The stress first decreased for 2 h and then actually increased until the test had progressed for about 40 h, when it again started to decrease. This stress enhancement was attributed to contraction of the hard segments brought about at the relatively high test temperature by conversion of branching biuret linkages to linear urea linkages in the presence of free amine. The resulting increase in density causes shrinkage in volume, thus produces stress buildup. After 40 h, the usual stress relaxation process becomes dominant again. This phenomenon was found to be closely associated to Caytur 21 and to depend strongly on the temperature and strain conditions. However, it was insensitive to isocyanate (NCO) content and Caytur amount.

KEY WORDS: negative stress relaxation, stress enhancement, stress buildup, stress relaxation, heat treatment, urea linkage, biuret linkage, free amine

The basic aspects of the chemistry of isocyanates and polyurethanes and their physical properties and rapidly expanding applications were discussed extensively in the two excellent volumes by Saunders and Frisch [*1,2*].[2] In a recent publication by Alliger et al [*3*], scientists at Firestone Central Research Laboratories discovered that MOCA extended Adiprene polyurethanes are stable, resilient rubbers with good viscoelastic properties when their stoichiometries (NH_2/NCO mole ratio) are equal or slightly greater than unity. Studies showed, for the first time, that some of the critical material properties, such as fatigue life, tear, and creep resistance

[1] Senior research scientist, Central Research Laboratories, The Firestone Tire and Rubber Co., Akron, Ohio 44317.

[2] The italic numbers in brackets refer to the list of references appended to this paper.

under dynamic loads, became optimum at a stoichiometry of 0.98 to 1.08. This was done without sacrificing Young's modulus. Only limited flex data on polyester MOCA and polyester Caytur 21 polyurethanes have been published [4].

Creep and stress relaxation are important properties of load-bearing structures, so any anomaly of these characteristics is of interest. During a stress relaxation test on Caytur 21 extended polyurethane, an unexpected increase rather than a decrease of stress occurred for part of the observation period. Such behavior is rare, and this instance cannot be attributed to the same mechanism as that responsible for the axial stress increase in *trans*-polyisoprene held at constant elongation [5] or the axial length decrease in cross-linked polyethylene held under constant force [6,7]. Both of these phenomena occurred during the later stage of crystallization. Gent [5] attributed his finding primarily to the relatively large volume contraction produced on crystallization of *trans*-polyisoprene, while in the latter case, the authors attributed the phenomenon to folded-chain crystallization.

The stress relaxation tests described here were made as part of a study on the morphology and kinetics of the molecular structure of Caytur 21 cured polyurethanes. This includes several component variations and changes in test conditions. Since the negative stress relaxation had been observed at the relatively high test temperature of 121°C (250°F), some investigations of the chemical processes and physical changes that occur at this temperature seem desirable.

Experiment

Material Preparation

The six polyurethane materials listed in Table 1 differ in prepolymer, curative, isocyanate (NCO) content and stoichiometry. The Adiprene prepolymers used were prepared from polytetramethylene ether glycols

TABLE 1—*Polyurethane materials.*

Stock	Prepolymer	NCO Content, %	Curative	Stoichiometry (NH_2/NCO)
A	Adiprene L367	6.45	Caytur 21	1.025
B	80/20 Adiprene L367/PPG 3025	5.67	Caytur 21	1.025
C	Adiprene L167	6.27	Caytur 21	1.025
D	77/23 Polymeg 1000/Hylene TM	4.88	Caytur 21	1.025
E	77/23 Polymeg 1000/Hylene TM	4.88	Caytur 21	1.100
F	Adiprene L167	6.27	MOCA	1.025

(PTMEG) and tolylene diisocyanate (TDI) with either Caytur 21 or MOCA as curatives. Some of the prepolymers were commercially available, and others were prepared in the laboratory to achieve desired NCO contents. They were prepared by first adding predried plasticizer, dioctylphthalate (DOP), and then curative into the degassed prepolymer. The resultant compound was poured into preheated molds and cured at 120°C for 2 h. The NH_2/NCO ratio was controlled by the NCO content in the prepolymer and the amount of curative. Twenty parts by weight of DOP were used in 100 parts of prepolymer for all specimens.

Specimens

Tension specimens, 6.34 mm (0.25 in.) wide and 152 mm (6 in.) long, were die cut from compression-molded slabs of 152 by 152 by 1.9 mm (6 by 6 by 0.075 in.). Gage length (distance between grips) was set to be 76 mm (3 in.) for all tests.

Apparatus

A floor model Instron tester was used for these stress relaxation tests. An air cylinder was installed between the lower-grip extension rod and cross-head to apply an "instant" step deformation. Temperature control was within ± 0.6°C (± 1°F).

Stress Relaxation Test

A step deformation was applied "instantaneously" at a rate of approximately 400 mm/s (15 in./s) by the air cylinder and held at a constant temperature. Unless otherwise specified, all tests were made on specimens of Stock A (see Table 1). Stress relaxation data were recorded on the Instron recorder.

Negative Stress Relaxation

Although the validity of time-temperature superposition as applied to materials other than homogeneous polymers is unproven, our studies suggested that relaxation moduli of several Adiprene polyurethane materials cured by either Caytur or MOCA are shiftable to follow a power law form [*3*]. Therefore, time-temperature superposition was used to construct master relaxation curves for these materials.

Since each master curve of stress as a function of relaxation time followed a straight line on a double logarithmic scale over most of its length, only a short segment of a master curve is needed to determine the slope that represents its viscoelastic property [3]. However, these straight lines dropped off sharply at long times, probably because of either viscoelastic terminal effect due to entanglement breakdown or chemical degradation. Therefore, stress relaxation results measured at a high temperature for a relatively short time may be used to represent the long-time response at a lower temperature. The straight line can be extended to the left on a log-log plot to cover the entire time range. The slope of this straight line is a viscoelastic property, and its value at very short time is an elastic modulus. Extension of this straight line to the right is not possible, since the time for onset of viscoelastic terminal zone or chemical degradation is unknown.

A stress relaxation test at the highest possible temperature can cover the widest time range; it may also explain the reasons for the sharp drop-off in master curves. Therefore, a test was made at 121°C (250°F) on Stock A. The test was continued for 65 h, which permitted measurements corresponding to more than five decades of real time in seconds. One percent strain was used in order to keep the viscoelastic response in the linear range. About four decades of good fit was found when a straight line was drawn through the data points on a log-log scale. After that, an unusual enhancement of stress was observed.

As shown in Fig. 1, the stress started to increase sharply after 2 h of relaxation time, then proceeded at the fastest rate for about 10 h. It reached a maximum plateau after 26 h and started to drop off slowly after 40 h. The stress remained 35 percent higher at 65 h than that at 2 h. A strong contraction mechanism obviously occurred, one that became greater after 2 h relaxation under 1 percent strain.

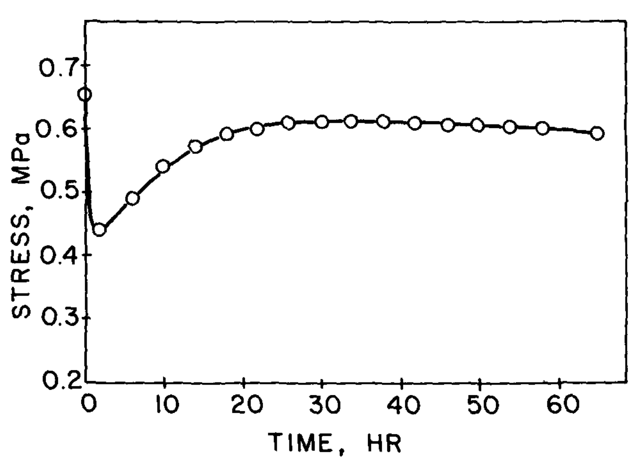

FIG. 1—*Negative stress relaxation of Caytur 21 cured polyurethane at 121°C (250°F) and 1 percent strain.*

Effect of Prepolymer and Curative

Prepolymer, curative, and cure condition control the molecular structure in polyurethane. The basic system studied in this paper consisted of Adiprene L367[3] as prepolymer and Caytur 21[3] as curative, that is, Stock A. A different composition was prepared in the laboratory by blending prepolymers of 20 parts by weight of polypropylene glycol (PPG-3025[4])-TDI and 80 parts of Adiprene L367 and then extended by Caytur 21, that is, Stock B. One day's stress relaxation data at 121°C and 1 percent strain, shown in Fig. 2, indicate that the presence of PPG-3025 reduced the buildup in stress by 65 percent. The stress reached a maximum at about 14 h, probably because polyurethane with PPG-3025 as prepolymer is more time dependent than that with Adiprene as prepolymer. The relaxation mechanism overcomes the shrinking force at an early time.

Caytur 21 is a complex of methylene dianiline with sodium chloride. The complex contains 92 percent of dianiline and is dispersed in DOP before adding to the prepolymer. MOCA is methylene bis-*o*-chloroaniline, a solid with low melting point. It is melted before being added to the prepolymer. Stress relaxation results in Fig. 2 showed almost negligible enhancement in stress for a MOCA cured stock, Stock F.

Effect of NCO Content and Stoichiometry

The function of NCO content in TDI prepolymer is to control the amount of hard segment generated. Therefore, the elastic modulus increases with increasing NCO content. Stoichiometry, in turn, is controlled by the amount of curative added at a given NCO level. The effect of stoichiometry on material properties is less than that of NCO content. The material properties become undesirable, however, when the stoichiometry falls lower or higher than the optimum level [*3*].

As shown in Table 1, different NCO contents in prepolymer were prepared for Stocks A, C, and D. Stress relaxation curves of these stocks in Fig. 3 show that they may be shiftable vertically. This indicates a strong dependence of elastic modulus on NCO content. However, the time-dependent enhancement in stress was not affected by changes in NCO content. Furthermore, a change of stoichiometry from 102.5 percent (Stock D) to 110 percent (Stock E) did not alter either the elastic or the viscoelastic response appreciably, as shown in Fig. 3.

Effect of Strain Level

Stress relaxations at 1 and 5 percent strains were studied and are com-

[3] Commercially available from E. I. duPont de Nemours & Company, Inc.
[4] Commercially available from Union Carbide Corp.

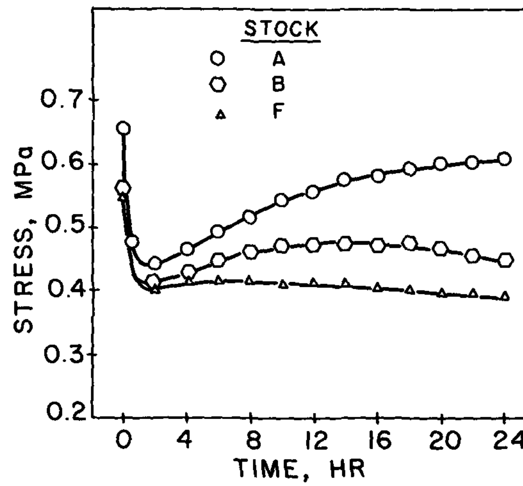

FIG. 2—*Effect of prepolymer and curative on stress relaxation at 121°C (250°F) and 1 percent strain.*

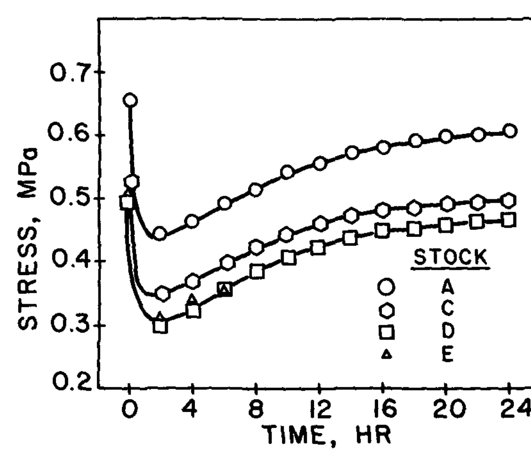

FIG. 3—*Effect of NCO level and stiochiometry on stress relaxation at 121°C (250°F) and 1 percent strain.*

pared in Fig. 4. The relaxation modulus at 5 percent shows continuous decay at 121°C, that is, the relaxation prevails over the relatively small contractive force.

Effect of Temperature

Stress relaxation tests were carried out with 1 percent strain at three temperatures—27, 93, and 121°C. The results are plotted in Fig. 5. No

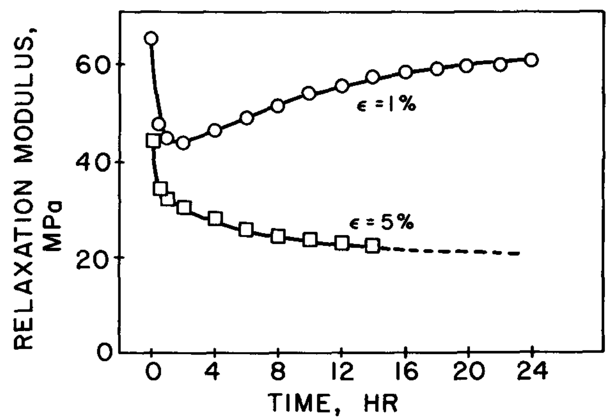

FIG. 4—*Effect of strain level on stress relaxation of Stock A at 121°C (250°F).*

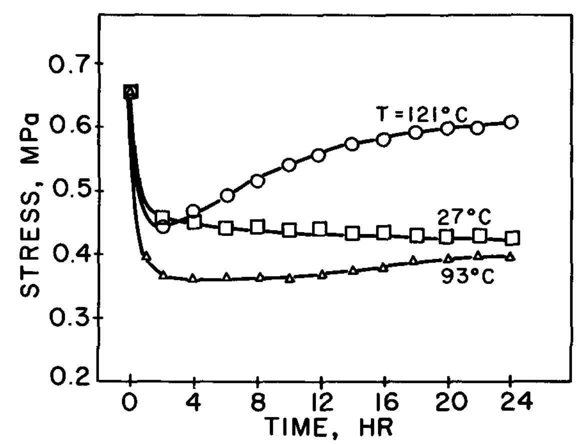

FIG. 5—*Effect of temperature on stress relaxation of Stock A at 1 percent strain.*

stress enhancement was found at 27°C. The stress relaxed more at 93°C than that at 27°C and showed a small stress buildup after 4 h of relaxation. However, a sharp increase in stress at 2 h was observed at 121°C, which indicates that a strong contractive force developed within the material at this temperature. Therefore, stress measured at 2 h is higher at 121°C than at 93°C. The elastic responses were approximately the same at all three temperatures.

Effect of Heat Treatment

It is apparent that this negative stress relaxation depends strongly on temperature. Different processes of heat treatment were given before stress relaxation tests. The results are shown in Fig. 6.

The stress enhancement becomes less prominent as the time in heat treatment increases. After 87 h treatment at 121°C, the stress relaxed continuously with 1 percent strain at 121°C. The same result can be achieved at shorter time with higher temperature (say 138°C for 24 h), which indicates the speedup of disappearance of the contractive phenomenon at a higher temperature. The elastic modulus was found to be unaffected by heat treatment while the ultimate properties—strength and elongation at break—were improved somewhat.

Normal relaxation in stress was observed for heat-treated (121°C for 96 h) specimens tested at three temperatures as shown in Fig. 7. The magnitude of stress decay increased with rising temperature. The contractive mechanism in Caytur 21 extended polyurethane disappeared from heat treatment (post cure) alone.

Discussion of Results

The stress enhancement observed in a stress relaxation experiment on Caytur 21 cured polyurethane specimen at 121°C and 1 percent strain indicates a change in its molecular structure during the test, which creates a strong contractive force. This phenomenon is related closely to Caytur 21 and depends strongly on temperature. It was also found to be insensitive to NCO content and Caytur amount. However, 20 parts of PPG blended with 80 parts of Adiprene in prepolymer reduced the stress buildup sub-

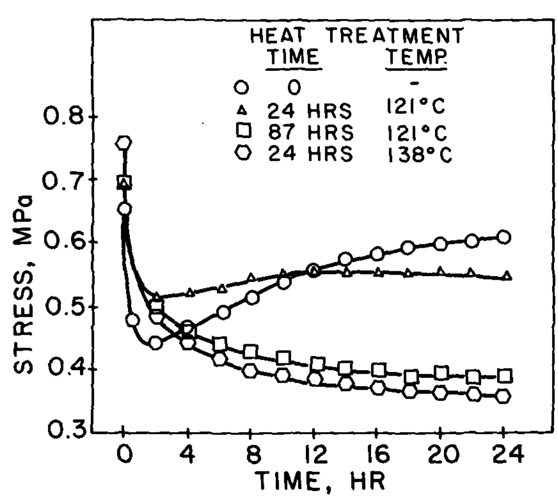

FIG. 6—*Effect of heat treatment on stress relaxation at 121°C (250°F) and 1 percent strain.*

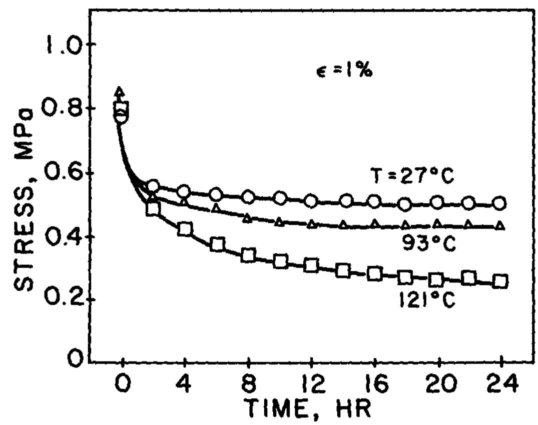

FIG. 7—*Effect of temperature on stress relaxation of Stock A heat treated at 121°C for 96 h.*

stantially. The following possible sources of negative stress relaxation have been studied.

Crystallinity

It has been reported that crystallization in either stress relaxation or creep may generate contraction in some polymers [5-7]. Therefore, the formation of crystals in the soft domain of polyurethane specimens during stress relaxation at 121°C under 1 percent strain might have caused the stress enhancement. Wide-angle X-ray diffraction examination of six specimens with different time history of stress relaxation, however, showed no detectable difference in amount of crystallinity. This indicates that the stress relaxation procedure does not change the crystal formation.

Weight and Volume Losses—DOP Migration

Since stress buildup can be a direct result of dimensional changes in a specimen, both weight and volume were measured for all specimens before and after either heat treatment or stress relaxation at 121°C. Results obtained from a Caytur 21 and a MOCA cured specimen are compared in Table 2. The Caytur 21 cured Stock A had more volume decrease than did the MOCA cured Stock F, (7.36 versus 5.0 percent). Yet their weight losses were the same, (5.11 versus 5.34 percent).

It was found later that the observed weight loss can be attributed primarily to the migration of DOP. The DOP contents of four specimens with different heat treatments and stress relaxation histories were determined by high-pressure liquid chromatographic analysis. The results are

TABLE 2—*Percent changes in size and weight after stress relaxation at 121°C (250°F) and 1 percent strain.*

Parameter	Percent Change	
	Stock A	Stock B
Length	0	0.50
Width	−3.26	−2.47
Thickness	−4.11	−3.68
Cross-sectional area	−7.26	−6.06
Volume	−7.36	−5.00
Weight	−5.11	−5.34

shown in Table 3. The values found for percent DOP were then used to calculate the weight losses assuming that DOP is the only component lost during heat aging.

Negligible stress enhancement was observed for MOCA cured Stock F, although it had about the same weight loss as did the Caytur 21 cured Stock A. In each case, the loss was attributed to DOP migration. The greater volume decrease in Stock A, which caused the stress buildup, must be due to other reasons.

Chemical Explanation

The basic chemical reaction during curing of either Adiprene and Caytur 21 or Adiprene and MOCA polyurethane is that of isocyanate (NCO) from prepolymer and amine (NH_2) from curative to form linear, hard urea linkages. The reaction of a Caytur 21 system relies on decomplexation of amine from sodium chloride at curing temperature. The free amine reacts very quickly with the surrounding isocyanate. As a result, the availability of amine becomes less as the curing progresses away from Caytur particles, some of the urea reacts with neighboring isocyanate to form biuret branches. Therefore, after 2 h of cure at 120°C, a polyurethane specimen is composed of urea, biuret, ether linkages, and unreacted amine. Although the chemistry is similar in MOCA system, the kinetics behind the reaction is quite different. The molten MOCA mixes homogeneously with the prepolymer. The resulting reaction, slowed by the presence of chlorine groups, proceeds more smoothly and with no large localized concentration of amine. Probably, less biuret and more linear urea groups are found in MOCA cured polyurethane.

Given heat, strain or not, free amine in the Caytur system starts to react with biuret to form urea [*8*]. It is believed that linear urea occupies less volume than the branched biuret. Thus, stress buildup is a direct result of shrinkage in volume produced from contractive forces between the hard segments. In a MOCA system, the same reaction occurs at a much slower

TABLE 3—*Correlation of weight loss and DOP migration in stock A.*

	Heat Treatment		Stress Relaxation				Weight Loss, %	
Specimen	Temperature, °C	Time, h	Temperature, °C	Strain, %	Time, h	DOP Found, %	Calculated	Observed
1 (control)	...	...	...	...	...	13.0	0.0	0.0
2	...	...	121	1	24	8.9	4.50	5.11
3	121	24	121	1	24	6.4	7.00	7.20
4	121	87	121	1	24	3.1	10.20	12.25

rate. The bulky chlorine groups in MOCA retard the reaction of free amine with biuret; therefore, the conversion of biuret to urea is slower and more uniform. Consequently, negligible enhancement in stress is found.

Heat under strain accelerated the chemical reaction. The stress buildup reached a maximum with 1 percent strain at about 24 h in Fig. 1, while continuous enhancement in stress was observed for a specimen heat treated for 24 h at the same temperature, 121°C, in Fig. 6.

In Table 4, a swelling experiment in 25/75 dimethyl formamide/tetrahydrofuran showed solubility of 43 percent for an untreated control specimen due probably to the presence of branching biuret. The material became more soluble when the relaxation time at 121°C and 1 percent strain was increased, which indicates the gradual disappearance of biuret. These relaxation times represent different stages of the stress buildup, which is shown in Fig. 1.

TABLE 4—*Effect of negative stress relaxation on solubility.*

	Stress Relaxation Test				
Specimen	Temperature, °C	Strain, %	Time, h	Stage of Negative Stress Relaxation	Percent of Solubility[a]
A-1 (control)	...	...	...	...	43.1
A-2	121	1	2	onset	52.9
A-3	121	1	10	highest rate	63.7
A-4	121	1	26	highest stress	69.6
A-5	121	1	65	longest test time	80.0

[a] In 25/75 dimethyl formamide/tetrahydrofuran.

Domain Formation

It was thought that the contractive force generated during stress buildup might create new domains. Two independent small-angle X-ray scattering inspections showed similar results. All five specimens at different stages of stress buildup in Table 4 showed unoriented domains of the order of 9.2 to 10.5 nm (92 to 105 Å) (distance between centers of two nearest neighboring domains). All five specimens appear to have fairly similar morphologies.

Attempts to inspect the domain formation of these specimens on a transmission electron microscope were not successful. These domains were too small—of the order of 2 nm (20 Å)—and too diffuse to be found. Therefore, we conclude that no significant difference in domain formation through the stress buildup process can be detected. The contractive force may lead to density increase in polyurethane only.

Conclusion

An unusual stress buildup phenomenon of Caytur 21 cured Adiprene polyurethanes was observed in stress relaxation experiments at 121°C and 1 percent strain. The stress increased sharply from 2 h of relaxation time to more than 40 h. It was found to be closely associated to Caytur 21 and to depend strongly on temperature. It was insensitive to NCO content and Caytur amount. However, 20 parts of PPG mixed with 80 parts of Adiprene in prepolymer reduced the stress enhancement substantially.

Several possible sources for this phenomenon have been investigated. Neither crystal nor domain formation can be detected from the available techniques. The observed weight and volume losses, which were results of DOP migration, were believed to have little, if any, effect on the negative stress relaxation. Finally, chemical reactions at 121°C in Adiprene polyurethanes extended by Caytur 21 seemed to generate contraction of the hard segments. The conversion of biuret linkages to urea linkages in the presence of free amine creates an increase in density and thus produces stress buildup. Better understanding of this phenomenon may result in improvement of product reliability of segmented polyurethane system.

Acknowledgment

The author wishes to thank many of his colleagues at Firestone Central Research Laboratories. In particular, Drs. G. G. A. Bohm, R. A. Hayes, and K. R. Lucas, and B. H. Werner and A. R. Cain for their stimulating discussions on physical and chemical aspects of polyurethanes. Without them the chemical explanation would not be possible. Acknowledgment is due to The Firestone Tire and Rubber Company for permission to present these results.

References

[*1*] Saunders, J. H. and Frisch, K. C., *Polyurethanes: Chemistry and Technology, Part I—Chemistry,* Interscience, New York, 1962.
[*2*] Saunders, J. H. and Frisch, K. C., *Polyurethanes: Chemistry and Technology, Part II—Technology,* Interscience, New York, 1964.
[*3*] Alliger, G. McGillvary, D. R., and Hayes, R. A., *Pure and Applied Chemistry,* Vol. 39, Nos. 1-2, 1974, pp. 45-56.
[*4*] Rogers, T. H., Finelli, A. F., Pearson, C. J., and Chung, D. A., *Journal of Elastomers and Plastics,* Vol. 8, 1976, pp. 116-131.
[*5*] Gent, A. N., *Journal of Polymer Science,* Part A-2, Vol. 4, 1966, pp. 447-464.
[*6*] Judge, J. T. and Stein, R. S., *Journal of Applied Physics,* Vol. 32, No. 11, 1961, pp. 2357-2363.
[*7*] Keller, A. and Machin, M. J., *Journal of Macromolecular Science,* Vol. B1, No. 1, 1967, pp. 41-91.
[*8*] Cain, A. R., Paper No. 50, presented at the 111th Meeting of the Rubber Division, American Chemical Society, Chicago, Ill., 1977.

DISCUSSION

A. Fox (written discussion)—In your test your are constraining the specimen at constant length and are measuring the change in constraining force as a function of time. Without prior heat treatment a time dependent decrease followed by an increase of force was shown, while after a 24 h, 138°C heat treatment the usual stress relaxation behavior is exhibited. It seems to me that when conducting this type of test on unaged material you are measuring a change in force induced by volume shrinkage. Do you have any comment on this?

A. Y. C. Lou (author's closure)—Yes, you are right. The stress buildup is a direct result of shrinkage in volume produced from contractive forces between the hard segments. The conversion of biuret linkages to urea linkages in the presence of free amine in the polyurethane system during heating creates an increase in density.

K. Amin[2]*(written discussion)*—Are these reactions going on at 121°C endothermic? We really are asking if the actual temperature of the specimen is changing during the test which may affect its stress relaxation?

A. Y. C. Lou (author's closure)—Yes, the reaction is endothermic. Heat is required to activate the free amine in the Caytur system. However, the actual temperature of the specimen remained near 121°C during the test because the reaction progressed at a very slow rate.

[1] Bell Laboratories, Murray Hill, N.J. 07974.
[2] Bendix Research Laboratories, Southfield, Mich. 48076.

Hold-Times Cyclic Effects and Residual Stress

F. T. Geyling[1] *and P. L. Key*[1]

Stress Relaxation of Residual Metalworking Stresses

REFERENCE: Geyling, F. T., and Key, P. L., "**Stress Relaxation of Residual Metalworking Stresses,**" *Stress Relaxation Testing, ASTM STP 676,* Alfred Fox, Ed., American Society for Testing and Materials, 1979, pp. 143-154.

ABSTRACT: The stress relaxation behavior of 1010 and 1020 steels was evaluated for an application involving the relaxation of mandrel-drawn, roller-straightened tubes. The distortions observed in full-sized tubes after annealing at 260 and 482°C are reported, as well as measurements of the actual residual stress levels in such tubes. Bending stress relaxation experiments were performed on strip specimens removed from full-sized tubes at temperatures of 23, 149, and 260°C for up to 2000 h. The relaxation of metalworking stresses was modeled using small beams plastically deformed in four-point bending. The curvature relaxation of the beams after annealing at 260 and 482°C was measured. The results of this work indicate that less than 10 percent of the initial stresses due to metal forming should relax in tubes in service at room temperature.

KEY WORDS: low-carbon steel, stress relaxation (metals), creep (metals), mechanical properties (metals), steel tubing, residual stresses

The usual occurrences of stress relaxation involve tensioned bolts, springs, or press fit assemblies. The initial stresses in these cases are intentionally introduced and desired. However, residual stresses resulting from inhomogeneous plastic deformation during metal forming operations can also provide an origin for stress relaxation considerations. The relaxation of such stresses can result in distortions that can be of significant concern for designs involving close dimensional tolerances, such as tooling, high-speed turbines, and precision optical instruments.

The development of a millimeter waveguide transmission system by the Bell System [*1*][2] led to an investigation of the relaxation of residual stresses in 1010 and 1020 steel tubes. A schematic of an installed waveguide is

[1]Members of technical staff, Metallurgical Engineering Department, Bell Laboratories, Murray Hill, N. J. 07974.

[2]The italic numbers in brackets refer to the list of references appended to this paper.

shown in Fig. 1. The waveguide itself consists of a 1010 steel tube (60 mm inside diameter, 67.4 mm outside diameter),[3] with an inner lining of 180 μm of polyethylene bonded to about 5 μm of electroplated copper. Flanges attached by electron-beam welding are used to join the individual sections (8.8 m long), which are buried in a protective steel sheath.

The attractiveness of millimeter waveguide as a transmission medium stems from the ability to obtain very high capacity (equivalent to almost 500 000 telephone circuits) coupled with low transmission loss. However, these features depend critically upon the right circular geometry of the waveguide, and deviations from this geometry lead to rapidly increasing losses. This geometric sensitivity required that the tubing be purchased to special dimensional specifications almost an order of magnitude more stringent than industry specifications. After substantial development work with tubing suppliers, we were pleased to find that tubes meeting our requirements could be produced by rather standard industry practices—electric-resistance welding of hollows, drawing the hollows over a mandrel, and roller straightening the finished tube [2].

Of course, it was also necessary to guarantee that the tubes would not significantly change in shape during service. To evaluate the likelihood and the consequences of such an event, a simple experiment was performed. A tube was accurately measured in the as-straightened condition and after a stress relief anneal of 1 h at 482°C. The results are shown in Fig. 2 and

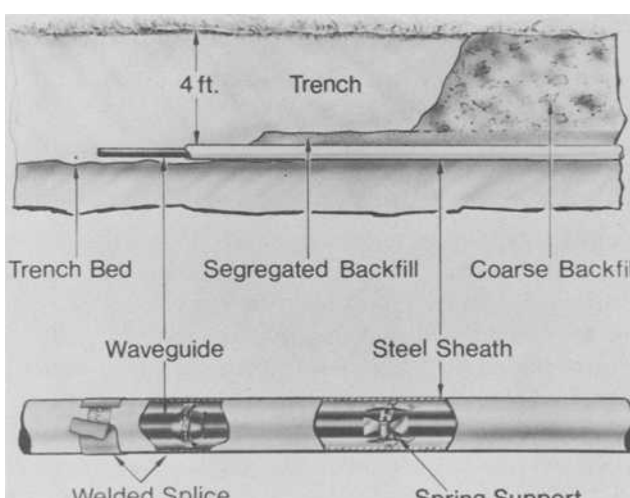

FIG 1—*Schematic of installed millimeter waveguide.*

[3]The experiments reported in this paper were actually performed on samples of a preliminary waveguide design with 51 mm inside diameter and 57.4 mm outside diameter.

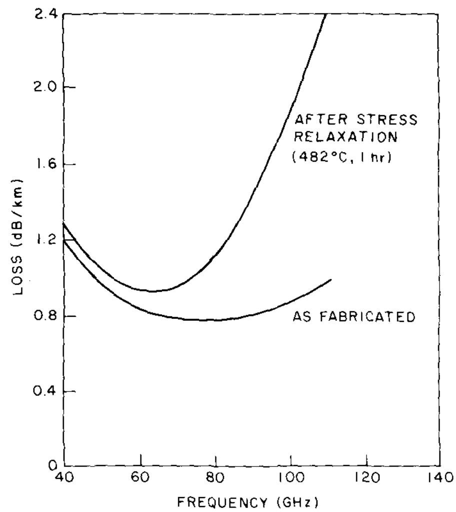

FIG. 2—*Effect of stress relaxation on waveguide (51 mm inside diameter) transmission losses.*

indicate a very large increase in loss for the relaxed tube, primarily due to the development of a bow. In another preliminary experiment, a tube held at 260°C for 1 week showed essentially no dimensional change. This latter experiment gave us confidence that the tubes probably would not relax in the service condition (40 years at 27°C). However, the potential consequences indicated by the 482°C experiment indicated that it would be prudent to examine stress relaxation of waveguide tubes in greater detail.

Experimental Program

A three-part effort was planned to determine if stress relaxation was a major problem for waveguide tubes.

Determination of Actual Residual Stress Levels

This portion of the effort was performed by the Columbus laboratory of Battelle Memorial Institute (BMI). Portions of nine waveguide tubes were provided to BMI. Three techniques for determining residual stresses were used:

1. Tube slitting [*3*]—Circumferential stresses were measured by slitting 50.8-mm lengths of tube along their lengths and measuring the diameter change with a micrometer. Longitudinal stresses were measured by slitting a longitudinal tongue 70 mm long by 7.6 mm wide in 152 mm lengths of

tube using a water-cooled abrasive wheel. Tongue deflection was measured with a dial gage.

2. X-ray diffraction [4]—Surface stresses (longitudinal and circumferential) were measured from the angular shift in the (211) diffraction peaks using filtered chromium Kα radiation.

3. Incremental removal [5]—The circumferential and longitudinal stresses were determined by simultaneously recording the strain on the inner surface of a 152-mm-long tube using 90-deg rosette strain gages, while the outer surface was removed by electropolishing in a solution of 10 volume percent hydrochloric acid in water.

Evaluation of Relevant Material Properties

The tensile, stress relaxation, and microcreep properties of 1010 and 1020 steels were evaluated. All tension testing was performed at room temperature in accordance with ASTM Mechanical Testing of Steel Products (A 370-76). Stress relaxation testing was performed at 23, 149, and 260°C with constant-moment, tapered cantilever beam specimens [6] using one of the methods described in ASTM Stress Relaxation Tests for Materials and Structures (E 328-75). Initial stress levels equal to the yield strength (0.2 percent offset) and to one half the yield strength were used. The specimens were machined from 0.31-mm-thick strip that had been processed from waveguide tubes to a strength level similar to the strength level in the waveguide tube. Specifically, this process included cutting a strip from a tube, cold rolling it to 0.38 mm, normalizing it (½ h, 927°C), and finally cold rolling it to 0.31 mm. Specimens were tested in both the as-rolled and the stress-relieved (482°C, 1 h) conditions.

Microcreep experiments at room temperature were performed by BMI. Pin-loaded tension specimens with a gage length of 25.4 mm and a gage width of 6.35 mm were machined from the walls of 1010 steel waveguide tubes. Prior to machining, the tubes were stress relief annealed for 1 h at 482°C. Strains were measured on opposite faces of the specimens with bonded foil strain gages. The microcreep behavior was determined at stress levels of 138, 276, and 414 MPa for up to 1000 h.

Analytical Simulation of Waveguide Relaxation

It was expected that, if the stress relaxation rates determined in the previous section were unexpectedly high, it would be necessary to carry out an analytical modeling of waveguide relaxation using a three-dimensional finite element model. To evaluate the modeling scheme and to establish numerical parameters for the creep law used in the simulation, a simplified experiment involving the relaxation of small bent beams was performed. The specimens were strips 6.35 mm wide by 3.18 mm thick by 140 mm long cut from a 1010 steel waveguide tube. The specimens were plastically deformed in four-point bending to various initial curvatures. After bending, the specimens were annealed in a salt bath at 260 and 482°C. The specimens were removed at selected intervals up to 3 h, and the relaxed curvature was measured on an optical comparator. The change in curvature was compared to theoretical predictions.

Results

Residual Stress Measurements

Tube Slitting—The values of the longitudinal and circumferential residual stresses at the outer surface calculated from the measured deflections of the slit tubes showed little variation from tube to tube or with longitudinal or circumferential location in a tube. The average values for as-straightened tubes ranged from +138 to +172 MPa (tensile) for circumferential stresses and +62 to +69 MPa (tensile) for longitudinal stresses. One tube was stress relieved at 482°C for 1 h, which reduced the circumferential stress to +21 MPa and the longitudinal stress to +7 MPa, indicating that the anneal was effective in relieving residual stresses.

X-ray Diffraction—The values of longitudinal and circumferential stresses at the outer surface calculated from the diffraction peak shifts showed large variations and differed substantially from the values determined by slitting. For example, the X-ray results indicated that longitudinal stresses were compressive rather than tensile. However, the absolute values of each of more than 70 separate X-ray stress determinations was less than 138 MPa.

Incremental Removal—The values of longitudinal and circumferential residual stresses were calculated from the strains measured on the inner surface. With this technique, the distribution of stress through the tube wall could be obtained, and values to a depth of about 1.3 mm were determined. The data indicate that both the longitudinal and circumferential stresses reached a maximum value somewhat below the outside surface and that both were tensile. The longitudinal stress, however, appeared to be near zero or compressive at the outer surface, whereas the circumferential stress remained tensile.

Material Properties

Tensile Properties—The tensile properties of the tubes and the strip prepared from the tubes for stress relaxation tests are given in Table 1.

Stress Relaxation Data—The stress relaxation data are presented as a percent of the initial applied stresses. The data for 1010 steel, stress relieved at 482°C for 1 h are shown in Fig. 3, while the data for 1020 are shown in Fig. 4 (as-rolled) and Fig. 5 (stress-relieved).

Microcreep Behavior—At each of the three levels of stress examined, the

TABLE 1—*Tensile properties.*

Material	Tensile Strength, MPa	0.2% Yield Strength, MPa	Total Elongation in 50.8 mm, %
1020 tube	598	479	19.5
1020 strip (0.31 mm), as rolled	659	633	1.8
1020 strip, annealed 482°C, 1 h	636	569	10.0
1010 tube	554	543	6.1
1010 strip (0.31 mm), as rolled	567	562	3.9
1010 strip, annealed 482°C, 1 h	512	483	10.0

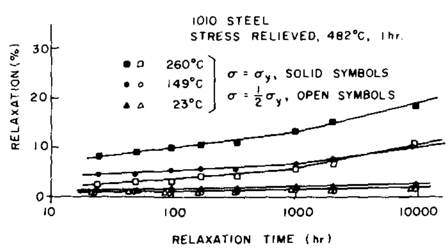

FIG. 3—*Stress relaxation of 1010 steel, stress relief annealed 482°C, 1 h.*

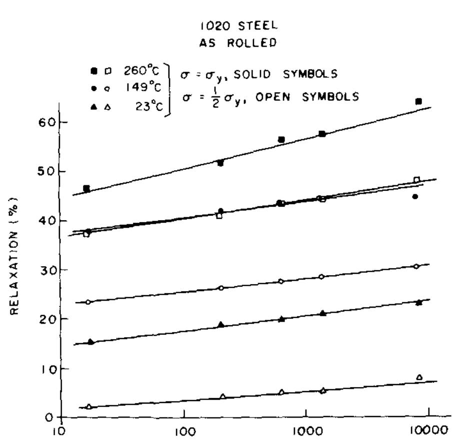

FIG. 4—*Stress relaxation of 1020 steel, as-rolled.*

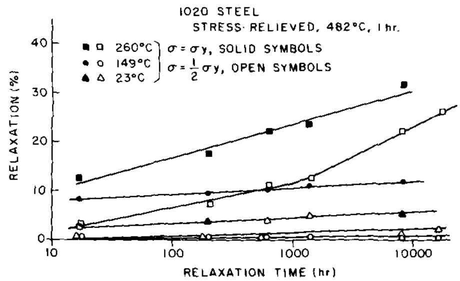

FIG. 5—*Stress relaxation of 1020 steel, stress relief annealed 482°C, 1 h.*

creep strain after 1000 h was very small. For example at 414 MPa, a total strain of only 6 to 7 $\times$ 10^{-6} was observed.

Beam Relaxation Experiments

One beam was relaxed at 260°C, and it was found that no measurable relaxation occurred for times up to 4 h. Eight beams were relaxed at 482°C; relaxation at this temperature was so rapid that most relaxation had occurred within 5 min. Figure 6 shows the total change in curvature after annealing at 482°C for 3 h as a function of the initial curvature. Both the curvature change and the initial curvature have been made dimensionless by dividing by the value of curvature corresponding to yielding in the outer fibers. This curvature is given by

$$K_y = \frac{2\sigma_y}{Et} \tag{1}$$

where σ_y, E, and t are the yield strength, Young's modulus, and thickness, respectively. For the 1010 steel tube used for this experiment, σ_y = 735 MPa, E = 207 GPa, and t = 3.18 mm, so K_y = 2.23 $\times$ 10^{-3} mm^{-1}.

Discussion

Residual Stress Measurements

Although the values of residual stress determined by the various techniques seem to differ, these differences were probably due to the techniques themselves. For example, with the X-ray diffraction method, local stresses were determined within a depth of about 25 μm of the surface and from an area of about 6 mm^2, whereas the slitting technique gave an average stress based on the entire distribution of stress through the tube wall. The value of stress calculated in the slitting technique depends critically upon

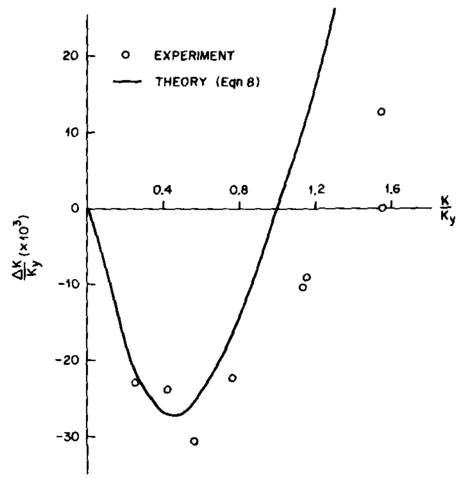

FIG. 6—*Curvature relaxation of 1010 steel beams plastically deformed in pure bending. Relaxation conditions, 482°C, 3 h.*

the assumptions used to relate tube deflections to stress. One such assumption is that the stresses were distributed linearly through the tube wall, but the results of the incremental removal method indicate that this assumption was not met. However, although the accuracy of individual stress values may be in doubt, the results show that the stress levels are relatively low—less than half the tensile yield strength in all cases.

Stress Relaxation Data—The strong dependence of stress relaxation on temperature and stress is clearly shown in Figs. 3 through 5. Comparison of Figs. 4 and 5 shows that significant reductions in stress relaxation resulted from the stress relief anneal. This anneal does not change the tensile properties significantly, but, as shown by residual stress measurements just mentioned, it effectively removes residual stresses. In effect, a rolled specimen has two applied stress systems—the nominally applied stress and the residual stresses from rolling. For this reason, stress relaxation test specimens should be stress relief annealed prior to testing. It is also a good practice to use a stress relief anneal with parts that undergo stress relaxation in service such as springs.

Beam Relaxation—The curvature changes accompanying the relaxation of plastically deformed beams illustrate the distortions possible with stress relaxation in general. The origin of the curvature change can be illustrated by considering the residual stress distribution in a beam plastically deformed with concave upward curvature shown schematically in Fig. 7. Equilibrium requires that the integral of the stress distribution and its first moment about the neutral axis vanish. The antisymmetry of the distribution ensures that its integral vanishes. Moment equilibrium can be thought of as a

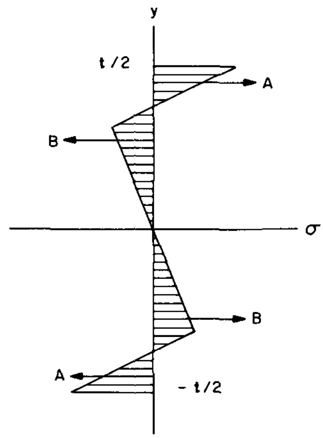

FIG. 7—*Schematic of residual stress distribution in a bent, elastic-perfectly plastic beam. Original curvature concave up.*

balance between a positive and a negative couple, shown as A and B, respectively. (Couple A tends to produce concave down curvature; couple B the opposite).

Assume now that a small increment of stress relaxation occurs reducing the stresses shown. If the stress reductions were proportional, then no distortion would occur, as the force and moment equilibrium would be maintained. However, relaxation is a nonlinear function of stress such that larger stresses relax more rapidly (see the data on 1010 and 1020 steels, Figs. 3 through 5). Thus, the couple associated with the largest stress will relax more rapidly, and the beam curvature must change to maintain moment equilibrium. In the case shown in Fig. 7, the positive couple (A) will relax more rapidly, so the beam curvature must change so as to increase couple A, requiring the beam to deflect in a concave downward direction and thus decreasing the original curvature. It is interesting to note that, as the initial curvature increases, the residual stresses associated with the negative couple increase relative to those of the positive couple. Hence, the sign of the curvature change would be expected to change from negative to positive as the initial curvature increased. Of course, for zero initial curvature, there should be no curvature change. This suggests that a plot of curvature change as a function of initial curvature should start at the origin, decrease to a minimum, and then increase through zero.

The behavior of the experimental curvature data shown in Fig. 6 follows the pattern just outlined. The results of an analytical simulation of this model (see Appendix) are also shown in this figure. The theoretical curve requires creep parameters for an independent prediction; in the absence of these parameters, the theoretical curve was fit to one point of the experimental curve. As shown in Fig. 6, there is qualitative agreement between theory and experiment. The principal difference appears to be in the transition region between positive and negative curvature changes. This transition occurs when the maximum absolute values of the residual stresses associated with the two couples are initially equal and is independent of creep behavior, suggesting there was a difference in the actual and the assumed residual stress distributions (Fig. 7). The residual metalworking stresses in the tube from which the beam specimens were cut is the most likely source of this difference.

Implications for Waveguide—The low levels of residual stresses, the small stress relaxation rate at room temperature, and the low microcreep rate all suggest that stress relaxation should not be a problem for the millimeter wavegide system. Using the stress relaxation data shown in Fig. 3, we estimated that less than 10 percent relaxation of the initial metalworking stresses should occur over the service life of 40 years. This level of stress relaxation leads to only a 1 percent increase in loss and is acceptable.

Acknowledgments

The authors would like to acknowledge E. O. Fuchs for much of the experimental work on stress relaxation and beam bending, R. J. Boyd for performing the relaxation experiments on full-sized tubes, and C. W. Marschall of BMI for the careful experimental work on residual stress measurements and microcreep. In addition, the formulation of the curvature rate equation described in the appendix is based on unpublished work by I. M. Levi and L. M. Slavin.

APPENDIX

Curvature Relaxation in Elastic-Perfectly Plastic Beams

Consider a rectangular beam of an elastic-perfectly plastic material deformed into the plastic range. The residual stress distribution is shown in Fig. 7. Assuming that plane sections remain plane, the bending strains will be linearly distributed

$$\epsilon = yK \tag{2}$$

where

ϵ = bending strain at a distance y from neutral axis and
K = curvature of the neutral axis.

We further assume that the constitutive relation (creep law) has the form

$$\dot{\epsilon} = \frac{\dot{\sigma}}{E} + F(\sigma) \tag{3}$$

where

$\dot{\sigma}$ = stress rate corresponding to the strain rate $\dot{\epsilon}$ and
$F(\sigma)$ = functional form for the stress dependence of $\dot{\epsilon}$.

Using the moment equilibrium equation, one can obtain a rate equation for curvature

$$\dot{K} = \frac{b}{I}\int_{-t/2}^{+t/2} yF(\sigma)\, dy \tag{4}$$

where I is the section moment of inertia and b and t are the width and thickness of the beam.

Combining Eqs 2 and 3 results in a relation for the stress rate

$$\dot{\sigma} = Ey\dot{K} - EF(\sigma) \tag{5}$$

Equations 4 and 5 can yield a solution for the stress and curvature as a function of time, provided the form of $F(\sigma)$ is known. Because of the nonlinear nature of the problem, the solution must be obtained numerically. To provide insight into the character of the solutions, we performed a perturbation analysis. Namely, we assumed that

$$F(\sigma) = \left(\frac{\sigma}{\zeta}\right) + \lambda\left(\frac{\sigma}{\zeta}\right)^2 + \lambda^2\left(\frac{\sigma}{\zeta}\right)^3 + \dots$$

and

$$\sigma = \sigma_1 + \lambda\sigma_2 + \lambda^2\sigma_3$$
$$K = K_1 + \lambda K_2 + \lambda^2 K_3$$

where λ is the perturbation parameter ($\ll 1$) and ζ is a constant.

Substituting these expansions into 4 and 5 results in the following expressions

$$\dot{\sigma}_1 = -E\left(\frac{\sigma_1}{\zeta}\right) \qquad \sigma_1(y, 0) = \sigma(y, 0) \tag{6}$$

$$\dot{K} = \frac{b\lambda^2}{I}\int_{-t/2}^{+t/2}\left(\frac{\sigma_1}{\zeta}\right)^3 y\, dy \qquad K(0) = 0 \tag{7}$$

The curvature change associated with annealing is obtained by integrating Eq 6, substituting the result into Eq 7, and integrating the resulting expression. Taking the asymptotic value gives the following expression for the total curvature change during annealing

$$\frac{\Delta K}{K_y} = \left(\frac{\lambda\sigma_y}{\zeta}\right)^2 \int_0^1 S^3(z, 0) z\, dz \tag{8}$$

where dimensionless variables have been introduced using $z = 2y/t$ and $S = \sigma/\sigma_y$. This expression contains a single creep parameter $\lambda\sigma_y/\zeta$, and depends on the initial residual stress distribution, which can be written down as a function of the initial curvature, geometry of the cross section, and the yield strength [*7*]. However, the residual stress distribution is involved, and its cube is so unwieldly that the integral was evaluated numerically.

References

[*1*] Alsberg, D. A., Bankert, J. C., and Hutchison, P. T., *Bell System Technical Journal,* Vol. 56, Dec. 1977, p. 1829.
[*2*] Boyd, R. J., Cohen, W. E., Doran, W. P., and Tuminaro, R. D., *Bell System Technical Journal,* Vol. 56, Dec. 1977, p. 1873.
[*3*] Polakowski, N. H. and Ripling, E. J., *Strength and Structure of Engineering Materials,* Prentice-Hall, Englewood Cliffs, N. J., 1966, p. 477.
[*4*] Cullity, B. D., *Elements of X-ray Diffraction,* Addison-Wesley, Reading, Mass., 1956, p. 431.
[*5*] Sachs, G. and Espey, G., *Iron Age,* Sept. 18, 1941, pp. 63-71.
[*6*] Fox, A., *Journal of Materials,* Vol. 6, No. 2, June 1971, p. 428.
[*7*] Timoshenko, S., *Strength of Materials,* Part II, D. Van Nostrand, Princeton, N. J., 1956, p. 377.

J. M. Beeston[1] *and T. K. Burr*[1]

In-Reactor Stress Relaxation of Type 348 Stainless Steel In-Pile Tube

REFERENCE: Beeston, J. M. and Burr, T. K., "**In-Reactor Stress Relaxation of Type 384 Stainless Steel In-Pile Tube,**" *Stress Relaxaton Testing, ASTM STP 676,* Alfred Fox, Ed., American Society for Testing and Materials, 1979, pp. 155–170.

ABSTRACT: The results of a slit tube test, which show that large residual stresses do not develop during irradiation of in-pile tubes at operating temperatures of 573 to 698 K are presented. The slit width measurement at ambient conditions indicates that the predicted stress gradient due to irradiation growth was completely relaxed, and the residual stress that opened the slit was caused by the tube wall temperature change (hot to cold) when the reactor was shut down. No voids were detected and no immersion density gradient or difference in transmission electron microscopic (TEM) observations of irradiation-produced defects was found through the wall thickness. The microstructural mechanism for plastic flow through irradiation creep could explain the relief of the differential swelling stresses.

KEY WORDS: stress relaxation, irradiated stainless steel, density, irradiation-produced defects, temperature range, slit width measurement, irradiation creep, irradiation swelling

Irradiation-induced swelling and creep in nuclear reactor systems, especially at higher temperatures where void swelling occurs, is recognized as one of the major problems in reactor design and operation. Core components must be designed or the reactor operated so that swelling and creep effects can be accommodated with a minimum impact on performance and plant availability. Swelling and creep in a reactor system are a function of temperature, stress, fluence, flux spectrum, and material. The slit tube test has been proposed [*1,2*][2] as a means of defining the swelling-creep superposition behavior and of confirming the resultant stress relaxation.

Other investigators [*3-5*] have used residual stress measurements in irradiated tubing to gain information on the swelling-creep relationships.

[1] Senior scientist and supervisor, TRA Structural Projects Section, respectively, EG&G Idaho, Inc., Idaho Falls, Idaho 83401.

[2] The italic numbers in brackets refer to the list of references appended to this paper.

Utilizing this work, the recent design and lifetime extension analyses of in-pile tubes has included an assumption that stresses due to radial thermal gradients and radial, irradiation-induced swelling gradients were relaxed during operation such that, eventually, the residual (reactor off) stress gradients are equivalent to a reversal of the initial (first cycle) thermal stress gradients. In-pile tubes in reactor cores are subjected, mainly, to a pressure load and a radial (through-the-wall) temperature gradient, which makes them ideal for slit width test verification of residual stress. The work described in this paper confirms the stress relaxation concepts with a slit width test on a highly irradiated in-pile tube cyclindrical section and with analytical results. The analytical results compare stresses in the reactor on and off conditions with and without stress relaxation. Immersion density and transmission electron microscopy (TEM) measurements are related to the observed swelling and creep as measured with a bore gage. The irradiation temperature was in the low mean metal-temperature range (583 to 698 K) for swelling and creep.

Stresses (No-Stress Relaxation)

Of very practical importance to the operation of the in-pile tubes is whether differential swelling gradients are generated through the wall thickness with attending large stresses. The literature [*2,4,5*] tends to show (not unambiguously) that irradiation creep increases as the swelling rate increases, and large stresses due to differential swelling do not develop. Some recent work [*6*] by the authors with the FW-HEDL computer code R1045 indicates that cyclic plastic strain is present and may contribute to the reduction in the differential swelling stresses. The FW-HEDL program performs a cyclic elastic-plastic creep analysis of an infinitely long thick-walled cylinder subject to pressure loads at the inner and outer surfaces, to axial loads, and to a radial thermal gradient through the tube wall. Additionally, the program includes the effects of irradiation-induced swelling and creep. It seems certain from operating experience and from the results of the slit-tube test presented in this paper that any residual stresses developed in the in-pile tubes operating with a mean metal temperature range of 583 to 698 K are not large, and the remaining question concerns their magnitude.

The in-pile tube from which the slit tube test section was cut had operated at power with a maximum mean metal temperature of 617 K, corresponding to temperatures at the inside diameter (ID) and outside diameter (OD) of 577 and 637 K, respectively. The internal pressure was 15.2 MPa (gage 2200 psig). The accuracy of the absolute wall temperatures is of concern in calculating stresses and swelling-creep interrelations, and measurement of thermal diffusivity to improve these calculations is planned in future work. The in-pile tube was operated to a fluence of 4×10^{22} n/cm^2, $E >$ 1 MeV. At temperatures at which the voids are indistinguishable, it is not apparent in these measurements whether there is an effect of stress on swelling. Growth occurs as a result of irradiation-produced defects. Some of these defects may be gas atoms, for example, helium in beryllium. The authors have had success in failure analysis of beryllium by describing the internal stress due to growth in terms of pseudotemperatures. Differential stresses are produced but no creep in irradiated beryllium at 373 K. In stainless steel at these conditions, we apparently have growth and creep and no differential stresses but will show this by calculations first as if the differential stresses were to develop and second when they do not develop.

Curves of pressure plus thermal elastic stresses and another of the pressure plus thermal plus differential swelling stresses are shown in Fig. 1*a* for the reactor on condition. For the reactor off condition, a residual stress from differential swelling would remain, as shown in Fig. 1*b*, if stress relaxation or an effect of stress on swelling does not occur. The stresses are tabulated in Table 1.

The differential swelling stress across the tube wall is calculated by converting the differential swelling to pseudotemperatures using adjusted equations from *Nuclear Systems Materials Handbook* [7]

$$\frac{\Delta V}{V} = R\Phi t + \frac{1}{\beta}\left[\ln \frac{1 + \exp \beta(\tau - \Phi t)}{1 + \exp \beta\tau}\right] \tag{1}$$

where

$R = 0.01 \exp[-49.77 + 0.196T - (1.87 \times 10^{-4})\, T^2]$,
$\beta = -1.2 + (6.9 \times 10^{-3})T$,
$\tau = (7.99 - (2.98 \times 10^{-2})\, T + (2.9 \times 10^{-5})\, T^2)^{-1}$,
Φt = fluence in units of 10^{22} n/cm^2 E > 0.1 MeV, and
T = temperature in degrees Celsius.

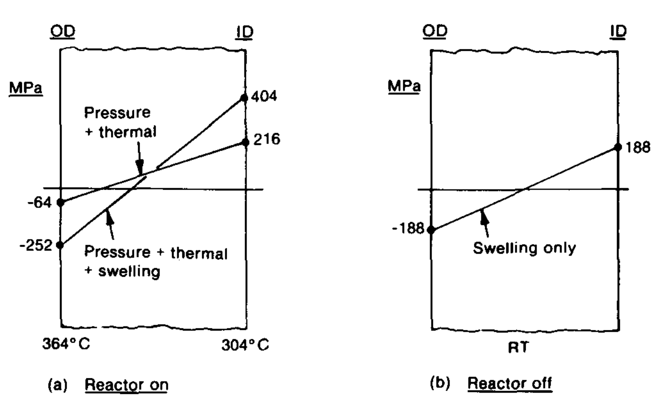

FIG. 1—*Through the wall circumferential stress (no stress relaxation).*

TABLE 1—*Tabulation of surface stresses.*

	Surface Stress, MPa	
	OD	ID
Pressure stress	69	83
Thermal stress[a]	−133	133
Swelling stress[b]	−188	188
No relaxation, reactor on		
Pressure + thermal	−64	216
Pressure + thermal + swelling	−252	404
No relaxation, reactor off		
Swelling only	−188	188
Stress relaxation, reactor on		
Pressure only	69	83
Stress relaxation, reactor off		
Pressure + reversed thermal	202	−50
Reversed thermal only	133	−133

[a] Thermal stress based on $\Delta T = 60$ K.
[b] Swelling stress based on pseudo $\Delta T = 85$ K.

and

$$\Delta T = \frac{\epsilon_0(F) - \epsilon_i(F)}{\alpha} = \frac{1}{3}\frac{(\Delta V/V)_0 - (\Delta V/V)_i}{\alpha} \quad (2)$$

where

$\epsilon(F)$ = elongation as a function of fluence on outside and inside wall and
α = thermal expansion coefficient in inverse Celsius degrees.

The differential swelling stress is given by

$$\sigma = \frac{\alpha E \, \Delta T}{2(1 - \nu)} = 188 \text{ MPa} \quad (3)$$

for temperatures at the ID and OD of 577 and 637 K, respectively, (reactor on). This differential swelling stress is of large magnitude, as indicated in Fig. 1.

Material and Irradiation History

The slit tube test section was taken from a Type 348 stainless steel in-pile tube irradiated in the Engineering Test Reactor (ETR) at the Idaho National Engineering Laboratory. The solution-annealed Type 348 stainless steel in-pile tube composition in percent was carbon, 0.034; manganese, 1.11; phosphorus, 0.014; sulfur, 0.006; silicon, 0.43; chromium, 18.03; nickel, 10.97; molybdenum, 0.13; copper, 0.13; columbium and tantalum, 0.60; tantalum, 0.02; and cobalt, 0.06. The section from the irradiated tube was 5 cm long, with 5.398-cm ID and 6.426-cm OD, and was irradiated in a position from 5 to 10 cm above the reactor core centerline. The irradiation history of the in-pile tube in the ETR was such that the section received a fluence of 3.4×10^{22} n/cm^2, $E > 1.0$ MeV, which corresponds to about 52 displacements per atom (dpa). Density decrease after irradiation to a fluence of 3.5 to 3.8×10^{22} n/cm^2, $E > 1.0$ MeV, amounts to 0.22 percent. The total hoop creep strain, calculated from bore gage measurements in the in-pile tube, at a fluence of 4×10^{22} n/cm^2, $E > 1.0$ MeV was 0.85 percent. The yield strength ranges of the material before irradiation at room temperature and 700 K were, respectively, 265 to 315 MPa and 207 to 241 MPa. The yield strength of specimens with fluence of 3.7×10^{22} n/cm^2, $E > 1.0$ MeV, that had been irradiated at temperatures of 583 to 617 K and tested at room temperature, 587 K, and 700 K were, respectively, 969, 865, and 763 MPa. The helium content was measured by a fusion technique on four specimens and gave an average of 546 atomic ppm of helium. The ferrite content on an irradiated specimen was measured by a Ferrit-Messer instrument at 0.1 percent, and metallography indicated the presence of the austenitic phase and small amounts of carbides.

Procedure

The schematic of the elastic stresses with no stress relaxation, shown in Fig. 1, is to be compared with the calculated stresses after the irradiation including stress relaxation and with the results of the slit width test. Before making the slit width test with the irradiated section of the tube, a test was conducted on a dummy section of 17-4 PH tube of the same size (5.398 cm ID, 6.426 cm OD, and 5.08 cm long), heat treated to simulate the strength [$R_c = 35$, $\sigma_{ys} = 966$ MPa (140 ksi)] and hardness of the irradiated test tube section. The dummy tube section was held in the fixture in the same manner, and the partial and final slits were made with a Con-O-Saw and water coolant with the same type of blade (918-150-025) as used subsequently on the test section. The hold-down clamps (one at each end of the tube section) had fingers tapered to the contour of the cylinder. Once the tube section was tightened in place on the fixture with the clamps, the tube and fixture were moved as a unit to make the successive cuts, locating the assembly by means of pins on the fixture bed.

The partial cut (the index) was made with a blade trimmed to a 7.62 cm diameter so that the plunge cut through the wall thickness resulted in a ligament about 0.51 cm long on each end of the OD of the tube and 1.59 cm long on each end of the ID. After the partial cut through the wall thickness, the slit index width was measured and was comparable (0.066 cm) with the blade width (0.064 cm). The final cuts of the ligaments were then made by moving the tube–fixture unit, and the slit width was then measured for the index position. The blade did not traverse the index position in the final cuts. The dummy tube measurements indicated no change from the index measurement, so that the clamping fixture and procedure seemed verified.

After the slit width measurement was made, the tube-fixture unit was moved so that two slices 0.64 cm wide by 5.08 cm long were cut for the density and TEM specimens. One slice was annealed at 1047 ± 14 K (1400 to 1450°F) for 1 h and air cooled. The specimens were cut on a Brownwill thin-sectioning saw so that successive wall thickness slices could be measured. Figure 2 shows the stub ends after removal of the 2.54-cm-long TEM and density slices. The slices were removed to ensure identification and were acid-polished (1 part nitric acid-2 parts hydrochloric acid-2 parts glycerol-1 part hydrogen peroxide) for 5 min to remove burrs before measurement.

Results of Slit Tube Test

A calculation of the expected slit width opening when only elastic thermal stresses are present can be made using a solution presented by Timoshenko [8]. For the hollow circular cylinder, described in Fig. 3, subjected to steady heat flow and a uniform radial temperature gradient around the circumference, the relative displacement of the slit faces is given by

$$v_b - v_a = B\,2\pi r \qquad \text{for} \quad u_b - u_a = 0 \tag{4}$$

where

$$A = -\frac{T_i - T_0}{\ln (r_0/r_i)} \qquad \text{and} \qquad B = (1 + \nu)\alpha A$$

In this formulation, $T_i > T_0$ implies tensile and compressive stresses on the ID and OD, respectively, for a negative value of B so that the gap will open. When complete stress relaxation occurs in the in-pile tube with the reactor on, $T_i < T_0$. However, cool-down creates tensile and compressive stresses on the ID and OD, respectively, and the slit gap will open. Since the residual stresses in the in-pile tube are created by cooling instead of heating, the negative sign for A, is dropped when determining $v_b - v_a$ for the ETR slit tube section.

For a mean metal temperature of 344°C (617 K) and temperatures of 304 and 364°C (577 and 637 K) on the ID and OD, respectively, the slit width opening is calculated as

$$v_b - v_a = -0.114 \text{ cm (0.045 in.) (slit opening)} \tag{5}$$

The measured slit width opening of the irradiated tube section was 0.130 cm (0.051 in.). The slit width opened up, as seen in Fig. 4.

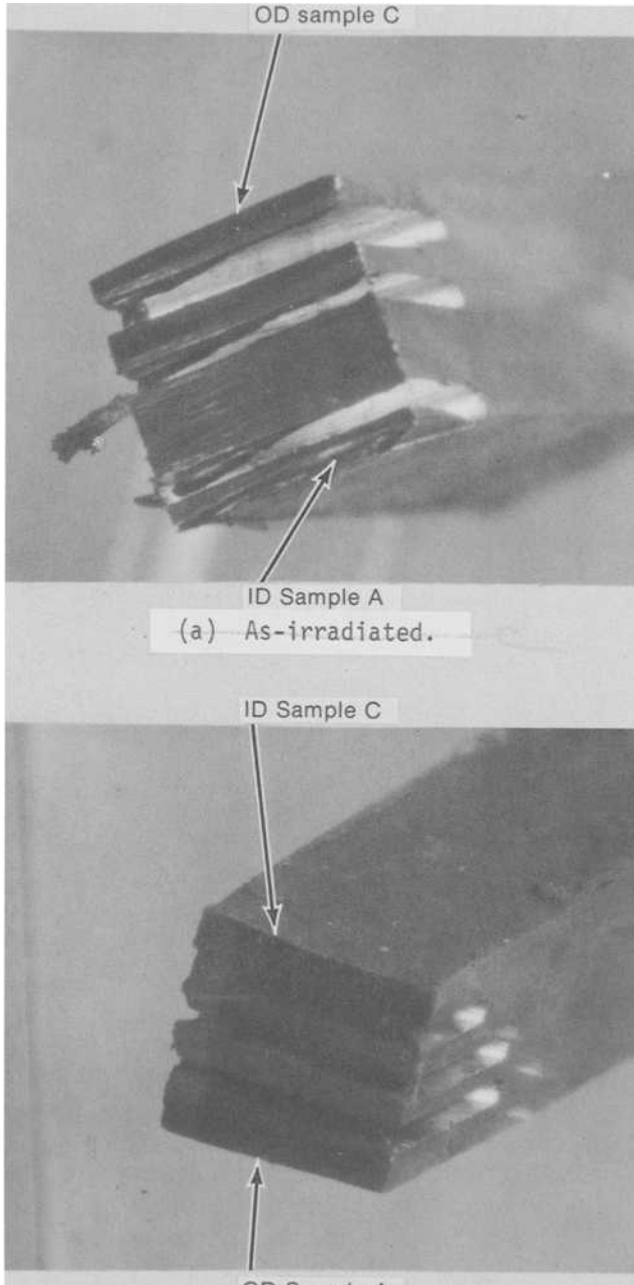

FIG. 2—*Photographs of stub ends of slices from which density and TEM specimens were taken: (a) as irradiated; (b) annealed at 774°C for 1 h prior to cutting.*

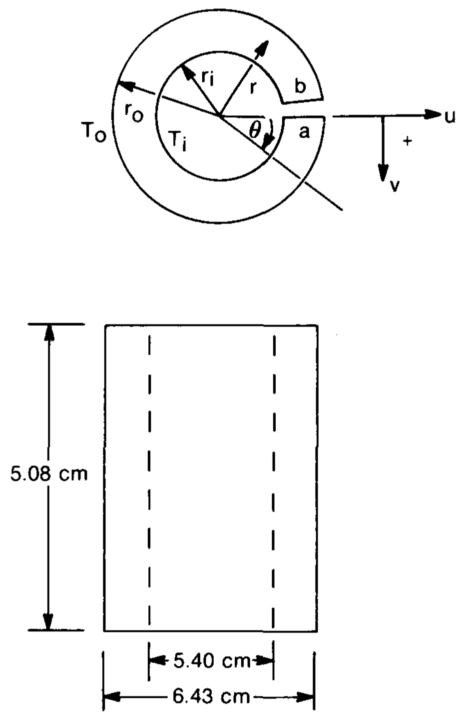

FIG. 3—*Schematic of slit width opening relationships.*

Stresses After Irradiation with Stress Relaxation

Since in-reactor stress relaxation is known to occur [*4,5,9*], the question of the amount of relaxation is pertinent. Kenfield et al [*9*] showed that the total in-reactor relaxation after a peak fluence of 2×10^{21} n/cm^2, $E > 0.1$ MeV, at 643 K is approximately 50 percent, whereas thermally activated relaxation at the time and temperature involved was only 15 percent. The mean temperatures are lower and the times much longer for the ETR in pile tube. A plot of the thermal plus pressure stresses with complete relaxation is shown in Fig. 5*a* with the reactor on, and a plot of the thermal bending stress after relaxation in Fig. 5*b* with the reactor off. The stresses were given in Table 1. It is apparent from the agreement of the calculated and measured slit width that the stress relaxation is nearly complete. The slit width measurement at ambient conditions indicates that the predicted stress gradient due to differential irradiation growth through the wall was completely relaxed and that the residual stress that opened the slit was due to the temperature change (hot to cold) when the reactor was shut down.

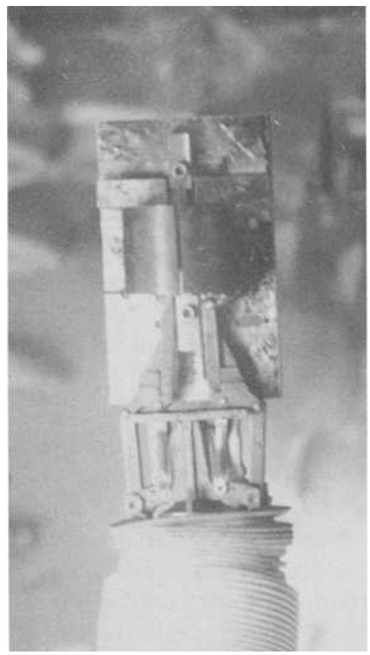

FIG. 4—*Photograph of slit width section after final cut showing opening of 0.196 cm (0.130 slit width plus 0.066 slit index width).*

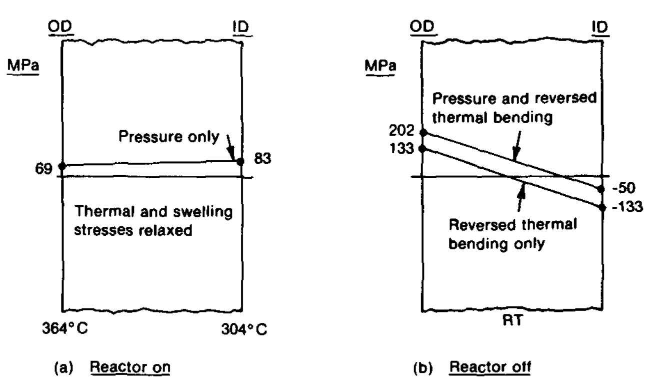

FIG. 5—*Through the wall circumferential stress (with stress relaxation).*

Density and TEM Measurements

As described in the procedure, specimens were taken for density and TEM measurements. The densities were determined using an Ainsworth balance that had been calibrated and the standard weights (500 mg, 1 g, and 2 g) checked within 0.0003 g. Water containing Photoflo and a 0.005-in.-diameter wire were used to obtain the wet weight W_2. The density was calculated from the equation

$$\rho = \frac{W_1 \rho H_2O}{W_1 - W_2} \tag{6}$$

where W_1 is the dry weight in air, and values were obtained for the as-irradiated material of $\rho_{a-i} = 7.9116 \pm 0.0016$ g/cm^3 for four specimens. The density grams per cubic centimeter of each of the four specimens from the annealed slice was $\rho_a = 7.9162 \pm 0.0065$. In neither slice could a trend indicating a gradient in the density through the tube wall be detected.

The TEM photographs of specimens from both the irradiated and the annealed slices were taken on a Hitachi 200 microscope. Three specimens were taken from each slice, one each from next to the ID and the OD and one in the middle. Stereophotographs were taken; from these the thickness of the film was determined. Voids could not be detected in any of the irradiated specimens, but a high density of loops was present (Fig. 6). No difference in the three TEM specimens from the as-irradiated slice could be detected; thus, no gradient in the irradiation produced defects could be determined. Since the ferrite content is less than 0.1 percent after irradiation, it appears that swelling is due to the presence of irradiation-produced defects, but a swelling gradient does not develop. The density of loops was determined to be 3×10^{16} loops/cm^3 with an average diameter of about 100 Å. The loops disappeared after annealing, but helium bubbles were present with a density of about 1.0×10^{16} bubbles/cm^3 (one third that before annealing) and an average diameter of about 40 Å (Fig. 7).

Discussion

The slit width measurement has indicated that an effective mechanism has operated in the reactor to relieve the residual stresses. Since the operating temperature was low (583 to 617 K), the amount of thermal relief of the stresses [*9*] should have been less than 15 percent. Plastic flow from either irradiation creep or cyclic strain will be examined for its contribution to the relief of the differential swelling stresses.

Detailed analyses [*6*] of a similarly constructed and operated in-pile tube indicated that cyclic strain accumulation due to thermal ratcheting is

FIG. 6—*TEM micrograph showing irradiation produced defects after a fluence equivalent to 52 dpa.*

less than 0.08 percent. Yield strength enhancement from irradiation allows for shakedown to elastic behavior after a fluence of 5×10^{21} n/cm^2, $E > 1$ MeV, or approximately eight operating cycles. Thus, the contribution of cyclic strain toward stress relaxation is considered to be small.

Various investigators [*2,10,11*] have identified the defects that contribute to the swelling-creep behavior as voids, dislocations, interstitial loops, and vacancy loops into which the point defects (vacancies and interstitials)

FIG. 7—*TEM micrograph showing bubbles and remains of some clusters, loops, and dislocations after annealing at 1047 K for 1 h.*

are absorbed to produce the swelling and creep. It has been shown [*10*] that vacancy loops do not contribute to steady-state creep processes, but act as recombination centers for vacancies and interstitials, thus reducing the number available for absorption in those defects contributing to plastic deformation. Using this microstructural model, we are left with dislocations and interstitial loops as the irradiation-produced defects contributing to the irradiation creep, although vacancy loops and voids of a size below the resolution detection limit may be present. The density of the dislocations in the solution-annealed tube will be low at the start of irradiation; the cyclic plastic strain will introduce dislocations during start-up and subsequent cycles until the yield strength exceeds the stress. The vacancy loops are created in the cascade collapse. Eyre and English [11] show that the calculated thermal shrinkage rates are negligible below ~873 K. Thus, no significant decrease in vacancy loop numbers would be expected if the vacancy loop generation rate is athermal in the temperature range 583 to 617 K.

Some microstructural mechanisms can be examined for their effect on the stress relief, although the transmission electron microcopy has not been detailed enough at this time to distinguish between the interstitial and vacancy loops. With the assumption that the vacancy loops contain the gas atoms and are equal to the number of bubbles after annealing, the number density of interstitial loops would be the difference between the total loops and bubble density of 2×10^{16} loops/cm^3. From a modification of the relationship of Eq 5 [2] and Eq 18 [10] the swelling, S, is given as

$$S = \pi \, r_{IL}^2 b N_{IL} = \frac{4\pi}{3} r_v^3 N_v = 0.0022 \tag{7}$$

with

$N_{IL} = 2 \times 10^{16}$ interstitial loops/cm^3,
$N_v = 1 \times 10^{16}$ vacancy loops/cm^3, and
$r_{IL} = 1.0$ pm.

then the Burgers vector $b = 1.4$ nm and the radius of vacancy loops $r_v =$ 3.8 nm.

The modification assumes the vacancies go to the vacancy loops as well as the voids, which for our case are indistinguishable. This means that the smaller loops are the vacancy loops, and since the lattice parameter of stainless steel is about 0.36 nm, the movement of the interstitial loops by about four lattice parameters would account for the in-reactor creep strain. Since the voids are not resolvable, if we assume they have an average diameter of about 2 nm, the swelling due to the voids with number density equal to the interstitial loops would be negligible or

$$S = \frac{4\pi}{3} r_v^3 N_v = 0.0001 \tag{8}$$

The immersion density after annealing of 7.912 ± 0.002 g/cm^3 was about the same as that of the specimens from the ID, middle, and OD of the wall of 7.916 ± 0.007 g/cm^3. This presumably results from the swelling due to bubbles of average diameter of 5 nm being approximately equal to the swelling from the presence of the interstitial loops that have annealed out. The number density of the interstitial loops in each of the three sections of the wall thickness was seen to be about the same in the transmission electron micrographs. The presence of helium bubbles of 5 nm diameter after annealing at 1047 ± 14 K in the specimens with 546 atomic ppm is consistent with the observations of Mazey and Francis [12], except they reported the presence of defect clusters and interstitial loops in addition to helium bubbles after the postirradiation annealing.

Upon reactor start-up, cyclic hardening of the solution-annealed in-pile tube material would be expected, but cyclic softening on cold-worked and weld material has been reported [13]. The rate at which the material hardens or softens depends on the plastic strain; for example, with 2 percent total strain, the maximum hardening occurs in about 10 cycles, while with 0.5 percent total strain, the maximum hardening may take 100 cycles or more. Irradiation hardening of the solution-annealed material also occurs so that the yield strength at temperatures of 583 to 617 K and fluences in 10^{21} n/cm^2, $E > 1.0$ MeV, would have doubled or tripled [14].

For the limited swelling and creep data on the ETR in-pile tube, the creep equation of Boltax et al (Eq 1) is given as

$$\frac{\epsilon}{\sigma} = C\phi t + DS \tag{9}$$

where

ϵ = creep strain = 0.0085,
σ = hoop stress = 79.4 MPa (11.5 ksi),
ϕt = fluence in units of 10^{22} n/cm^2, $E > 0.1$ MeV = 12, and
S = fractional swelling = 0.0022.

The constant C can be expressed as 5.88×10^{-8}, where D is taken [2] as 1.5×10^{-5} and the value of C is calculated from the measurements.

The value of the constant, C, for the ETR data is a factor of 2.6 greater than suggested [2] for fast reactor creep. Foster et al [15] report that the constant C is increased by a factor of about 2.5 for fast to thermal reactor irradiation. In considering the parameters that affect the swelling and creep, the effect of flux spectrum is the most likely parameter causing this increase. The effect of temperature, which is in the low range for swelling and creep, should be to reduce the swelling and creep. While the flux after a correction for the displacement cross section for stainless steel for an ETR flux spectrum with neutron energies $E > 0.1$ MeV would be equivalent to a fast reactor [Experimental Breeder Reactor-II (EBR-II) at the Idaho National Engineering Laboratory], flux of 9.4×10^{14} n/cm^2·s at the position where the creep and swelling were measured, it would be 8.3×10^{14} n/cm^2·s at the position of the tube section for the slit width test.

These equivalent fluxes would produce displacements per atom per second of about 4 to 5 $\times$ 10^{-7}, which although in the low range, are comparable with EBR-II data. The effect of the flux spectrum is to provide a substantial component of thermal flux that acts to reduce recombination of vacancies and interstitials in the vacancy loops, thus providing more interstitials for interstitial loop formation and increased creep.

Thus, the microstructural mechanism for plastic flow through irradiation creep appears adequate to explain the relief of the differential swelling stresses. There would be a contribution to the relief of these stresses from the cyclic strain; however, irradiation hardening would decrease the contribution. The amount of plastic strain determines the rate and magnitude of the stress relief contribution.

Conclusions

1. The slit width measurement at ambient conditions indicates that the predicted stress gradient due to differential irradiation growth through the wall was completely eliminated by relaxation and that the residual stress that opened the slit was due to the tube wall temperature change (hot to cold) when the reactor was shut down.
2. The estimate of the slit width opening if thermal stresses only were present indicates that significant residual thermal stresses exist in the in-pile tubes during the reactor off condition.
3. The microstructural model and analysis of transmission electron micrographs indicate that interstitial loops with a Burgers vector of about four lattice parameters would account for the in-reactor creep strain.
4. Swelling is due to the presence of the interstitial and vacancy loops and not to the presence of the unresolved voids or increased ferrite content. Since the density of the vacancy loops tends to saturate, the swelling will not be large until the voids can be resolved.
5. Large residual stresses due to differential swelling gradients will not be generated in the presence of irradiation creep.
6. The larger value of the creep equation constant indicates that thermal neutrons in the spectrum are having an effect of reducing recombination of vacancies and interstitials in the vacancy loops, thus providing more interstitials for interstitial loop formation and increased creep.

Acknowledgments

This work was performed under contact to the Department of Energy, Contract EY-76-C-07-1570.

References

[1] Pennell, W. E., *Nuclear Technology*, Vol. 16, Oct. 1972, pp. 332–353.

[2] Boltax, A., Foster, J. P., Weiner, R. A., and Biancheria, A., *Journal of Nuclear Materials,* Vol. 65, 1977, pp. 174–183.
[3] Foster, J. P., Wolfer, W. G., Biancheria, A., and Boltax, A., *Irradiation Embrittlement and Creep in Fuel Cladding and Core Components,* British Nuclear Energy Society, London, 1973, pp. 273–281.
[4] Wolfer, W. G., Foster, J. P., and Garner, F. A., *Nuclear Technology,* Vol. 16, Oct. 1972, pp. 55–63.
[5] Flinn, J. E., McVay, G. L., Walters, L. C., *Journal of Nuclear Materials,* Vol. 65, 1977, pp. 210–223.
[6] Burr, T. K., unpublished data, 1978.
[7] TID-26666, *Nuclear Systems Materials Handbook,* Vol. 1, Design Data Property Code 3304 (E-1), p. 1.0, Section 4; Section 5, Revision 2, 4-16-75 and 6-19-74.
[8] Timoshenko, S. and Goodier, J. N., *Theory of Elasticity,* McGraw-Hill, New York, 1951, pp. 427–431.
[9] Kenfield, T. A., Busboom, H. J., and Appleby, W. K., *Journal of Nuclear Materials,* Vol. 66, 1977, pp. 238–243.
[10] Weiner, R. A., and Boltax, A., *Journal of Nuclear Materials,* Vol. 66, 1977, pp. 1–16.
[11] Eyre, B. L. and English, C. A., *Consultant Symposium on the Physics of Irradiation Produced Voids, Harwell 9-11 September 1974,* R. S. Nelson, Ed., AERE-R7934, British Atomic Energy Research Establishment, Jan. 1975, p. 239.
[12] Mazey, D. J. and Francis, S., "Observations of Dislocation Structure and Cavities Formed by Annealing in Type 316 Steel after Ion Irradiation at Ambient Temperature," AERE-R7934, British Atomic Energy Research Establishment, p. 257.
[13] "Mechanical Properties Test Data for Structural Materials, Quarterly Progress Report for Period Ending July 31, 1974," ORNL 4998, Oak Ridge National Laboratory, Contribution from Aerojet Nuclear Company, p. 6 and Table 1.1.
[14] Martin, W. R. and Weir, J. R., *Flow and Fracture of Metals and Alloys in Nuclear Environments, ASTM STP 380,* American Society for Testing and Materials, 1965, p. 259.
[15] Foster, J. P., Weiner, R. A., and Boltax, A., *Oxide Fuel Element Development for Period Ending Sept. 30, 1975,* WARD-OX 3045-20, pp. 6-2 to 6-7.

J. A. Kapp,[1] J. H. Underwood,[1] and J. J. Zalinka[1]

Crack Growth Retardation in Two Low-Strength Materials Under Displacement Controlled Cyclic Loading

REFERENCE: Kapp, J. A., Underwood, J. H., and Zalinka, J. J., "**Crack Growth Retardation in Two Low-Strength Materials Under Displacement-Controlled Cyclic Loading,**" *Stress Relaxation Testing, ASTM STP 676,* Alfred Fox, Ed., American Society for Testing and Materials, 1979, pp. 171-181.

ABSTRACT: Several experiments have been performed to determine the tolerance to defects of two low-strength materials used on cannon tube components subjected to displacement-controlled fatigue loading. The study was initiated to determine acceptable flaw sizes for hoops used to stabilize large cannons during recoil. A simple specimen was devised to approximate the axisymmetric, displacement-controlled actual loading of hoops. The results show that under this loading, a fatigue failure is not possible in either material because of the combination of the reduced stiffness of the structure containing fatigue cracks and general cross-sectional yielding.

KEY WORDS: fatigue (materials), crack propagation, fracture mechanics, stress relaxation

Modern large-caliber cannons are massive structures of up to 6 m in length and 4500 kg of mass. When the cannon is fired, it recoils through approximately 1 m in a few milliseconds. To ensure that this recoil motion is stable, the gun tube is guided through this stroke along a rail system. The rails are connected to hoops, which in turn are shrink-fitted around the tube (Fig. 1). Since hoops are not considered critical items, they are made of either of two low-cost, low-strength materials—mild cast steel or cast ductile iron.

Hoops are of basically simple geometry—a uniform thin shell connected

[1]Mechanical engineer, materials engineer, and mechanical engineering technician, respectively, Benet Weapons Laboratory, U.S. Army Armament Research and Development Command, LCWSL Watervliet Arsenal, Watervliet, N.Y. 12189.

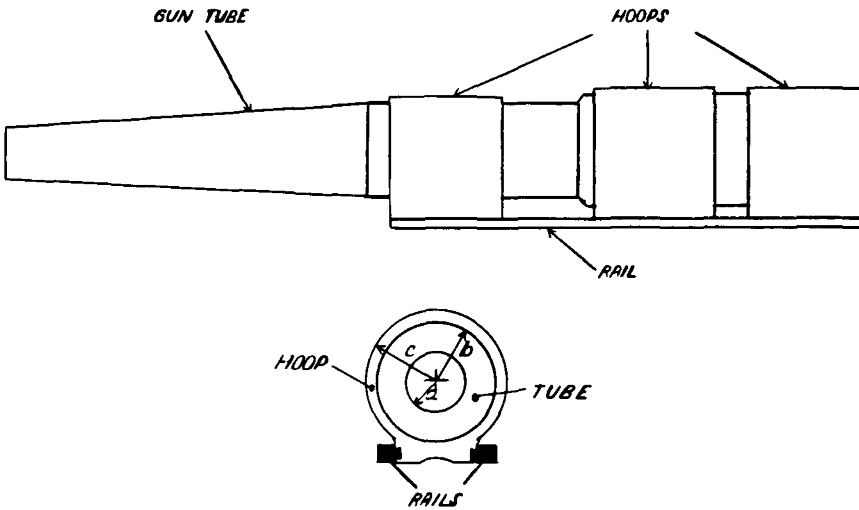

FIG. 1—*Typical hoop-tube-rail assembly.*

with a built-up rail section, as pictured in Fig. 2. The nonuniformity of the hoop cross section makes it susceptable to defect formation during the casting process. The heavier rail section will act as a heat sink, which results in a slower rate of solidification there. When liquid metal transforms to a solid, there is an accompanying volumetric contraction; a mass of solid steel takes less space than the same mass of liquid steel. If there is not sufficient liquid metal to fill the voids resulting from solidification, a shrinkage defect is formed. Other defects may also occur in hoops, but shrinkage is the most common and the most serious.

Shrinkage defects often occur near a surface or may intersect the surface. These defects may be detected by a nondestructive inspection, but such testing is quite expensive and is applied sparingly to samples of castings. Thus, hoops containing casting defects often reach the shop floor. When they are machined, the defects will generally become readily visible.

The objective here is to describe the procedure and results of analyses and tests that were performed in order to develop maximum acceptable flaw-size criteria for hoops containing defects.

Procedure

Load Analysis

Hoops are subjected to several applied loads when a cannon is fired, in addition to the residual load from the shrink fitting. The firing loads include impulsive body forces from the rapid recoil, twisting due to projectile-tube

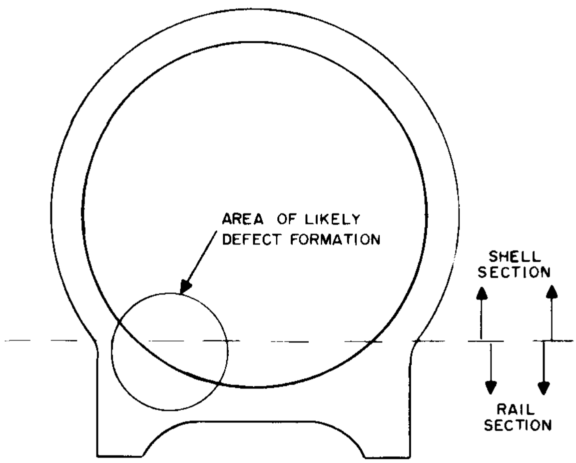

FIG. 2—*Typical hoop casting.*

rifling interactions, and dilation caused by the tube expanding from the applied pressure. Analysis reveals that the dominant firing load is the dilation and that the total hoop load is well approximated by the combination of the cyclic dilation load and the static shrink-fit load.

It should be noted that both the dilation and the shrink-fit loads result from the enforced displacement of the inside diameter (ID) of the hoop, and are not directly applied forces. Hence, the proper form of analysis to be used in determining the operating hoop loads is a displacement analysis, from which elastic stresses can be approximated using Hooke's law. When such fixed displacement loads are applied to a structure, cracking and yielding of the structure can lead to a significant relaxation of stress within the structure. This will be shown to be the case with the displacement loading of the hoops discussed here.

A description of the service stresses and strains in a hoop before any stress relaxation occurs is obtained from fundamental strength of materials relationships available in such basic texts as Timoshenko [*1*].[2] The expression for the circumferential strain at the hoop-tube interface of a hoop subjected to dilation from the pressurized tube and to an interference shrink fit is

$$\epsilon_{\text{total}} = \frac{Pa^2}{E(c^2 - a^2)} \left[1 - \nu + \frac{c^2}{b^2}(1 + \nu) \right] + \frac{\delta}{2b} \qquad (1)$$

The first term in Eq 1 represents the alternating strain ϵ_p at the hoop-tube interface due to internal pressure P applied to the tube; E and ν are the elastic

[2]The italic numbers in brackets refer to the list of references appended to this paper.

modulus and Poisson's ratio, respectively, and a, b, c, are the radii shown in Fig. 1. The second term in Eq 1 represents the residual strain ϵ_r at the hoop-tube interface due to the shrink-fit interference δ between the tube and the hoop ID. Equation 1 was used to calculate the various circumferential strains for two hoop-tube combinations that are reported in Table 1. The values of E and ν used are 207 000 MPa and 0.3, respectively; the values of P and δ in Table 1 represent the most severe operating conditions.

The calculated strain values listed in Table 1 are those that occur at the hoop ID, which is the location of maximum loading in the hoop. The strain will gradually decrease through the hoop thickness, but the change is quite small. Thus, we assumed that hoops are uniformly loaded at the strain levels of Table 1.

Tests Performed

Two hoops, one each of iron and steel, were used for specimens. The basic mechanical properties and composition of the materials were measured to ensure that the specimens were typical of ductile iron and cast steel. The results of these measurements are listed in Table 2. The mechanical tests were performed using the standard ASTM Methods of Tension Testing of Metallic Materials (E 8-78) and Methods for Notch Bar Impact Testing of Metallic Materials (E 23-72 (1978)) for tension and impact tests. The results are within the expected ranges, so the results from further testing of these sample hoops can be used to develop general flaw-size criteria for hoops.

Two general types of tests were performed on specimens from the sample hoops—fracture property measurements related to service loading and direct service simulation tests. The fracture property tests measured fracture toughness and fatigue strength. The specimens used were patterned after the C-shaped fracture specimen [2], which is simply a segment of a disk cut from a hollow cylinder with the inside diameter (ID) and outside diameter (OD) surfaces preserved. The test specimen geometries are shown in Fig. 3.

The fatigue life tests were conventional, unnotched, constant force-amplitude, cyclic-life-to-failure tests at two loads (Table 3). The applied loads used in the tests correspond approximately to the alternating and total strains for the two hoop-tube conditions, ϵ_p and ϵ_{total}, in Table 1. The frac-

TABLE 1—*Circumferential strain in hoop for two hoop-tube combinations.*

Hoop-Tube Dimensions, mm			Internal Pressure	Strain Due to Pressure	Shrink-Fit Interference	Strain Due to Shrink-Fit	Total Strain
a	b	c	P, MPa	ϵ_p, %	δ, mm	ϵ_r, %	ϵ_{total}, %
108	190	212	400	0.157	0.28	0.074	0.231
107	216	238	317	0.088	0.25	0.058	0.146

TABLE 2—*Measured properties of hoop materials.*

Material	Mechanical Properties					Composition, Percent by weight				
	0.1 Percent Yield Stress, MPa	Ultimate Stress, MPa	Tensile Elongation, %	Charpy Energy						
				−40°C *J*	+20°C *J*	C	Mn	P	S	Si
Iron	298	438	16	2.2	13	2.33	0.28	0.012	0.014	1.50
Steel	285	498	15	4.2	37	0.30	0.68	0.012	0.012	0.45

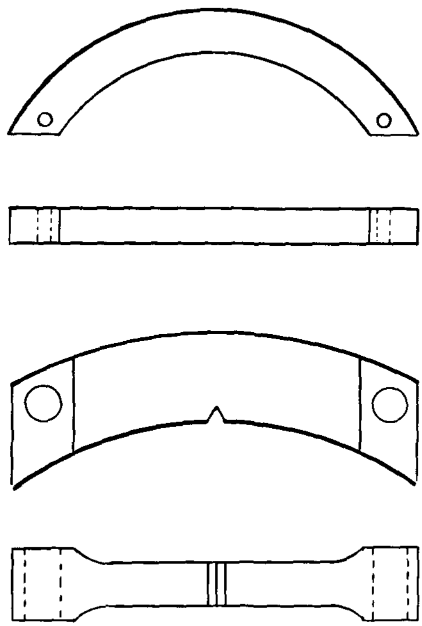

FIG. 3—*Fatigue and fracture specimens for hoops.*

TABLE 3—*Test conditions and results for fatigue life and fracture toughness tests.*

Material	Fatigue Life, cycles to failure		Fracture Toughness, MPa m$^{1/2}$
	$\Delta\epsilon = 0.10$, $\epsilon_{max} = 0.17\%$	$\Delta\epsilon = 0.18$, $\epsilon_{max} = 0.25\%$	
Iron	>1 000 000	214 000	151
Steel	>1 000 000	211 000	200

ture toughness measurements were made using the Landes and Begley J_{Ic} method [3]. The specimens were fatigue-precracked from the notch and then loaded to the point where further crack growth had just begun. By measuring the load and deflection that occurred up to the point of first crack growth, a measure of the materials' resistance to crack growth can be obtained. This measure of fracture toughness can be roughly compared to plane strain fracture toughness K_{Ic} as obtained using ASTM Test Methods for Plane Strain Fracture Toughness of Metallic Materials (E 399-78).

The service simulation tests required a unique specimen and test procedure. Since the actual loading is an axisymmetric deflection of the hoop ID, no bending through the hoop thickness is allowed, even if a casting defect or a fatigue crack is present. The specimen used was that shown in Fig. 4. When this specimen is loaded along the shoulders across the entire wall thickness,

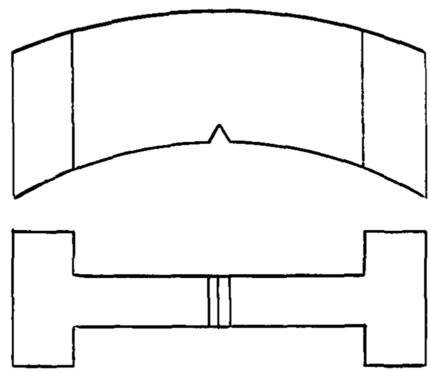

FIG. 4—*Specimen for simulation of cyclic service loading for hoops.*

only minimal through-thickness bending is allowed, resulting in a close approximation to the axisymmetric loading. Starter notches with root radii of 0.25 mm were used to simulate worst-case casting defects.

The service simulation specimens were tested on a hydraulically operated, servocontrolled, axial loading machine, pictured schematically in Fig. 5. Specimen displacement was measured with a linear variable differential transformer (LVDT). The servo valve was controlled by the LVDT electronic output. The force applied during each cycle was measured using a load cell and recorded on a strip chart.

The most important feature of the tests in regard to a proper simulation of service loads is that the specimen loading was limited by a fixed total displacement. Referring to Table 4, the initial loading cycle for specimen S-8 was chosen so that the 70-mm shoulder-to-shoulder gage length was increased by a ΔL = 0.12-mm. For all additional load cycles, this specimen

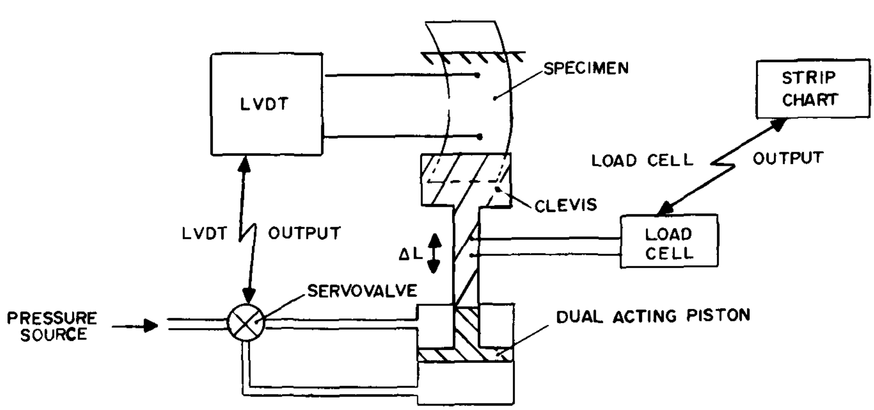

FIG. 5—*Sketch of test apparatus for simulation of service loading.*

TABLE 4—*Test conditions and results for displacement-limited service simulation tests.*

		Fatigue				
Material	Specimen	Initial $\Delta\epsilon$, %	Initial ΔL, mm	Cycles Applied	Crack Growth, mm	Fracture ΔL Required, mm
Steel	S-8	0.17	0.12	12 000	0.2	2.3
	S-9	0.26	0.18	93 000	9.4	2.3
Iron	I-8	0.17	0.12	10 000	0.5	1.4
	I-9	0.26	0.18	76 000	8.9	1.3

was stretched to the 70.12-mm total length. Tests were performed at two levels of displacement, which were chosen so that the initial $\Delta\epsilon$ values were 15 percent higher than the total strains expected in service, (ϵ_{total} in Table 1).

The test results will show that as the test proceeded at a fixed total displacement, the combination of plastic deformation and crack growth in the specimens caused a significant drop in the required maximum load. This, we believe, is a direct simulation of the displacement-limited loading of hoops in service.

Results and Discussion

The results of the unnotched fatigue life tests show that the two materials respond in a similar manner. As the results in Table 3 show, at the lower strain level there was no specimen damage in either material after 1 000 000 load cycles. At the higher strain level for both materials more than 200 000 cycles were required to grow a crack to midthickness of the specimen, which was considered the failure criterion. Since the constant force amplitude fatigue life is more than a factor of ten greater than the service life of a hoop, a fatigue failure of a hoop containing no processing defects appears to be very unlikely even under the maximum possible loading.

The broken fracture toughness specimens are shown in Fig. 6, and the associated fracture toughness values are presented in Table 3. In examining the deformed shape of the broken specimens, it is observed that the fracture was accompanied by large amounts of plastic deformation. Although the fracture toughness values are an estimate of K_{Ic}, the large amount of plastic deformation tends to verify that K_{Ic} for the two materials is at least 100 MPa m$^{1/2}$. For K_{Ic} at this value and using 290 MPa as the yield stress σ_y, the required specimen size for a brittle fracture and a valid measurement of K_{Ic} can be calculated as follows from E 399

$$\text{size} = 2.5\left(\frac{K_{Ic}}{\sigma_y}\right)^2 = 297 \text{ mm} \tag{2}$$

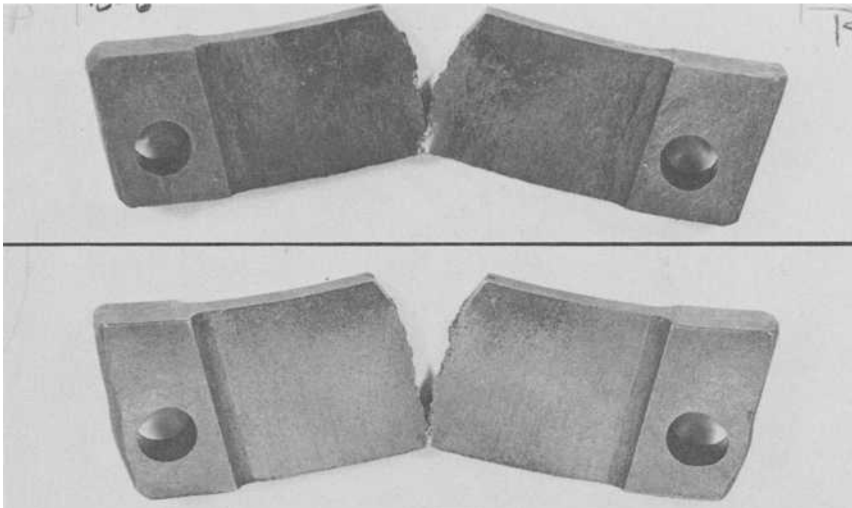

FIG. 6—*Broken fracture toughness specimens:* (top) *steel,* (bottom) *iron.*

Since the wall thickness of the hoops is less than one tenth of this size, a brittle, plane strain fracture appears to be impossible in the hoops.

The most interesting and conclusive results were obtained from the service simulation tests. When these specimens were cycled at either initial strain range $\Delta\epsilon$, fatigue cracks initiated at the root of the starter notches (Table 4). This indicates that casting defects could begin to grow under normal operating conditions. Cycling of the specimens loaded at high initial $\Delta\epsilon$ was continued to determine the extent to which the cracks would grow.

The total notch-plus-crack depth and the maximum applied force during each loading cycle were recorded for one specimen of each material. These results are presented in Fig. 7. They show that under fixed-displacement loading condition, the specimens undergo a very significant load relaxation. As the cycling proceeded and the crack grew, the maximum force required to produce the fixed displacement steadily decreased to about 20 percent of the initial value. The crack growth rate per cycle first increases, reaches a maximum, and then declines to a value so low that the crack essentially stops growing.

We believe the observed load relaxation is the combined result of two phenomena—gross cross-sectional yielding and reduction of the specimen stiffness due to the growing fatigue crack. At the suggestion of an ASTM reviewer, an analysis has been performed to determine how much of the load relaxation is due to yielding and what portion can be attributed to the propagating crack. The analysis involved the integration of Irwin's expression relating the change in specimen compliance as a function of crack depth to

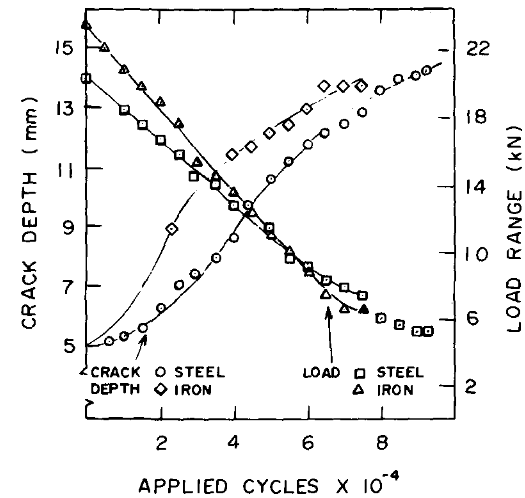

FIG. 7—*Service simulation test results.*

the stress intensity factor [*4*] using Pook's stress intensity factor solution for the single-edge notched, restrained-end specimen [*5*].

The analysis shows that during the early stages of cycling, the load drop-off is due primarily to plastic deformation. Using the steel specimen for example, the initial load required to produce the maximum displacement, assuming the specimen remains elastic, is 114 kN, while the actual load was 20.5 kN. In addition, after cycling for about 2×10^4 cycles, growing the crack to a total depth of 6.4 mm, the predicted load decrease is 2.6 kN and the actual decrease was 4 kN. Thus, it seems that during this initial period, the crack growth accounts for little more than half of the observed load decrease. After the specimen is cycled for an additional 2×10^4 cycles, advancing the crack to 7.8 mm in length, the predicted load drop-off was 2 kN, while 1.8 kN was observed. During this period, the entire load decrease can be attributed to the propagating crack. Thus, the analysis shows that the initial load decrease is dominated by specimen yielding, and the later portion can be attributed to the advancing crack.

Following the fatigue portion of the service simulation tests, the specimens were then loaded to fracture, and the change in specimen length at fracture was measured. These measurements are reported in Table 4. They further indicate that the hoops are highly resistant to brittle fracture, since the total elongation required for fracture was generally ten times larger than that which is applied to the hoops in service.

Conclusion

The various results lead to the conclusion that in-service hoop failure is quite impossible, even if the hoop contains large defects. The tests performed modeled only straight fronted defects, while those actually appearing are of various curved-fronted shapes. Straight-fronted cracks are more severe than curved cracks in every loading condition, so it is safe to assume that failure from a naturally occurring casting defect is impossible. Using this knowledge, conservative defect criteria were developed.

The basic rationale of the recommended criteria is based on the result that, because of stress relaxation, the maximum occurring operating stresses occur during the initial loading of the hoops. We decided to limit the allowable defects to those that will result in an arbitrarily low value of stress intensity factor K—about 10 percent of K_{Ic} when the hoop is initially loaded. The maximum defect dimensions for several defect geometries were determined, and these criteria are now being implemented.

Acknowledgments

The authors wish to thank A. Hess and J. Bak for their assistance in gathering test material and specimen preparation. We also wish to acknowledge the help of R. Farrara and N. Placido, whose many suggestions and comments are greatly appreciated.

References

[1] Timoshenko, S., *Strength of Materials, Part II*, Van Nostrand, Princeton, N.J., 1956.
[2] Underwood, J. H. and Kendall, D. P. in *Developments in Fracture Mechanics Test Methods Standardization, ASTM STP 632*, W. F. Brown, Jr., and J. G. Kaufman, Eds., American Society for Testing and Materials, 1977, pp. 25-38.
[3] Landes, J. D. and Begley, J. A. in *Developments in Fracture Mechanics Test Methods Standardization, ASTM STP 632*, W. F. Brown, Jr., and J. G. Kaufman, Eds., American Society for Testing and Materials, 1977, pp. 57-81.
[4] Irwin, G. R., *Applied Materials Research*, Vol. 3, 1964, p. 65.
[5] Pook, L. P., *International Journal of Fracture Mechanics*, Vol. 4, No. 3, 1968.

J. H. Laflen[1] *and C. E. Jaske*[2]

Cyclic Relaxation Response Under Creep-Fatigue Conditions

REFERENCE: Laflen, J. H. and Jaske, C. E., "**Cyclic Relaxation Response Under Creep-Fatigue Conditions**," *Stress Relaxation Testing, ASTM STP 676,* Alfred Fox, Ed., American Society for Testing and Materials, 1979, pp. 182–206.

ABSTRACT: The path and history dependence of elevated-temperature, time-dependent deformation response is investigated for three alloy steels—2¼Cr-1Mo steel, Type 304 stainless steel, and Type 316 stainless steel. The scope is limited to uniaxial loading under isothermal conditions. Relaxation data are evaluated for several prior cyclic (fatigue) loading histories. Results of these evaluations are compared with creep data for the same histories. To analyze stress relaxation data, creep equations are chosen and integrated using the time-hardening rule to develop closed-form expressions for relaxation response. Coefficients for these relaxation expressions are obtained using nonlinear least squares techniques. The appropriateness of using linearized transformations compared with direct nonlinear approaches is treated. For tensile hold-time creep-fatigue tests, the dependence of the coefficients on initial stress level is evaluated. Finally, the dramatic effects of both loading sequence and strain (both monotonic and cyclic) are discussed for one particular experimental case.

KEY WORDS: creep, fatigue (materials), stress relaxation, austenitic stainless steel, ferritic low-alloy steel, stresses, strains, hardening

An accurate assessment of time-dependent deformation response is essential in structural analysis. For example, it is used in design analysis to assess the total amount of deformation that occurs during service so that dimensional clearances can be maintained. Alternately, it is used in stress analysis to determine stress and strain fields in a component, which serve as input to damage analysis to avoid creep-fatigue cracking and fracture. The need for adequate descriptions of the time-dependent deformations is well known. Nevertheless, an accurate computational scheme for predicting these deformations in a unified way for all of the phenomenological manifes-

[1] General Electric Company, Cincinnati, Ohio 45215; formerly with Battelle's Columbus Laboratories, Columbus, Ohio 43201.
[2] Senior research scientist, Battelle's Columbus Laboratories, Columbus, Ohio 43201.

tations of each of the potential microprocesses is not currently available. There are several reasons for this, as discussed in the background section.

Generally, material behavior is both path and history dependent. In this paper, the word "history" will be used to indicate prior history, in other words, the effects that appear to be the result of previous events. The word "path" will be used to indicate the current direction and magnitude of stress or strain in a uniaxial test specimen. Note, then, that the relaxation and creep of two specimens with identical history to a given point will follow different paths during creep and relaxation. Therefore, materials that exhibit path dependency potentially will not exhibit creep and relaxation behavior that correspond in a one-to-one manner. Conversely, the effects of history could result in, for example, cycle-dependent creep and relaxation behavior.

The objective of this paper is to investigate these dependencies for three alloy steels—2¼Cr-1Mo steel, Type 304 stainless steel, and Type 316 stainless steel—at specific temperatures. Obviously, such a broad objective is beyond the current state of technology. Hence, the scope of this paper will be limited to investigating the path and history dependence of these materials using simple state-of-the-art approaches. In so doing, the path dependence will be examined by treating creep and relaxation as inverse processes and examining the subsequent correlations. History dependence is indicated by the analysis of relaxation data with different prior loading histories.

To examine path dependence, relaxation data are analyzed and compared with creep data generated on material with the same prior history. The feasibility of such an approach has been evaluated in only a few past studies, for example, [*1,2*].[3] The practical benefit of such a capability is enormous. Generally, elevated temperature fatigue data are obtained under strain control where hold times give rise to stress relaxation curves. If it were possible to convert relaxation data to creep data, then one could measure the influence of cyclic history on creep. Given sufficient information of this type, memory and history rules could be developed such as the Masing hypothesis [*3*] and the accumulated plastic strain measures of cyclic softening or hardening [*4*], which are used to model uniaxial stress-strain response under cyclic loading. Given the ability to develop isothermal creep curves from relaxation data, one would require the results of only a few experiments (ideally only one) to synthesize the creep curves. This is in contrast to the multiple experiments that are currently required, thereby providing an obvious potential for cost savings.

To develop creep curves from a relaxation curve, an analytical representation of the physical process (or, alternatively, reasonable assumptions) and a decision process that determines the best representation of the

[3] The italic numbers in brackets refer to the list of references appended to this paper.

relaxation curve are required. In this paper, simple analytical representations [5] of the creep curve and the time-hardening rule (equivalent to assuming negligible recovery and anelastic effects) are assumed for computational simplicity. The creep equation is integrated to develop a stress relaxation function, which is then fitted to stress relaxation data using the method of nonlinear least squares. Since a goal of this effort was to evaluate only the feasibility of predicting creep from relaxation, other more complicated but more correct expressions for the creep curve are not used; therefore, restrictions are placed on the accuracy of both the method and the resulting creep-curve predictions. The creep curves so derived are compared to creep curves obtained under loading histories comparable to those used to obtain the relaxation data. These comparisons show reasonable correlations between the two. Data for two austenitic steels (Types 304 and 316) and one low-alloy ferritic steel (2¼Cr-1Mo) are examined at different temperatures, and various nonlinear least squares techniques are investigated. Finally, limitations of the approach are discussed and recommendations for further work are given.

Background

There are several complicating factors that make it difficult to represent time-dependent material deformation responses obtained from creep and stress relaxation on a common basis without accounting for differences in path. Four of the more important reasons are as follows:

1. The thermally activated micromechanisms are stress and temperature dependent. As such, one must represent each of the different mechanisms in the context of each of the potential phenomenological manifestations of these microprocesses. Since the analytical forms for representing these mechanisms are known to be different, the form of phenomenological models is constrained by the active microprocess.
2. The creep is history dependent, as shown, for example, by differences between monotonic and cyclic creep response [5,6]. This fact, which is not really surprising when one considers the differences between cyclic and monotonic stress–strain response at lower homologous temperatures, is seldom taken into account.
3. Recovery and anelasticity are often observed in metals and alloys after a stress reduction, giving rise to a distinct possibility for differences between the time-dependent response measured in creep and stress relaxation. Accounting for these differences requires more than just the proper analytical form for the creep curve or the most correct hardening rule (for example, strain or time hardening) for transferring from one creep curve to another as stress is reduced.
4. While the above-mentioned micromechanisms are important, con-

siderations such as environmental attack (for example, oxidation and corrosion) and grain boundary movement can also play important roles in what is normally referred to as time-dependent deformations. Such mechanisms clearly lie outside the above-mentioned functional forms, and their unique inclusion into deformation response prediction schemes requires more developmental work.

While these complicating factors are of real concern, they do not preclude achieving the objective of this paper. Thus, it is still reasonable to expect that creep and relaxation can be treated as inverse processes when the material response is path independent (for example, this can restrict applications to the mild homologous temperature range). However, given the complex metallurgical make-up of elevated-temperature alloys, it is difficult to predict this path-independent regime without recourse to a detailed metallurgical evaluation. In this paper, we avoid this problem by dealing with data where the time-dependent response is path insensitive (other than that, we use the time-hardening rule to model the stress relaxation).

Analytical Considerations

Several key assumptions are necessary in order to develop an algorithm for predicting creep curves from relaxation data. These include the form of the creep curve, the selection of a hardening rule, and an approach for fitting the relaxation equation. Each of these items will be discussed separately.

Creep Equation

Since only isothermal relaxation and creep response are treated in this paper, the following equations are given without including the temperature variable T. In general applications, temperature should be included. As previously mentioned, it is desirable to use a creep equation that is consistent with the microprocess of the material at hand. Since the goal of this paper is to initially investigate the feasibility of predicting creep curves from relaxation test results, this prescription is not followed precisely. Rather, simple creep equation forms are deduced from mechanistic models of secondary (or linear) creep so that closed-form equations for the stress relaxation curve are obtained. This procedure necessarily limits the accuracy of the resulting creep predictions, which might be improved by assuming more precise analytical expressions for the creep curve. Such creep-curve expressions would not result, in general, in closed-form expressions for the relaxation curve, and the procedure to be described would involve a numerical integration. While conceptually no more difficult, the current method is simpler and adequate in the context of this paper's limited scope.

To begin, we choose the form for climb of edge dislocations given by Conrad [7]

$$\dot{\epsilon}^c = f(\sigma) = K'\sigma^n \sinh(\beta\sigma^m) \tag{1}$$

where

$\dot{\epsilon}^c$ = creep rate,
σ = applied stress, and
K', n, β, and m = material constants.

Equation 1 provides a very flexible format in that it includes other mechanisms as special cases and thus yields well-known approximate creep curves by specifying certain constants. For instance, if in Eq 1 $n = 1$ and $m = 0$, one has the result that

$$\dot{\epsilon}^c = K\sigma \tag{2}$$

where $K = K' \sinh \beta$, which is the form for diffusion creep [7]. For the present, three specific forms of Eq 1 are used, one of them being Eq 2. By setting $m = 0$, one has the log-linear relation

$$\dot{\epsilon}^c = K\sigma^n \tag{3}$$

and if $n = 0$ and $m = 1$, one has a hyperbolic sine equation

$$\dot{\epsilon}^c = K' \sinh(\beta\sigma) \tag{4}$$

These equations model only secondary creep, whereas real creep curves exhibit a nonlinear (in time) primary creep stage that can be modeled as follows.

Primary Creep Modeling—Assuming that Eqs 1 through 4 specify the stress dependence of the creep rate and that the time and stress dependence are uncoupled, the creep rate can be written as

$$\dot{\epsilon}^c = f(\sigma)g(t) \tag{5}$$

where $f(\sigma)$ is given by Eqs 2 through 4. It is assumed that

$$g(t) = mt^{m-1}$$

Combining Eqs 3 through 5 and recognizing that Eq 2 is merely a special case of Eq 3 (with $n = 1$), the two creep equations utilized in this paper are given as

$$\dot{\epsilon}^c = mK\sigma^n t^{m-1} \tag{6}$$

$$\dot{\epsilon}^c = mK' \sinh(\beta\sigma)\, t^{m-1} \tag{7}$$

Hardening Rules

A critical item in development of creep curves from relaxation data is the selection of a hardening rule. Several choices are possible, including time hardening [*8*], strain hardening [*8*], Hart's approach [*9*], and the nonlinear viscoelastic theories (for example, [*10,11*]). Of these methods, Hart's is not applicable, since constant states of hardness are assumed for relaxation results. Relaxation results from experiments at more than one constant strain level are necessary in order to uniquely determine his parameters. Thus, while his approach is important, it is not useful in the current context. Nonlinear viscoelastic formulations—the multiple integral formulation [*10*] and the single kernel function representation [*11*]—are not considered either, because the former requires the determination of several kernel functions, while the latter represents all primary creep as being anelastically recoverable, as is not generally true for metals. While the single kernel function approach recently has been improved to alleviate this anelastic assumption [*12*], the approach is still cumbersome. This leaves us with the choice of either strain or time hardening.

In comparing the strain- and time-hardening rules, normally the strain-hardening rule is preferred, because it tends to represent a reactivation of primary creep during a stress increase and a creep rate decrease during a stress reduction (more than is predicted by time hardening). However, at least one author [*13*] has concluded that the time-hardening rule should not be rejected on physical grounds (since both are engineering approaches), and remarks that comparisons between the two formulations often show small differences. Indeed, the two approaches are identical for the extreme case of materials that exhibit only secondary creep. In this work, we adopt the time-hardening rule, since it leads to closed-form solutions for the relaxation curve using Eqs 6 and 7.

In closing this section, we remark that at least two other "hardening rules" are possible, the Besseling approach [*14*] and that described by Pugh et al [*15*]. Both of these approaches require numerical integration of the creep curves to determine the relaxation curve, and therefore are not used. All such rules are necessarily approximations that do not identically model the physical realities of the microprocesses that give rise to phenomenological observations such as recovery and anelasticity. Until such models are developed, one must choose according to his own preferences, guided by the requirements at hand.

Relaxation Equations

To determine the form of the relaxation curve, it is assumed that the total strain ϵ is composed of elastic, plastic, and creep components

$$\epsilon = \epsilon^c + \epsilon^p + (\sigma/E)$$

where ϵ^p is the plastic (time-independent) strain and E is the elastic modulus. Differentiating with respect to time, assuming that the plastic strain rate is zero during stress relaxation and noting that total strain is constant, one has, after rearranging

$$\dot{\sigma} = -E\dot{\epsilon}^c \tag{8}$$

Substituting Eq 5 into Eq 8 and integrating gives

$$\int_{\sigma_0}^{\sigma} \frac{d\sigma}{f(\sigma)} = - \int_0^t Eg(t)\, dt \tag{9}$$

where σ_0 is the initial stress at the onset of relaxation. Substituting Eq 6 into Eq 9 one obtains

$$\sigma = [(n - 1)EKt^m + \sigma_0^{(1-n)}]^{(1-n)^{-1}} \tag{10}$$

while Eq 7 gives

$$\sigma = \frac{1}{\beta} \ln \left(\frac{e^y + 1}{1 - e^y} \right) \tag{11}$$

where

$$y = -\beta EK't^m + \ln \left| \tanh \frac{\beta\sigma_0}{2} \right| \tag{12}$$

Equation 10 does not apply when $n = 1$, so substituting Eq 2 for $f(\sigma)$ in Eq 9 yields

$$\ln \frac{\sigma_0}{\sigma} = EKt^m \tag{13}$$

Equation 13 has the form of the Gittus equation [16], which has been used in previous studies of short-term cyclic relaxation behavior (for example, [17,18]). Considering its basis (Eq 2), Eq 13 appears to be valid for diffusional creep processes only. However, as discussed in detail later, this is a rather narrow perspective, as equations of the form of Eq 2 (or Eqs 3 and 4) certainly would be reasonable mathematical approximations over limited stress ranges, regardless of the mechanisms involved.

Nonlinear Least Squares Techniques

Two alternative approaches were used in the study. The first of these, which was applied to Eqs 10 and 13 only, was based on Eq 10 rearranged so that, once the natural logarithm was taken, the following form was obtained

$$\underline{\overline{\mathrm{Y}}} = \ln\left(\frac{\sigma^{(1-n)} - \sigma_0{}^{(1-n)}}{n-1}\right) = \ln(EK) + m \ln t \tag{14}$$

Using specified values of n in the left-hand side of Eq 14, a linear least squares approach was employed in terms of the variable $\underline{\overline{\mathrm{Y}}}$. That is, the nonlinear problem has been linearized, giving the usual form

$$\mathrm{SSD}\underline{\overline{\mathrm{Y}}} = \sum_{i=1}^{N} (\underline{\overline{\mathrm{Y}}}_i - \underline{\overline{\overline{\mathrm{Y}}}}_i)^2 \tag{15}$$

where $\underline{\overline{\mathrm{Y}}}_i$ was the left-hand side of Eq 14, $\underline{\overline{\overline{\mathrm{Y}}}}_i$ was the right-hand side, N was the number of relaxation data points used to determine ln (EK) and m via linear least square regression analysis, and $\mathrm{SSD}\underline{\overline{\mathrm{Y}}}$ denotes the sum of the squares of the deviations of $\underline{\overline{\mathrm{Y}}}$. The range of $1 \leq n \leq 10$ was considered, such that minimum values in the error of the variable $\underline{\overline{\mathrm{Y}}}$ were obtained. A second approach using these equations was also pursued in which the error in stress was computed via the equation

$$\mathrm{SSDS} \equiv \sum_{i=1}^{N} (\sigma_i - \overline{\sigma}_i)^2 \tag{16}$$

where σ_i was the stress after t_i hours of stress relaxation, $\overline{\sigma}_i$ was the predicted stress at time t_i, and SSDS denotes the sum of the squares of the deviations of stress. Note that the second approach does not resort to a linearization of the format of the relaxation equation for purposes of analysis. Note, too, that the error is being minimized on different variables, with only the second using a pure stress basis. Therefore, as might be expected, minima in Eqs 15 and 16 were not found at the same values of ln (EK) and m.

In addition to the previously noted aspects, it should be noted that due to the transformed nature of Eq 14, the global minimum of Eq 16 could not be found by this approach. Thus, an available subroutine [*19*] that included the Levenberg-Marquardt approach [*20,21*] was used to ensure that the global minimum of Eq 16 was located. The Levenberg-Marquardt approach, which ensured decreased values of SSDS before a change in the coefficients was made, was found to be more reliable than Brown's approach [22], which was also available in the same subroutine. Brown's approach did not ensure that SSDS was decreased before a change in the variables was made, and was found to diverge for bad initial values. An alternative approach, which utilized Newton's method, which was a part of the Levenberg-Marquardt approach, was also attempted. However, the approach generally failed to converge and was not used in most cases.

Results

The least squares approach was used to evaluate three groups of stress relaxation data:

1. Stabilized cyclic relaxation response of Type 316 stainless steel for hold-time (0.1 to 5.0 h) fatigue tests at 566°C (1050°F) and 649°C (1200°F) that were conducted by Jaske et al [23].
2. Relaxation response (20 to 150 h) of Type 304 stainless steel after fatigue precycling to cyclically stabilized condition at 593°C (1100°F). One test was conducted by Leis [24], and two tests were conducted by Jaske [25].
3. Relaxation response (80 h) of 2¼Cr-1Mo steel after fatigue precycling to a stabilized condition at 510°C (950°F) as reported by Jaske et al [6], and relaxation response (12 to 96 h) of 2¼Cr-1Mo steel as a function of plastic strain history from data reported by Pugh [26].

Predictions of creep data are made using the constants in Eqs 6 and 7 obtained from relaxation curve fits. Upon integration for constant stress, Eqs 6 and 7 become

$$\epsilon^c = K\sigma^n t^m \tag{17}$$

and

$$\epsilon^c = K' \sinh(\beta\sigma)\, t^m \tag{18}$$

respectively. Since both of these equations are linear on logarithmic coordinates of ϵ^c and t, this format provides a convenient basis for graphical comparison of predictions with the data. Three generic cases are examined:

1. Cases involving relaxation after prior initial constant-amplitude strain cycling (which was adequate to stabilize the hysteresis response). In these cases, direct comparison of predictions with creep data after the same initial cycling is made.
2. A cursory evaluation of the dependence of the relaxation coefficients on the initial stress level.

3. A case which demonstrates the potential history-path dependence of the time-dependent flow due to more complex strain cycling conditions.

Results for each of these cases are presented in turn.

Comparisons of Creep Predictions with Data

Three specimens of solution-annealed Type 304 stainless steel were subjected to hold periods at maximum tensile strain after 20 cycles of straining at a rate of 0.005 min^{-1}, a strain amplitude of ± 0.3 percent, and a temperature of 593°C (1100°F). Two of these (Specimens 9 and 9A) were from work of Jaske [*25*], and the other one (Specimen BR-1) was from work of Leis [*24*]. Results of the data analyses using the transformed Eqs 14 and 15 are given in Table 1, while the results from the analyses using the Levenberg-Marquardt approach are given in Table 2. The results obtained from the analysis of the data for Specimen 9A are presented later, in the discussion section. Figure 1 compares results of the three types of analytical approaches with the base relaxation data. As shown, all approaches give good agreement with the data. Although some cases are worse, Fig. 1 is typical of all such comparisons; hence, further comparisons of the analyses with the baseline data will not be given in presenting the other results.

Using the coefficients in Eqs 17 and 18 obtained from the relaxation analyses, creep curve predictions can be made. The comparison of these predictions with creep data collected following the same prior cyclic history are shown in Fig. 2, where good agreement is indicated for two of the approaches. Figure 3 shows a similar comparison of analytical results with the creep data reported by Leis [*24*]. In this case, the results from applying the transformed approach did not agree with the relaxation data as well as those from the Levenberg-Marquardt approach, and consequently the creep predictions are not as good. Figure 4 shows yet another comparison of the predictions of the analytical results with other data from Leis [*24*]. The data in this figure are for an unusual control condition, where the product of stress and strain is maintained constant. The predictions (the darkened symbols) are the results obtained by numerically imposing this control condition utilizing an iterative algorithm. The constants that are used in the analysis are those obtained from the fit of the relaxation data.

Relaxation data reported by Jaske et al [*6*] for 2¼Cr-1Mo steel at 510°C (950°F) are examined next. One specimen (KB-17) was subjected to a stabilizing cyclic strain history prior to relaxation testing. In this case, using Eq 10 and the Levenberg-Marquardt fitting technique resulted in a negative stress exponent ($n < 0$). When Eqs 11 and 12 were used in conjunction with the Levenberg-Marquardt approach, this problem was not encountered directly. However, a low enough value of β was obtained that the hyperbolic sine term was approximately equal to its argument

TABLE 1—*Stress relaxation results for strain hold times after 20 cycles of straining (transformed approach).*

Specimen	Tension Length of Hold Time, h	Precycling Total Strain Range, %	Maximum Sress, MPa (ksi)	Best-Fit Values Based on SSDY[a]		
				n	$m - 1$	$A(EK)$
Type 304 Stainless Steel at 593°C (1100°F)						
9	110	±0.3	173 (25.1)	2.76 (1)	−0.578 (−0.681)	4.60×10^{-4} (0.0757)
9A	150	±0.3	170 (24.7)	1.0	−0.775	0.0632
BR-1	20.5	±0.3	145 (21.1)	1.0	−0.722	0.0665
2¼Cr-1Mo Steel at 510°C (950°F)						
KB17	80	±0.2	276 (40.0)	1.0	−0.787	0.0363

[a] Values in parentheses are those for the Gittus-type relation when it did not give the best fit to the data.

TABLE 2—*Results using the Levenberg-Marquardt approach (nonlinear least squares).*

Type of Steel	Specimen No.	Temperature, °C (°F)	EK (Eq 10)	n (Eq 10)	m (Eq 10)	EK' (Eq 11)	β (Eq 11)	m (Eq 11)	Reference
Type 304	9	593 (1100)	5.894 E-4	2.9611	0.4362	6.003 E-2	0.2386	0.5389	[25]
	BR-1	593 (1100)	2.240 E-4	3.394	0.4744	0.17614	0.21162	0.4763	[24]
2¼Cr-1Mo	KB-17	510 (950)	NC[a]	NC[a]	NC[a]	132.66	1.075 E-3	0.2768	[6]
	FCM-1 (1-1)[b]	538 (1000)	0.8381	0.5193[c]	0.1693	31.28	7.574 E-3	0.1795	[26]
	FCM-1 (2-3)[b]	538 (1000)	1.338 E-2	2.599	0.3143	3.337 E-2	0.5683	0.5342	[26]
	FCM-1 (3-1)[b]	538 (1000)	4.581 E-3	3.533	0.413	NC[d]	NC[d]	NC[d]	[26]

[a] Convergence actually obtained yielded $n < 0$ for Eq 10. Using Eq 11, the small β-value forces the effective use of Gittus relation Eq 13.

[b] Numbers in parentheses indicate (segment number-event number) as discussed previously.

[c] $n < 1$ is not a physically realistic value of the exponent. Using Eq 11, the small β-value forces the effective use of Gittus relation Eq 13.

[d] Convergence not obtained due to numerical insensitivity of Eq 11 when β is high. In this case, assuming $\sinh \beta\sigma \simeq e^{\beta\sigma}$ and integrating might yield a useful approach.

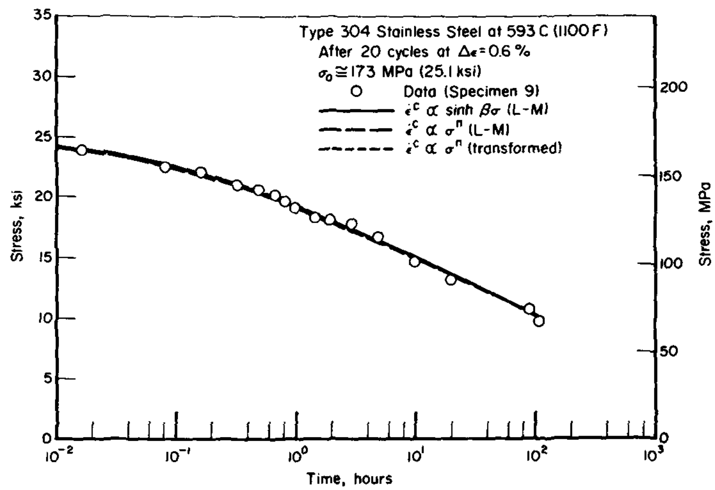

FIG. 1—*Results of regression analyses compared to Type 304 stainless steel relaxation data (Specimen 9).*

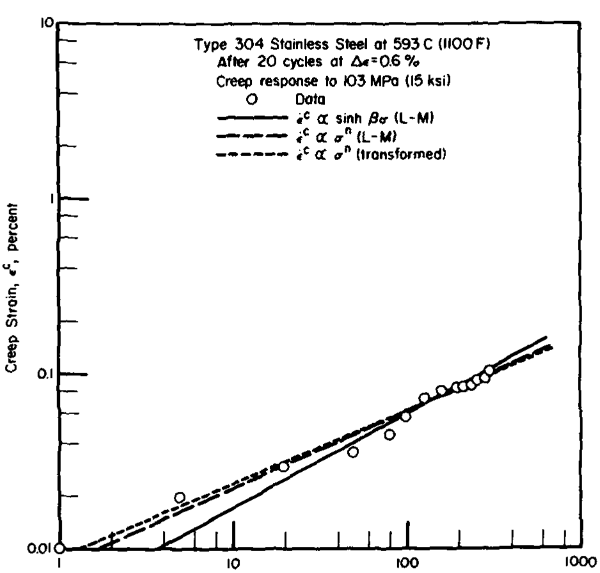

FIG. 2—*Comparison of creep data to predictions for Type 304 stainless steel.*

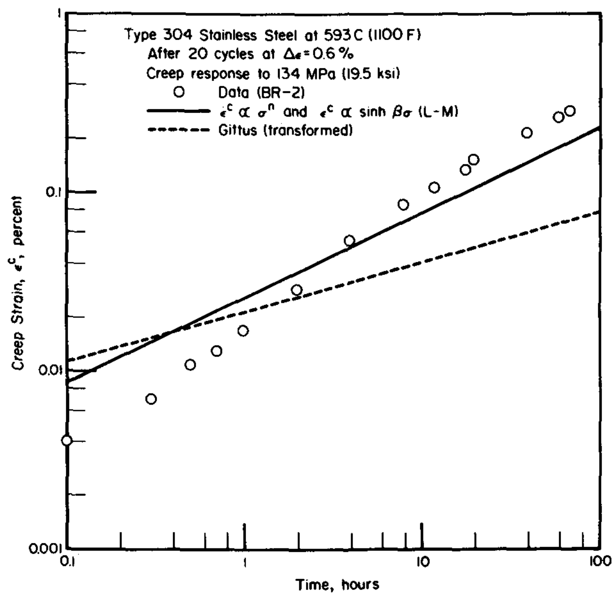

FIG. 3—*Comparison of creep data to predictions for Type 304 stainless steel (Specimen BR-2).*

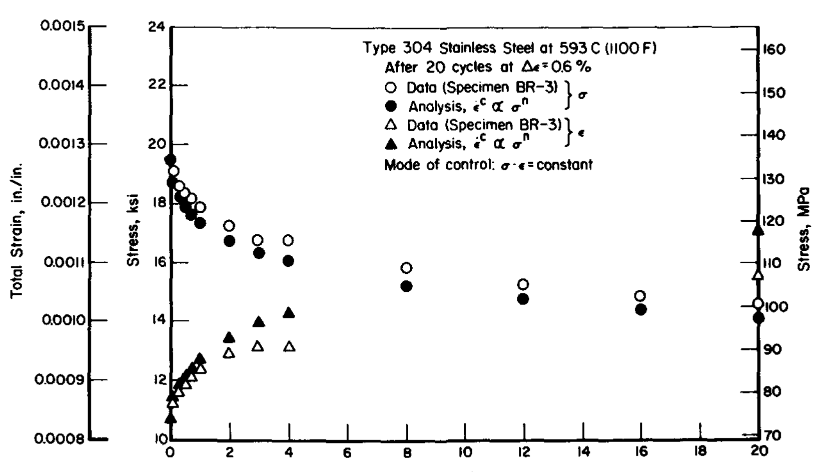

FIG. 4—*Comparison of product control data to predictions for Type 304 stainless steel (Specimen BR-3).*

over the range of stresses in the relaxation data set. Also, the transformed approach indicated the Gittus relationship ($n = 1$). Thus, both approaches indicated the same functional stress dependence. However, since the two approaches optimize different measures of error (Eqs 15 and 16), the results were slightly different, as shown in Fig. 5, where the predicted lines are compared to the corresponding creep data.

Dependence of the Coefficients on the Initial Stress Level

The preceding analyses have examined the potential of predicting creep from relaxation data. Here we examine briefly the uniqueness of these coefficients as a function of the initial stress level. Due to the fact that the relaxation times considered are small, these results may be of limited applicability. However, they may indicate trends that should be considered before applying them to data obtained from a single relaxation test.

Data were analyzed from 10 hold-time fatigue experiments of Type 316 stainless steel at 566°C (1050°F) and 14 hold-time fatigue experiments of the same alloy at 649°C (1200°F) [*23*]. In all cases, the relaxation data were for a stabilized cycle at approximately half the number of cycles to failure. Total strain ranges and hold times were kept constant throughout

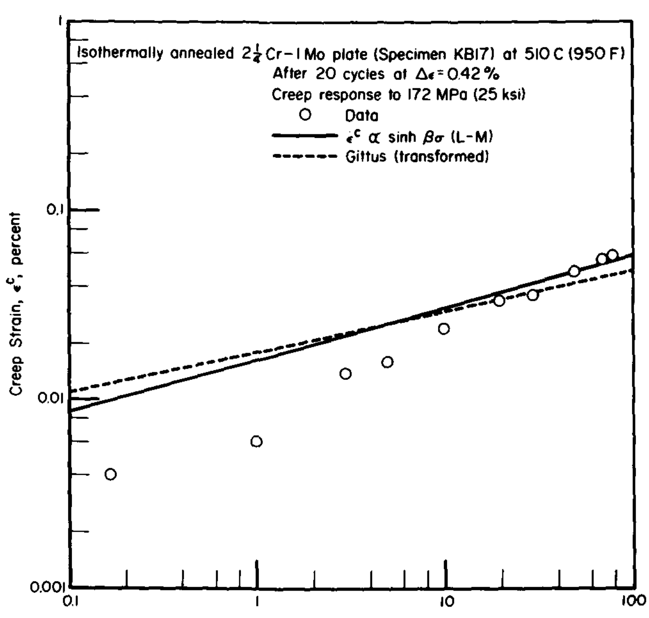

FIG. 5—*Comparison of creep data to predictions for 2¼Cr-1Mo steel (KB-17).*

each test, and a hold period was introduced at the peak tensile strain in every cycle. Hold times of 0.1 and 5.0 h[4] and total strain ranges of 0.5 to 2.1 percent were used. Since these hold time lengths were relatively short, the amount of stress relaxation was correspondingly small. In most cases, the relaxed stress σ_r at the end of a hold period was greater than 70 to 80 percent of the maximum (or initial) stress σ_{max}. For this example, only the transformation approach (Eq 15) was used.

For these shorter hold times and smaller amounts of relaxed stress, the Gittus-type relaxation equation ($n = 1$) gave a satisfactory representation of the relaxation response, even though it was not always the case of optimum least squares fit. For 13 of the 24 experiments, the Gittus relation ($n = 1$) gave the best fit (i.e., $\text{SSD}\overline{\text{Y}}_{min}$). In the other eleven cases, the best-fit values of n ranged from 1.83 to 9.62. In these cases, the value of SSDS_{min} was only 0 to 15 percent smaller than the value of SSDS at the conditions where $\text{SSD}\overline{\text{Y}}_{min}$ was computed.

An empirical approach was developed for approximating the best-fit constants A (EK) and m, as a function of strain range and test temperature. Upon determination of these terms, an application to continuous cycling data is made as follows. For fully-reversed, continuous-fatigue cycling, Morrow [*27*] has observed that stable cyclic stress-strain response can be described by a power law:

$$\sigma_{max} = K_H(\Delta\epsilon^p/2)^{nH} \tag{19}$$

where

σ_{max} = maximum stable cyclic stress amplitude,
$\Delta\epsilon^p$ = stable plastic (time-independent) strain range,
K_H = cyclic strength coefficient, and
nH = cyclic strain hardening exponent.

For the hold-time tests of Type 316 stainless steel, the data were well approximated by Eq 19 using the constants listed in Table 3. Similar constants for continuous cycling fatigue (without hold times) also are listed. Although these cyclic stress-strain relationships were not a significant function of hold time (0.1 to 5 h), they are different than those for continuous cycling.

Once a value of σ_{max} is computed from Eq 19, one needs to know the appropriate values of A and m in order to compute stress relaxation response with the Gittus-type relation. For the data under consideration,

[4] Fifteen tests were with 0.1-h hold periods, 3 were with 0.5-h hold periods, 5 were with 1.0-h hold periods, and 1 was with a 5.0-h hold period. Thus, a majority of the tests were for relatively short hold times.

it was found that A had an approximately constant (within experimental scatter) value at each temperature:

$$A = 0.0304 \quad \text{at } 566^\circ\text{C } (1050^\circ\text{F})$$
$$A = 0.367 \quad \text{at } 649^\circ\text{C } (1200^\circ\text{F})$$

The constant m was treated as a function of stable maximum cyclic stress amplitude:

$$m = 1 - (\sigma_{max}/C_H)^h \qquad \text{for} \quad \sigma_{max} \leq 379 \text{ MPa } (55.0 \text{ ksi})$$
$$m = 0.10 \qquad \text{for} \quad \sigma_{max} > 379 \text{ MPa } (55.0 \text{ ksi})$$

where C_H was a constant equal to 402 MPa (58.3 ksi) and h was a constant equal to 1.80 for both material conditions and both temperatures. This is equivalent to assuming A is independent of the strain history, while m is dependent on the strain history. Temperature dependence is assumed for A, while m is independent of the temperature level.

Using Eq 19 and values of m and A (as just formulated), one can use Eq 13 to predict relaxation for a given value of $\Delta\epsilon^p$. Two measures of how well this average approach works are shown in Fig. 6. There is a wide scatter in the relative error of the amount of relaxed stress, $\sigma_{max} - \sigma_r$, as shown in Fig. 6*a*; however, the average ratio is fairly close to unity. When actual values of σ_r are compared with calculated ones on an absolute basis, a much better apparent correlation is shown (see Fig. 6*b*). All but 4 of the 24 data points fall within a scatter hard of ± 20 MPa (2.9 ksi). Thus, this approach can give a reasonable assessment of the absolute relaxed stress level, but the computed amount of relaxation ($\sigma_{max} - \sigma_r$) may be subject to errors as large as about ± 100 percent when this amount is a small ($\leq \sim 10$ percent) fraction of the actual value of σ_{max}.

TABLE 3—*Constants for power law*[a] *cyclic stress-strain curve for type 316 stainless steel.*[b]

Temperature, °C (°F)	Material Condition	Values of Constants: For Hold-Time Tests K_H, MPa (ksi)	For Hold-Time Tests nH	For Continuous Cycling K_H, MPa (ksi)	For Continuous Cycling nH
566 (1050)	annealed; aged[b]	1124 (163)	0.218	2034 (295)	0.317
649 (1200)	annealed	855 (124)	0.214	1248 (181)	0.250
649 (1200)	aged[b]	752 (109)	0.214	1062 (154)	0.250

[a] $\sigma_{max} = K_H (\Delta\epsilon^p/2)^{nH}$, $0.001 \leq \Delta\epsilon^p/2 \leq 0.01$.
[b] Data reported by Jaske et al [23].
[c] Aged for 1000 h at indicated test temperature before testing was initiated.

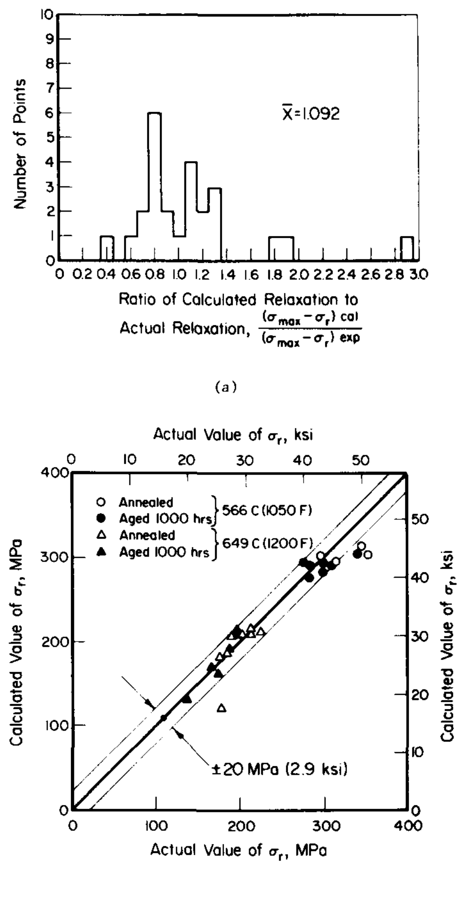

FIG. 6—*Error in averaged calculation of relaxation behavior for Type 316 stainless steel.* (a) *Histogram of relative error in calculating relaxation response.* (b) *Calculated stress at end of hold time.*

Influence of Sequence and History Dependence

Figure 7 shows a schematic of a loading history imposed on a specimen of 2¼Cr-1Mo steel at 538°C (1000°F) [*26*] from which the last examples are extracted. Though no comparable creep data are directly available, these examples are used to illustrate the pronounced effect of loading sequence or history or both. Figure 8 shows the relaxation data and the corresponding predictions. Note that each data set shows drastically different relaxation response (that is, compare the amount of relaxation). Such response differences, quite clearly, show the need for the development of methods that can predict such behavior. These differences give rise to

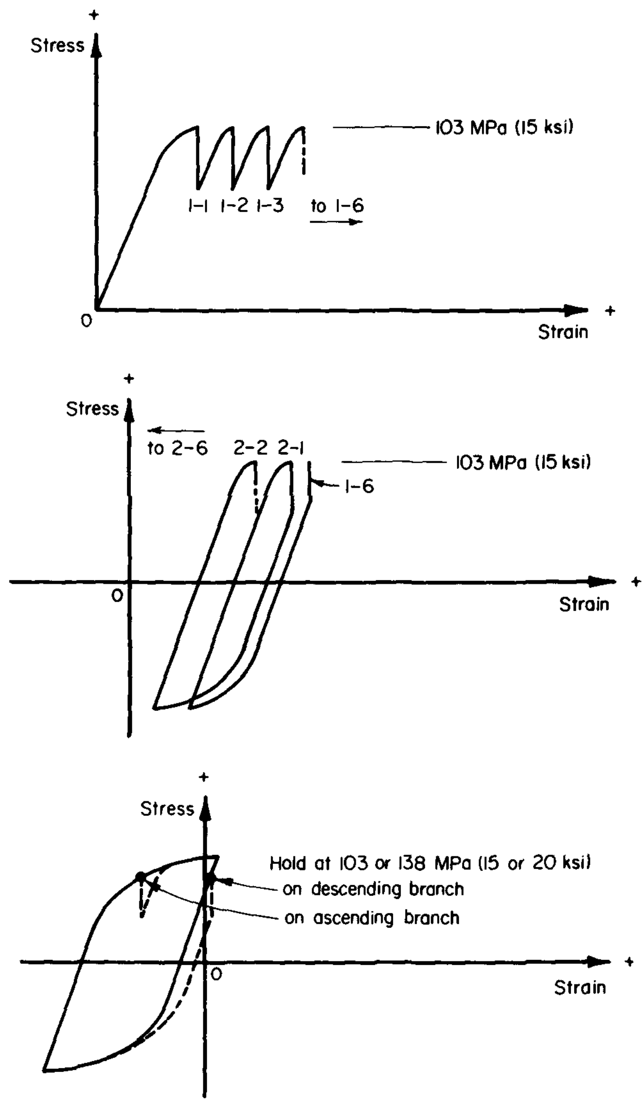

FIG. 7—*Schematic illustration of three types of tensile strain hold segments used in test of Specimen FCM-1 or 2¼Cr-1Mo steel at 538°C (1000°F).*

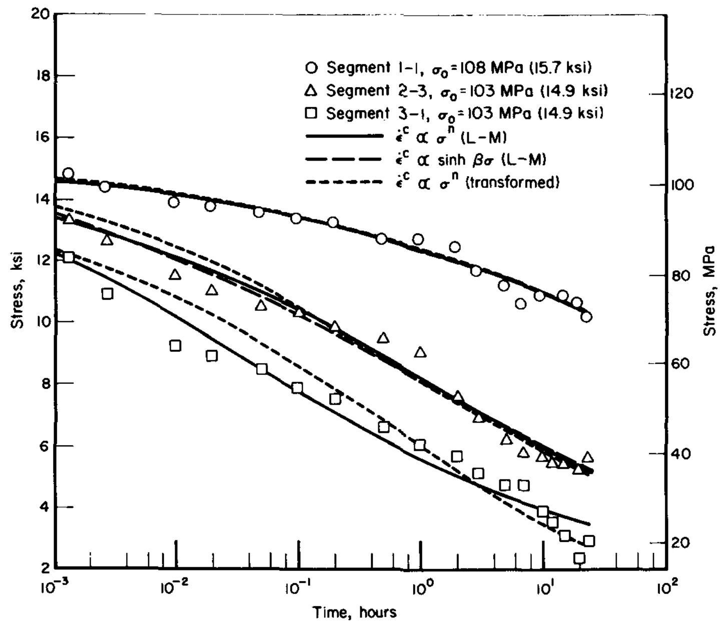

FIG. 8—*Results of regression analyses compared with data for relaxation test of Specimen FCM-1 of 2¼Cr-1Mo Steel at 538°C (1000°F).*

the predicted creep curves shown in Figure 9. As shown, a large dependence of creep upon sequence (or history) is apparent.

In Figure 9, the influence of these different loading segments on the derived creep curves is compared to an Oak Ridge National Laboratory (ORNL) creep equation [*28*], which is reported to be an average representation of several heats of 2¼Cr-1Mo steel over a broad range of temperatures and stress. As shown, the creep curves derived from the relaxation data for Segment 1-1 cross this curve at approximately 20 h, whereas the predicted creep response for the other segments are substantially above this curve. Segment 1-1 corresponds to the initial relaxation before any strain cycles and would be most comparable to this creep curve. While the correspondence between the present predicted curve and the ORNL curve is poor, there is substantial scatter in the reported data on which the ORNL curve is based. A comparison of the ORNL curve with data at 538°C (1000°F) and a stress of 103 MPa (15 ksi) shows that the times to 0.5 percent creep strain vary from approximately 32 h to 3200 h, with the ORNL curve representing the upper bound [*28*]. Comparisons at other creep strain levels are not available from this reference, so the tendency of the ORNL curve at lower creep strain levels is not known. The inference that can be made is that the current predictions may be reasonable for the

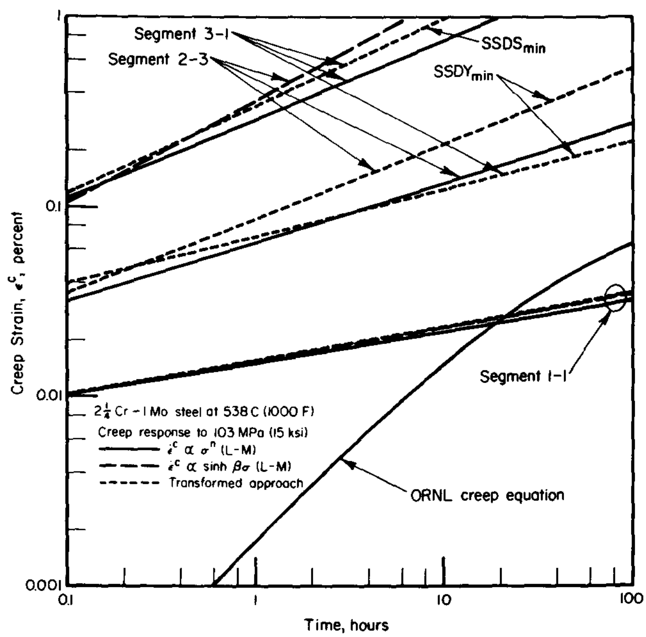

FIG. 9—*Comparison of the creep predictions for three segments of an experiment in 2¼Cr-1Mo steel to an ORNL creep equation.*

particular heat from which the relaxation data are obtained, but this cannot be verified directly.

Discussion

The objective of this paper is to evaluate the feasibility of obtaining physically meaningful results from the analysis of relaxation data using simplified approaches. As can be seen in Figs. 2 through 5, reasonably accurate predictions of creep data can be obtained with the approaches under evaluation. However, easy interpretation of these results is somewhat confounded by the following intertwined factors: (*a*) material variability versus experimental error, (*b*) numerical considerations, (*c*) material history dependence, (*d*) material path dependence, and (*e*) the limitations of the assumed creep equations and hardening rules. These factors will be discussed in the ensuing paragraphs.

One nagging concern is the lack of repeatability of the derived coefficients. This was observed to different extents in the evaluation of all three materials. One explanation is the material variability versus experimental error aspects as is shown through the discussion of Fig. 10. The data in Fig. 10 are from results obtained from identical testing of two

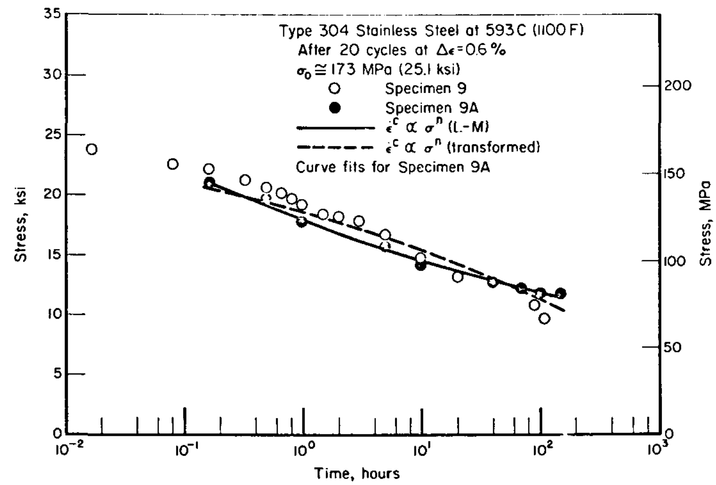

FIG. 10—*Influence of test-to-test variation on the calculated relaxation curve.*

different specimens of nominally the same material. The analytical results of the data for specimen 9 were presented earlier in Figs. 1 and 2, and the coefficients from this analysis are consistent with those obtained from the analyses associated with the data in Figs. 3 and 4 (see Table 2). Included in Fig. 10 are the predictions obtained from the nonlinear Levenberg-Marquardt approach (solid line) and the Gittus relationship (dashed line) for the results from specimen 9A. Comparing the predictions to the data, it is seen that the Levenberg-Marquardt approach gives a better representation of the data than that obtained from the Gittus equation. However, the constants are not physically realistic ($n \sim 20$, $m > 1$). Considering these results contrasted to those for specimen 9, it is apparent that rather large discrepancies can be obtained from single-specimen analyses. Therefore, further analysis of this type should use an approach that would group all specimens for a given material with the same previous history into a single population. The results so obtained would tend to eliminate the specimen-to-specimen variations and measurement errors and increase the overall confidence in the approach.

Concerning the comparison of the two fitting techniques (the transformed and Levenberg-Marquardt approaches), it was observed that in general, the transformed approach that minimized SSD$\overline{\underline{Y}}$ (Eq 15), gave rise to different coefficients and exponents than the nonlinear approach that minimized SSDS (Eq 16). Considering the transformed approach, it is seen, through Table 1 and the analysis of the Type 316 stainless steel data, that the Gittus relationship was most often obtained. Furthermore, using SSD$\overline{\underline{Y}}$ as the error measure resulted in a reversal in trends between the creep predictions for Segments 2-3 and 3-1 (see Fig. 9). When the SSDS error measure was used, the results were as expected. Conversely, the Levenberg-Marquardt approach yielded a consistent formulation for the two materials that were evaluated using it (see Table 2). In the case of 2¼Cr-1Mo steel, it was found that in two cases the creep exponent n was less than unity. In both of these cases, the hyperbolic sine stress-dependence formulation resulted in a β term sufficiently small that a linear stress dependency (as with the Gittus relationship) was indicated over the range of stresses included in the data sets. From a mathematical viewpoint, the hyperbolic sine relationship has the advantage over the log-linear form of ensuring that the stress exponent is never less than unity. Apparently, as shown in Figs. 5 and 8, this was a sufficiently accurate stress dependence in these cases. Whether or not this result is an artifact of the approximations involved in the creep equations and hardening rule (as discussed in the next paragraph) or is physically realistic was not investigated.

The assumed creep curve that is used in the analysis of the relaxation data is greatly simplified in order to yield a simple algorithm for evaluating the viability of the approach. As such, it is possible that the use of more sophisticated creep curves (and hardening rules) could yield better results. Whatever approach is assumed, it will presuppose a form of the relaxation curve and will be forced into agreement with the relaxation data via the regression analysis technique. Thus, the approach as used should ideally match the physical process in order that the results be realistic. However, while it is desirable to believe that adding sophistication to the analysis procedure (for example, better creep equation and hardening rules) would decrease some of the sensitivities observed in the current analyses, it is also possible that the converse is true. That is, due to the complexities of the physical process, the actual information available through a relaxation experiment (sensitivity of the results to the physical processes) and the potential measurement and control errors (particularly at long times), the use of more sophisticated approaches may result in only more degrees of freedom for forcing a curve fit without yielding physically viable measures of actual processes. This was observed in the present program in that the Gittus relationship resulted in answers that in some cases were more desirable than those obtained by more realistic stress dependences. As such, the current level of development may represent the terminal state that is necessary to obtain physically meaningful results.

With regard to the potential for path dependency and the subsequent inability to simultaneously model creep and relaxation, it is noted that Figs. 2 through 5 tend to imply that these alloys at the given temperatures are not strongly path dependent. Noting that the predicted creep curves are not optimum, the differences between predicted and actual results may be due to path dependence. However, since the assumed creep equations would be considered to be a model of only one creep stage, whereas there are generally three creep stages, it is also possible that the discrepancies are due to the assumed creep-curve model. Additional modeling would be required to determine which reason is correct.

Considering the history dependence, it is seen that history strongly affects the subsequent relaxation behavior and hence the predicted creep behavior (see Figs. 7, 8, and 9). Such a result demands further work toward the development of accurate history measures and constitutive theories. The brief study of the short hold time data for Type 316 stainless steel indicates that the coefficients obtained by the transformed approach may depend on the initial stress level and, more expectedly, temperature. Such a result may be an outcome of the assumed creep law, short hold times, or regression technique.

Conclusions

Four main conclusions can be drawn from this study:

1. In general, the nonlinear regression analysis technique is more reliable than the transformed-linear approach.
2. The results suggest that creep can be predicted from relaxation data. However, in the case of the 2¼Cr-1Mo steel, the stress exponent was unity, a result that, while yielding an apparently reasonable approximation, was not expected physically. This suggests that more sophisticated models of the creep process may be necessary to predict creep response from relaxation data in a completely consistent manner. However, owing to the mathematical nature of the curve fitting technique, the material variability versus experimental error problems, and the amount of relaxation observed, such approaches may also be confounded. More work is required in this regard.
3. History and sequence are shown to have a dramatic influence on the subsequent relaxation and predicted creep response.
4. Path dependency was not directly observed in the present examples. In cases where path dependency is large, the approach would not be successful.

Acknowledgments

Some of the data used in this study were from work performed at Battelle's Columbus Laboratories (BCL) for Oak Ridge National Laboratory operated by Union Carbide Corporation for the U. S. Department of Energy. The authors are indebted to T. Forte of BCL for his programming assistance and to B. N. Leis for his review of the manuscript and his helpful comments throughout the course of this investigation.

References

[1] Trumpler, W. E., Jr., *Journal of Applied Physics*, Vol. 12, 1941, p. 248.
[2] Kennedy, C. R. and Douglas, D. A., "Relaxation Characteristics of Inconel at Elevated

Temperatures," USAEC Report ORNL-2407, Oak Ridge National Laboratory, Oak Ridge, Tenn., 1960.

[3] Masing, G., "Eigenspannungen and Verfestigung Beim Messing," *Proceedings*, 2nd International Congress of Applied Mechanics, Zurich, Switzerland, 1926.

[4] Eisenberg, M. A., *Journal of Engineering Materials and Technology*, Vol. 98, 1976, pp. 221-228.

[5] Manson, S. S., Halford, G. R., and Spera, D. A., in *Advances in Creep Design*, A. I. Smith and A. M. Nicolson, Eds., Halstead Press Division, Wiley, New York, 1971, pp. 229-249.

[6] Jaske, C. E., Leis, B. N., and Pugh, C. E. in *Structural Materials for Service at Elevated Temperatures in Nuclear Power Generation*, American Society of Mechanical Engineers, 1975, pp. 191-212.

[7] Conrad, H. in *Mechanical Behavior of Materials at Elevated Temperatures*, J. E. Dorn, Ed., McGraw-Hill, New York, Chapter 8, p. 149, 1961.

[8] Manson, S. S., *Thermal Stress and Low-Cycle Fatigue*, McGraw-Hill, New York, 1966.

[9] Hart, E. W., Li, C. Y., Yamada, H., and Wire, G. L. in *Constitutive Equations in Plasticity*, A. Argon, Ed., The Massachusetts Institute of Technology Press, Cambridge, Mass., pp. 149-197, 1975.

[10] Green, A. E. and Rivlin, R., *Archive for Rational Mechanics and Analysis*, Vol. 1, pp. 1-21, 1957.

[11] Stouffer, D. C., *International Journal of Nonlinear Mechanics*, Vol. 7, 1972, pp. 465-472.

[12] Laflen, J. H., "A Constitutive Theory for Metal Creep," Ph.D. dissertation, University of Cincinnati, June 1976.

[13] Krempl, E., *Welding Research Council Bulletin*, No. 195, June 1974, pp. 63-123.

[14] Besseling, J. F., *Journal of Applied Mechanics*, Vol. 80, Dec. 1958, pp. 529-536.

[15] Pugh, C. E., Liu, K. C., Corum, J. M., and Greenstreet, W. L., "Currently Recommended Constitutive Equations for Inelastic Design Analysis of FFTF Components," ORNL/TM-3602, Oak Ridge National Laboratory, Oak Ridge, Tenn., Sept. 1972.

[16] Gittus, J. H., *Philosophical Magazine*, Vol. 9, 1964, pp. 749-753.

[17] Berling, J. T. and Conway, J. B. in *Proceedings*, 1st International Conference on Pressure Vessel Technology, Part II, American Society of Mechanical Engineers, New York, 1969, pp. 1233-1246.

[18] Jaske, C. E., Mindlin, H., and Perrin, J. S. in *Fatigue at Elevated Temperatures, ASTM STP 520*, American Society for Testing and Materials, 1973, pp. 365-376.

[19] Computer Subroutine Libraries in Mathematics and Statistics, IMSL LJB-0005, International Mathematical and Statistical Libraries, Houston, 1975.

[20] Levenberg, K., *Quarterly Journal of Applied Mathematics*, Vol. 2, 1944, pp. 164-168.

[21] Marquardt, D. W., *Journal of Society for Industrial and Applied Mathematics*, Vol. 11, No. 2, June 1963, pp. 431-441.

[22] Brown, K. M. and Dennis, J. E., *Numerische Mathematik*, Vol. 18, 1972, pp. 289-297.

[23] Jaske, C. E., Mindlin, H., and Perrin, J. S. in *Proceedings*, International Conference on Creep and Fatigue in Elevated-Temperature Applications, Institution of Mechanical Engineers, London, 1973, pp. 163.1-163.7.

[24] Leis, B. N. in *Proceedings*, Second International Conference on Mechanical Behavior of Materials, American Society for Metals, Aug. 1976, pp. 876-882.

[25] Jaske, C. E. in *High-Temperature Structural Design Methods for LMFBR Components Progress Report for Period Ending March 31, 1973*, ORNL-TM-4089, Oak Ridge National Laboratory, Oak Ridge, Tenn., pp. 231-239.

[26] Pugh, C. E. in *High-Temperature Structural Design Program Semiannual Progress Report for Period Ending December 31, 1976*, ORNL-5281, Oak Ridge National Laboratory, Oak Ridge, Tenn., pp. 24-30.

[27] Morrow, JoDean in *Internal Friction, Damping, and Cyclic Plasticity, ASTM STP 378*, American Society for Testing and Materials, 1965, pp. 45-87.

[28] Booker, M. K., Hebble, T. L., Hobson, D. O., and Brinkman, C. R., *International Journal of Pressure Vessels and Piping*, Vol. 5, 1977, pp. 181-205.

Summary

Summary

This book is arbitrarily divided into three sections which are interrelated to some degree. The first section consists of four papers involving mainly phenomenological theory, modeling, and constitutive relations. The second section contains five papers dealing with practical materials and product related stress relaxation problems, and the third section contains five papers dealing with the interrelation of stress relaxation and residual stress and cyclic loading.

An invited paper by Hart critically examines the load relaxation measurement in a uniaxial tensile stress relaxation test involving both machine and specimen compliance and relates the load-time record to a specimen history of stress versus strain rate, as a function of time at a given temperature. Hart then uses the stress versus strain rate relationship as a tool for establishing a material's inelastic constitutive relations. The stress versus strain rate curves for an idealized material in a uniaxial load relaxation test are examined (1) for a simple viscous flow relation, (2) viscous flow in combination with an internal stress (a condition found for many metals at low homologous temperatures), and (3) inelastic (visco-elastic) behavior. Hart relates these idealized conditions to a model which quantitatively accounts for differences in behavior at both high and low homologous temperatures, and discusses its applicability to real materials and complex loading histories.

Rhode and Swearengen use a power law relation between inelastic strain rate and stress to predict the stress relaxation behavior of high-purity aluminum. Although similar in format to Hart's model of viscous flow with an internal stress, their power law equation contains a drag stress term physically related to a microstructural dependent internal state variable. These authors postulate that the power law exponent, n, in stress relaxation is nearly equal to that for steady-state creep. They conducted both stress relaxation and creep experiments on 99.99 percent pure aluminum to experimentally verify this.

A paper by Parikh and Shapiro examines the effects of cold work and recovery on the stress relaxation behavior of two copper base alloys, CA 510 (Cu-5Sn-0.2P—phosphor bronze) and CA 638 (Cu-2.8Al-1.8Si-0.40Co—silicon aluminum bronze). These authors show that prior stress relaxation exposure can decrease the stress relaxation rate. They attribute their observations to rearrangements of dislocations rather than changes in dislocation density.

A paper by Glodowski and Hoff discusses a procedure for evaluating the prestress loss in prestressed concrete structures. This loss results from stress relaxation of the steel tendons, volume shrinkage of the concrete, and concrete creep. The paper examines the use of stress relaxation data obtained under conditions of approximately constant total strain as recommended in ASTM E 328 for a variable strain condition found in the steel tendons in actual structures by comparing data obtained from tests made at constant strain with those obtained under variable strain conditions.

Four of the papers in the second section discuss the problem of stress relaxation of spring materials and one involves stress relaxation of plastics. The paper by Idermark and Johansson reports results for room temperature stress-relaxation measurement in tension on wires made from AISI Type 301 austenitic stainless steel, a martensitic stainless chromium steel (Type 420), a texture rolled carbon steel (Type 1078), and a hardened and tempered carbon steel (Type 1074). These data, which were obtained by means of a vibrating string technique, are compared to test data obtained on helical extension springs held at constant length. Data are also presented for springs coiled from 17-7 precipitation hardenable steel and AISI 302 austenitic stainless steel.

The paper by Fox reports results on stress relaxation in bending on AISI 301 type austenitic stainless steel strip in the temperature range 23 to 93°C (73 to 200°F) made in accordance with ASTM E 328 and compares the data to load relaxation data on complex clamp springs whose main stress mode is bending.

A paper by Filer and Scorey evaluates stress relaxation in bending of three copper beryllium alloys in strip form, in the temperature range 22 to 200°C (72 to 392°F). The alloys studied by these authors were CA 170 (Cu-1.7Be), CA 172 (Cu-1.9Be), and CA 175 (Cu-2.5Co-0.6Be). Data are also presented for CA 260 (Cu-30Zn, 70 percent cartridge brass), CA 510 (Cu-5Sn-0.2P-Grade A, 5 percent phosphor bronze), CA 521 (Cu-8Sn-Grade C, 8 percent phosphor bronze), CA 725 (Cu-9.5Ni-2.3Sn) and CA 770 (Cu-27Zn-18Ni).

A fourth paper in this section is a report on a round robin test program utilizing ASTM Recommended Practice E 328, Part C, Conducting Stress Relaxation Bending Tests of Materials. Tests were conducted utilizing elastic springback, continuous force measurement, and lift off techniques. All showed agreement within 10 percent of the observed loss in stress. The materials used in this investigation were C 110 (electrolytic tough pitch copper) and CA 260 (Cu-30Zn, 70 percent cartridge brass) in strip form.

A paper by Lou shows that for some plastics such as polyurethane the conventional stress relaxation test can actually produce an increase rather than a decrease in stress, due to volume shrinkage of the material under conditions of constant extension. This points out the fact that just as in metals the investigator must be aware of structural changes that are taking place in the material as the test progresses or some erroneous conclusions may be drawn.

The third section of the book consists of four papers; three of these involve studies of the stress relaxation of residual stresses present in tubes and the fourth, the effect of cyclic loading on the subsequent stress relaxation behavior.

A paper by Geyling and Key evaluates the stress relaxation behavior of mandrel drawn, roller straightened tubes made from AISI 1010 and 1020 steel. The relaxation of residual stresses resulting from inhomogeneous plastic deformation during metal drawing operations was modeled. Residual stresses in the straightened tubes were measured by both X-ray and deflection techniques. These measurements were complemented by microcreep experiments on tension specimens cut from the walls of tubes and stress relaxation experiments on constant curvature bend test specimens. The curvature relaxation of small beams deformed plastically in four point bending was measured and compared to an analytical model.

A paper by Beeston and Burr presented results of a slit-tube test used in measuring residual stress during irradiation of inpile tubes made from AISI 348 stainless steel in the temperature range 300 to 425°C (527 to 797°F). Their measurements indicated that the stress gradient which opened the slit was due to wall temperature change (hot to cold) during reactor shutdown and that the stress gradient due to irradiation growth was completely relaxed. These tests were complemented by density and transmission electon microscope (TEM) measurements. A discussion of the microstructural mechanisms believed to be operating due to irradiation creep and differential swelling is presented.

A paper by Kapp, Underwood, and Zalinka discussed cyclically induced load relaxation in mild cast steel and cast ductile iron used in large caliber cannons. Fracture property measurements and service simulation tests were made on specimens made from sample hoops. The service simulation tests, made at constant displacement levels showed a significant relaxation in load due to a combination of inelastic deformation and fatigue crack growth. An analysis relating the change in specimen compliance as a function of crack depth is used to determine the relative losses in load due to stress relaxation and due to crack propagation, respectively.

A paper by Jaske and Laflen examines effect of load path and history on three alloy steels: 2.25Cr-1.0Mo, steel, AISI Type 304 stainless steel, and AISI Type 316 stainless steel. Relaxation data and creep data for the identical histories are compared. The prediction of creep from relaxation data is discussed as well as the effects of holdtimes on cyclic stress strain behavior.

The application of the analytical models presented by some of the authors needs to be applied to materials of different histories as well as other metals and alloys for which actual test data are available. This, in combination with microstructural observations would contribute to a better understanding of the physical behavior and is an area where much additional work seems indicated. Another area would be the effect of the mode of stressing on stress relaxation behavior. For example Idermark and Johanssen present stress relaxation data for AISI Type 301 stainless steel in the tension and torsion mode, while Fox presents data in bending. An analysis of effects of stressing mode on those results would also prove a fruitful new area of research.

Alfred Fox

Bell Laboratories, Murray Hill, N.J. 07974; symposium chairman and editor.

Index

D

E

H

I